SLU

DOCTORAL THESIS NO. 2023:25
FACULTY OF LANDSCAPE ARCHITECTURE, HORTICULTURE
AND CROP PRODUCTION SCIENCE

Developing affordable high-throughput plant phenotyping methods for breeding of cereals and tuber crops

FERNANDA LEIVA-SANDOVAL
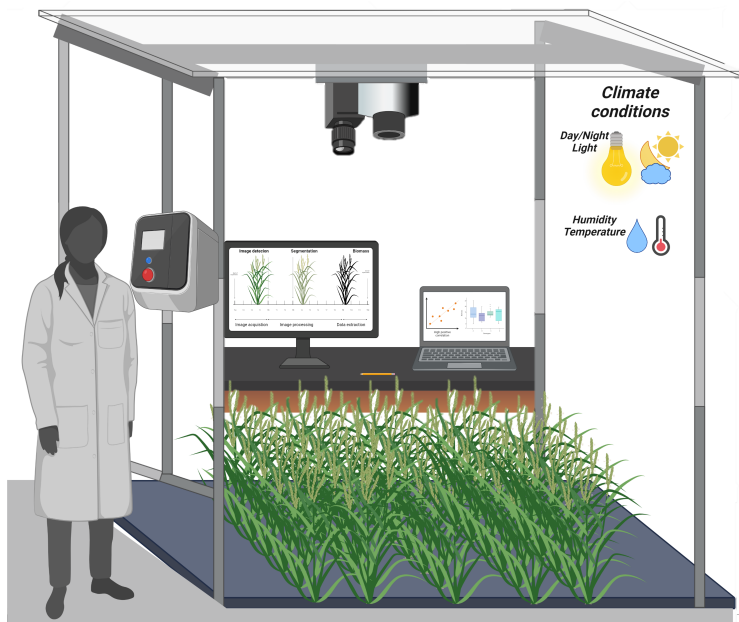
Developing affordable high-throughput plant phenotyping methods for breeding of cereals and tuber crops

Fernanda Leiva-Sandoval

Faculty of Landscape Architecture, Horticulture and Crop Production Science
Department of Plant breeding
Alnarp

SLU

SWEDISH UNIVERSITY
OF AGRICULTURAL
SCIENCES

DOCTORAL THESIS

Alnarp 2023

Cover: An illustration of Phenocave and the data processing
(Illustration by Fernanda Leiva-Sandoval in BioRender)

Abstract

High-throughput plant phenotyping (HTPP) is a fast, accurate, and non-destructive process for evaluating plants' health and environmental adaptability. HTPP accelerates the identification of agronomic traits of interest, eliminates subjectivism (which is innate to humans), and facilitates the development of adapted genotypes. Current HTPP methods often rely on imaging sensors and computer vision both in the field and under controlled (indoor) conditions. However, their use is limited by the costs and complexity of the necessary instrumentation, data analysis tools, and software. This issue could be overcome by developing more cost-efficient and user-friendly methods that let breeders, farmers, and stakeholders access the benefits of HTPP. To assist such efforts, this thesis presents an ensemble of dedicated affordable phenotyping methods using RGB imaging for a range of key applications under controlled conditions.

The affordable Phenocave imaging system for use in controlled conditions was developed to facilitate studies on the effects of abiotic stresses by gathering data on important plant characteristics related to growth, yield, and adaptation to growing conditions and cultivation systems. Phenocave supports imaging sensors including visible (RGB), spectroscopic (multispectral and hyperspectral), and thermal imaging. Additionally, a pipeline for RGB image analysis was implemented as a plugin for the free and easy-to-use software ImageJ. This plugin has since proven to be an accurate alternative to conventional measurements that produces highly reproducible results. A subsequent study was conducted to evaluate the effects of heat and drought stress on plant growth and grain nutrient composition in wheat, an important staple cereal in Sweden. The effects of stress on plant growth were evaluated using image analysis, while stress-induced changes in the abundance of key plant compounds were evaluated by analyzing the nutrient composition of grains via chromatography. This led to the discovery of genotypes whose harvest quality remains stable under heat and drought stress.

The next objective was to evaluate biotic stress; for this case, the effect of the fungal disease Fusarium head blight (FHB) that affects grain development in wheat was investigated. For this purpose, seed phenotyping parameters were used to determine the components and settings of a statistical model, which predicts the occurrence of FHB. The results reveal that grain morphology evaluations, such as length and width, were found to be significantly affected by the disease. Another study was carried out to estimate the disease severity of the common scab (CS) in potatoes, a widely popular food source. CS occurs on the tubers and reduces their visual appeal, significantly affecting their market value. Tubers were analyzed by a deep learning-based method to estimate disease lesion areas caused by CS. Results showed a high correlation between the predictions and expert visual scorings of the disease and proved to be a potential tool for the selection of genotypes that fulfill the market standards and resistance to CS. Both case studies highlight the role of imaging in plant health monitoring and its integration into the larger picture of plant health management.

The methods presented in this work are a starting point for bridging the gap between costs and accessibility to imaging technology. These are affordable and user-friendly resources for generating pivotal knowledge on plant development and genotype selection. In the future, image acquisition of all the methods can be integrated into the Phenocave system, potentially allowing for a more automated and efficient plant health monitoring process, leading to the identification of tolerant genotypes to biotic and abiotic stresses.

Keywords: Phenotyping, affordable, user-Friendly, RGB imaging, image analysis.

Sammanfattning

High-throughput plant phenotyping (HTPP) är en snabb, exakt och icke-destruktiv process för att utvärdera växters hälsa och miljöanpassning. HTPP kan påskynda identifieringen av agronomiska egenskaper av intresse, eliminera subjektivism, och underlätta utvecklingen av anpassade genotyper. Nuvarande HTPP-metoder förlitar sig ofta på bildsensorer och datorseende både i fält och under kontrollerade förhållanden i växthus. Användningen av dem begränsas dock av höga kostnader och av komplexiteten i den nödvändig utrustningen, dataanalysverktygen, och programvaran. Dessa problem skulle kunna lösas genom att utveckla mer kostnadseffektiva och användarvänliga metoder som låter växtförädlare, lantbrukare och andra intressenter få tillgång till fördelarna med HTPP. Denna avhandling presenterar en ensemble av dedikerade prisvärda fenotypningsmetoder som använder RGB-avbildning för en rad nyckelapplikationer under kontrollerade förhållanden för att överkomma dessa hinder.

Det prisvärda Phenocave-avbildningssystemet har utvecklats för att underlätta studier av effekterna av abiotiska stressfaktorer under kontrollerade förhållanden. Detta har gjorts genom att samla in data om viktiga växtegenskaper relaterade till tillväxt, skörd och anpassning till odlingsförhållanden och odlingssystem. Phenocave stöder bildsensorer inklusive synlig (RGB), spektroskopisk (multispektral och hyperspektral) och termisk avbildning. Dessutom implementerades en pipeline för RGB-bildanalys som en plugin för den kostnadsfria och lättanvända programvaran ImageJ. Denna plugin har sedan dess utveckling visat sig vara ett alternativ till konventionella mätningar och ger mycket reproducerbara resultat med hög noggrannhet. En efterföljande studie genomfördes för att utvärdera effekterna av värme- och torkstress på växttillväxt och spannmålsnäringssammansättning i vete, ett av de viktigaste sädesslagen i Sverige. Effekterna av stress på tillväxt utvärderades med hjälp av bildanalys, medan stressinducerade förändringar i förekomsten av essentiella ämnen utvärderades genom att analysera näringssammansättningen i vetekärnan via kromatografi. Detta ledde till upptäckten av genotyper vars skördekvalitet förblev stabil under värme- och torkstress.

Nästa målsättning var att utvärdera biotisk stress genom undersökning av effekten av svampsjukdomen Fusarium head blight (FHB) som påverkar spannmålsutvecklingen i vete. För detta ändamål användes fenotypningsparametrar för vetekärnor för att bestämma komponenterna och inställningarna för en statistisk modell, som kan förutsäga förekomsten av FHB. Resultaten avslöjar att egenskaper för kärnmorfologi, såsom längd och bredd, var signifikant påverkade av sjukdomen.

En annan studie genomfördes för att uppskatta infektionsintensiteten av potatisskabb (CS), Streptomyces scabies, i potatis, Solanum tuberosum. CS förekommer på knölarna och förstör dess utseende, vilket avsevärt påverkar deras marknadsvärde. Knölar analyserades med en djupinlärningsbaserad metod för att uppskatta sjukdomsskador orsakade av CS. Resultaten visade en hög korrelation mellan prediktionerna från modellen och visuella poängsättning av sjukdomen gjord av en expert på området, och visade sig vara ett potentiellt verktyg för val av genotyper som uppfyller marknadsstandarder och resistens mot CS. Båda studierna belyser bildens roll vid övervakning av växthälsovård och dess integration i ett större sammanhang för växtskyddshantering.

De metoder som presenteras i detta arbete är en utgångspunkt för att överbrygga gapet mellan bildteknik till kostnader och tillgänglighet. Resurserna är prisvärda och användarvänliga och kan generera avgörande kunskap om växtutveckling och genotypval. I framtiden kan bildinsamling av alla metoder integreras i Phenocave-systemet, vilket potentiellt möjliggör en mer automatiserad och effektiv växthälsoövervakningsprocess, vilket leder till identifiering av toleranta genotyper mot biotiska och abiotiska stressfaktorer.

Nyckelord: Fenotypning, prisvärd, användarvänlig, RGB-avbildning, bildanalys.

Dedication

To all my loved ones, my parents, sister, brother, my special you, and in loving memory of my forever beloved Sofy, who has gone from my sight but never from my heart.

"…What matters in life is not what happens to you but what you remember and how you remember it…"

Gabriel Garcia Marquez.

Contents

List of publications

This thesis is based on the work contained in the following papers, referred to by Roman numerals in the text:

I. Leiva, F., Vallenback, P., Ekblad, T., Johansson, E., Chawade, A.* (2021). **Phenocave: An Automated, Standalone, and Affordable Phenotyping System for Controlled Growth Conditions**. Plants, 10 (2021). DOI: 10.3390/plants10091817

II. Leiva F.*, Zakieh M., Alamrani M., Dhakal R., Henriksson T., Singh P.K., and Chawade A. (2022). **Phenotyping Fusarium Head Blight (FHB) through seed morphology characteristics using RGB imaging.** Frontiers in Plant Science, 13 (2022). DOI: 10.3389/fpls.2022.1010249

III. Lama S.*†, Leiva F. †, Vallenback P., Chawade A., and Kuktaite A. (2023). **Heat, drought and combined stress impact on yield, phenotypic and gluten protein traits: Capturing stability of spring wheat in excessive environments. International journal in molecular biology**. (Accepted)

IV. Leiva F*, Abdelghafour F, Davik J, and Chawade A. (2023). **ScabNet, A user-friendly application for detecting Common Scab in potato tubers using deep learning and morphology traits**. (Manuscript).

The contributions of Fernanda Leiva-Sandoval to the papers included in this thesis were as follows:

I. Designed the experiment together with the co-authors, performed sample preparation, acquired data and images, developed an image processing pipeline, analyzed data, and wrote the manuscript with the co-authors.

II. Designed the study together with co-authors, processed and analyzed all data, and wrote the manuscript with the co-authors.

III. Designed the study together with co-authors. Planned and performed some of the experimental work together with co-authors. Analyzed the phenotyping data and wrote the manuscript with the co-authors.

IV. Designed the study together with co-authors. Planned and performed image and data acquisition. In collaboration with the second author, developed algorithms for image processing and analyzed data. Finally, wrote the manuscript with the co-authors.

Other publications not included in the thesis:

Zakieh M, Gaikpa DS, Leiva F, Alamrani M, Henriksson T, Odilbekov F and Chawade A. (2021). **Characterizing Winter Wheat Germplasm for Fusarium Head Blight Resistance Under Accelerated Growth Conditions.** Frontiers in Plant Science, 12 (2021). DOI: 10.3389/fpls.2021.705006.

Abbreviations

CMYK	Cyan, Magenta, Yellow, Key/Black
CNN	Convolutional Neural Network
CS	Common Scab
DL	Deep Learning
DON	Deoxynivalenol
FHB	Fusarium Head Blight
HPLC	High-Performance Liquid Chromatography
HSB	Hue, Saturation, and Brightness
HSL	Hue, Saturation, and Lightness
HTTP	High-Throughput Plant Phenotyping
LAB	Luminance and color channels AB
LUPP	Large Unextractable Polymeric Proteins
ML	Machine learning
NDVI	Normalized Difference Vegetation Index
NIR	Near Infrared
QTL	Quantitative Trait Locus
QY	Quantum Yield
RGB	Red, Green, and Blue
TKW	Thousand Kernel Weight
TMP	Total Monomeric Proteins
TOTE	Total extractable protein
TOTU	Total SDS-unextractable proteins
TPP	Total Polymeric Proteins
UPP	Unextractable Polymeric Proteins

1.   Introduction

Greenhouse gas emissions are increasing worldwide because of the rapid growth of the human population and increasing consumption of goods and services, exacerbating the impact of climate change. This has increased the severity and frequency of extreme weather events including heatwaves, droughts, storms, and flooding (Altieri and Nicholls, 2017), all of which jeopardize food security and create risks of large-scale malnutrition. Research-based solutions have been proposed to accelerate plant breeding by developing genotypes that are better able to adapt to abiotic stresses and have the potential to increase crop yields (Phillips, 2010). While these approaches have yielded some new lines with improved adaptability to certain pedoclimatic factors, phenotyping continues to bottleneck breeding programs (Araus and Cairns, 2014). Some currently used phenotyping methods still rely on low-throughput visual assessments and manual measurements, which suffer from low accuracy and reproducibility on top of being time-consuming, labor-intensive, and subjective (Chawade et al., 2019; Fu and Jiang, 2022). However, advances in computer vision, data analytics, and machine learning have created new opportunities in plant research and breeding. Phenotyping methods combining these tools can reduce breeding costs and have made it economically feasible to expand field trials, accelerating progress in crop selection (van Dijk et al., 2021). For instance, high throughput phenotyping methods have been combined with genotypic data to analyze yield, yield components, and quality traits while also evaluating abiotic and biotic stress resistance (Chawade et al., 2019; Fu and Jiang, 2022). In addition, newly developed controlled growth facilities have enabled simulation of prolonged exposure to extreme conditions that adversely affect plant development, leading to significant losses of yields and

food quality as well as possibly stimulating the development of bio-aggressors. However, the digital divide has left many people on the margins of these developments because of a lack of expertise with the necessary technologies, the high labor intensity of their implementation, the cost of acquiring equipment, or the need for familiarization with new protocols that are not considered to offer significant advantages over conventional approaches. To overcome some of these problems, simple methods for evaluating plant cover have been developed in which a single camera is used to capture images in the visible red, green, and blue (RGB) spectrum before extracting leaf area, green biomass, or senescence and color vegetation index data (Casadesús et al., 2007; Arvidsson et al., 2011; Berger et al., 2012; Easlon and Bloom, 2014; Joalland et al., 2016; Armoniene et al., 2018). Methods of this sort have been used successfully to evaluate plant health, growth rate, abiotic stresses, and early vigor. Similarly, morphological analysis of leaves, seeds, and/or tubers (in the case of the root vegetable crops) has proven to be effective for evaluating quality parameters and disease severity for certain bio-aggressors (Wiwart et al., 2001; Tanabata et al., 2012; Whan et al., 2014; Komyshev et al., 2017; Si et al., 2017; 2018; Caraza-Harter and Endelman, 2020; Neilson et al., 2021; Miller et al., 2022). Solutions using more complex equipment to capture images in the VIS-NIR domain (multispectral and hyperspectral cameras) have been also proposed to evaluate moisture and nutrient content, plant health, seed water content composition and structure parameters, and vegetation indexes (Garcia et al., 2021; Mortensen et al., 2021; Femenias et al., 2022; Rangarajan et al., 2022; Ryckewaert et al., 2022; Yipeng et al., 2022; Qi et al., 2023; Solgi et al., 2023). However, simpler approaches may produce inconsistent outputs, while more advanced ones are costly and often impractical or unsuitable for use in real-scale trials. There is thus a need for new robust, user-friendly, and affordable phenotyping methods that have greater reproducibility than current methods while also being less time-consuming and labor-intensive. The work presented in this thesis was conducted to develop affordable and user-friendly methods for screening diverse germplasm in order to accelerate the discovery of new genotypes that can tolerate severe climate conditions under sustainable cultivation. Such methods would be of considerable value in Sweden's highly diverse plant breeding sector.

2. Background

2.1 Plant Breeding

Plant breeding, which is also known as crop development, cultivar improvement, and seed improvement, is a science-based activity whose practitioners seek to develop improved plant varieties that can adapt to specific conditions and be cultivated economically in commercial cropping schemes (Breseghello and Coelho, 2013). Breeding programs typically require rapid and accurate testing of large numbers of crosses in diverse environments because the likelihood of identifying the best progeny increases with the number of tests that are conducted (Araus and Cairns, 2014). Its concept entails three operations:

- Develop genetically variable germplasm.
- Identify and select better genotypes with all of the desirable characteristics/traits necessary for use in a production system.
- Multiply and stabilize these desired genotypes and release them for commercial production.

Plant breeders may work in either the private or the public sector. Private and public sector breeding programs mainly differ in terms of the time available for variety release, the cultivar types that are created, and prioritization of character selection criteria. For instance, private-sector breeders are likely to have a defined target of creating new lines as quickly as possible. Conversely, public-sector breeders also have to develop new varieties and may have more diverse responsibilities than their private-sector counterparts, including duties relating to academic activities or extension services. However, it should be noted that this is a very generalized description of the situation, and plant breeders in both sectors have wide-ranging responsibilities. In particular, they must be familiar with and manage work in diverse disciplines including plant evolution, genetics, biology, botany, pathology, biometry, molecular biology, and food science in order to successfully develop genotypes adapted to adverse climate conditions (Brown and Caligari, 2011).

However, not all challenges facing breeders relate to knowledge requirements or the diversification of responsibilities. Because the global population is growing rapidly, there is an urgent need to increase the efficiency of food production to ensure food security, now and in the future. Therefore, improving multiple traits of interest simultaneously is the main objective of current plant breeding efforts. This is difficult to achieve because physical linkages between genes controlling different traits of interest may give rise to undesirable correlations such that improvement with respect to one trait is accompanied by poorer performance with respect to another (Breseghello and Coelho, 2013). Crop selection is typically performed on the basis of empirical observations together with knowledge of genetic backgrounds and the products encoded by new genes. Information on genetic backgrounds and new gene products is typically gathered through laboratory-based studies whereas observations are typically acquired by using plant phenotyping methods to characterize novel cultivars in trials conducted under controlled or field conditions.

2.2   Plant phenotyping

The term "phenotyping" was introduced by the Danish plant scientist Wilhelm Johannsen and has been commonly used since the 1960s. Johannsen stated that if an organism can be discriminated from others of its species by direct examination or by more precise measurements of its anatomical, ontogenetic, physiological, or biochemical attributes, then it constitutes a distinct phenotype (Walter et al., 2015). These phenotypic attributes are governed by the interactions between an organism's genotypic background and the various micro- and mega-environments it encounters in its lifetime (Fasoula et al., 2020). Phenotyping involves the quantitative characterization of an organism's phenotypic attributes (Walter et al., 2015), (Figure 1). In crop science, plant phenotyping is an important tool for understanding plant behavior and optimizing crop management practices. Consequently, many plant phenotyping studies have been and are being conducted in order to improve crop yields and develop new lines with improved adaptability in the face of climate change. Some of these studies are conducted indoors, in greenhouses or controlled facilities, while others are conducted under real (or

"field") conditions (Pieruschka and Schurr, 2019). These two approaches have different advantages, disadvantages, and bottlenecks, but whichever approach is used, there are two central questions that must be answered in any phenotyping study: what should be measured, and how should it be measured?
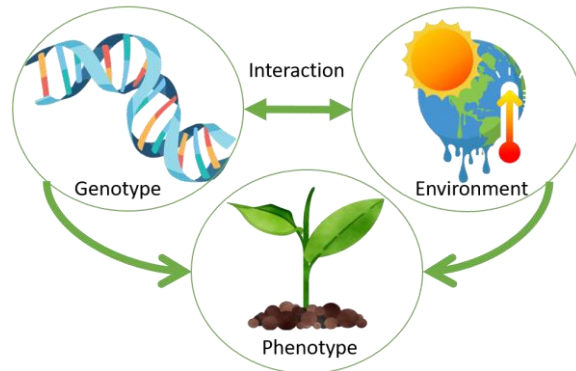
Figure 1. The interaction of a genotype and an environment to produce a phenotype.

2.3   Methods for plant phenotyping

Plant phenotyping methods can be classified as either low-throughput or high-throughput depending on their throughput, spatial resolution, and dimensionality (Dhondt et al., 2013). The term "throughput" refers to the number of discrete units that can be characterized with respect to a given set of plant traits (which may be canopy-level traits or traits relating to other organs) in a given amount of time. Spatial resolution refers to the scale at which plant traits can be measured using a given technique; the most high-resolution techniques may enable quantification of traits in individual cell components (e.g., plastids or cell walls), while techniques with coarser resolutions may only permit quantification at the level of whole cells, tissues, organs, or even at the level of entire fields. Finally, dimensionality refers to the variety of traits that can be evaluated in terms of categories and spatial and temporal resolutions. In phenomics, the term dimensionality corresponds to the number of genotypes and the diversity of environmental conditions that can be included in an analysis (Großkinsky et al., 2015).

2.3.1 Low-throughput plant phenotyping

Low-throughput phenotyping refers to traditional or conventional methods for evaluating plant traits. These methods are popular because they are cost-effective and can provide detailed information on specific traits, but they also generally have low sample throughput and are time-consuming and labor-intensive, making them unsuitable for use in large-scale studies (Araus et al., 2018). Notable low-throughput phenotyping techniques include visual assessment, gravimetric measurements, and biochemical assays.

- **Visual assessment***: Visual assessment involves using the naked eye to evaluate an individual's observable characteristics. These characteristics may include plant morphology parameters such as the height and number of leaves, color parameters such as the color of the leaves, or visible symptoms that might be caused by a bio-aggressor.

- **Gravimetric measurements**: Gravimetric measurement involves measuring the weight of whole plants or specific plant parts such as fruit, leaves, or roots.

- **Biochemical assays**: Biochemical assays are used to measure the concentrations of substances such as proteins, sugars, amino acids, and enzymes in plant tissues and cells. For example, sugar content measurements are important indicators of fruit quality.

2.3.2 High-throughput plant phenotyping

High-throughput phenotyping is a non-destructive approach in which automated or semi-automated methods are used to measure multiple traits in large populations of plants. It uses technologies such as sensors, imaging systems, and machine learning algorithms to quickly and accurately process and analyze data. High-throughput phenotyping is becoming increasingly important in plant breeding because it can accelerate the breeding process by providing insights into genotype-phenotype interactions and the influence of environmental factors on phenotype (Araus et al., 2018; Chawade et al., 2019; Fu and Jiang, 2022). However, high-throughput phenotyping is still a

developing field and faces several challenges in areas including standardization of methods, data management, and cost-effectiveness (Chawade et al., 2019). High-throughput phenotyping methods may be sensor-based, imaging-based, or robot-based.

- **Sensor-based phenotyping:** This approach uses sensors such as chlorophyll meters, fluorescence sensors, and thermal cameras to monitor physiological processes such as photosynthesis, water use, and stress responses in real-time and to detect changes in plant physiology. For example, thermal cameras can detect changes in plant temperature that may indicate water stress.

- **Imaging-based phenotyping:** This approach uses imaging systems such as RGB, multispectral, and/or hyperspectral cameras to capture images of plants, sometimes in conjunction with LiDAR (Light Detection and Ranging). These images can be analyzed to extract information on changes in traits such as biomass, leaf area, plant height, senescence, and early disease symptoms before they can be detected by the naked eye.

- **Robot-based phenotyping:** This approach uses systems equipped with various sensors and cameras to automate the measurement of plant traits. These systems can move through fields of crops or growth facilities and can collect data on multiple traits in real-time.

2.3.3   Instrumentation for plant phenotyping

Several sensing devices have been developed in recent decades and have become essential tools for quick and accurate assessment of plant characteristics. The main advantages of these instruments are their non-invasive nature and their ability to evaluate large numbers of genotypes to quickly identify those tolerant of and susceptible to specific environments (Pieruschka and Schurr, 2019).   Instruments commonly used for plant phenotyping include imaging systems such as RGB, multi or hyperspectral, and fluorescence cameras as well as sensors that measure plant height, biomass, and leaf area. Remote sensing techniques such as LiDAR and UAV-based systems are also gaining popularity because they can capture high-

resolution data over large areas (Yang et al., 2013; Fahlgren et al., 2015; Araus et al., 2018).

- **Remote sensors** are devices that can collect data from a distance without direct physical contact with the object or environment being measured. They are used in diverse applications, providing valuable information on environmental parameters such as temperature, humidity, and atmospheric conditions as well the location and movement of objects (Chawade et al., 2019). Common types of remote sensors include:

  - **LiDAR sensors:** LiDAR (Light Detection and Ranging) sensors use laser beams to measure the distance to an object or surface. They are commonly used in mapping, surveying, and geological applications.

  - **GPS sensors**: GPS (Global Positioning System) sensors use satellite signals to determine the location and movement of objects. They are commonly used in navigation, mapping, and surveying applications.

  - **UAV-based systems (drones):** UAV systems can capture high-resolution images and data over large areas. They typically use an unmanned aerial vehicle (UAV) equipped with sensors such as RGB or multispectral cameras, LiDAR, or thermal cameras to capture detailed images of plants from above for data extraction.

- **Handheld sensors** are portable devices that can be used to measure various environmental parameters. They are very popular due to their ease of use, portability, and affordability. Some common types of handheld sensors are chlorophyll meters, fluorometers, NDVI meters, spectrophotometers, and quantum yield meters (Chawade et al., 2019)

  - **Chlorophyll meters** measure the chlorophyll content in plant leaves, which can be used to estimate plant health, growth, and stress levels.

  - **Fluorometers** measure the fluorescence emitted by chlorophyll in response to light, which can be used to estimate photosynthetic activity and stress levels in plants.

- **NDVI (Normalized Difference Vegetation Index) meters** measure the amount of visible and near-infrared light reflected by plants, which can be used to estimate plant biomass, growth, and stress levels.

- **Spectrophotometers** are used to measure a sample's light absorption at specific wavelengths. They are commonly used in environmental testing, water quality analysis, and food safety testing.

- **Quantum Yield meters** measure the efficiency of photosynthesis in converting light energy into chemical energy, which can be used to estimate plant health and stress levels.

- **Other sensors:**

  - **Gas exchange meters** measure the exchange of gases such as carbon dioxide and oxygen, between a plant and its environment. They can be used to measure photosynthetic rates and water use efficiency.

  - **Soil meters** measure the soil's physical and chemical properties, including its moisture content, pH, and nutrient levels. They can be used to determine the availability of nutrients and water to plants.

- **Imaging systems** is a term that may refer to any digital or electronic instrument that captures images of plants for analysis and measurement of their physical and biological characteristics. This includes cameras operating in different spectral domains and any other instrument that can capture visual information on an object. Examples include RGB, near-infrared (NIR), thermal, multispectral (MSI), and hyperspectral (HSI) cameras (Araus and Cairns, 2014).

  - **RGB cameras** are commonly used and capture color images in the visible light spectrum. Such images can be used to analyze plant traits such as leaf area, plant height, and canopy cover.

- **NIR cameras** capture images in the near-infrared range, which extends from 700 to 1400 nm and is just below the wavelength range of visible light. This is useful in many applications where visible light cameras cannot capture useful information. NIR cameras are commonly used to study plant growth and health.

- **Thermal cameras** capture images of plants based on the heat they emit, providing information about temperature and stress responses.

- **MSI cameras** are specialized instruments that capture images in multiple wavelengths or spectral bands, often in the visible and near-infrared ranges. This allows them to capture information beyond that visible to the human eye, which can be used to analyze objects or scenes in greater detail. MSI cameras have diverse applications in agriculture, environmental monitoring, and remote sensing.

- **HSI cameras** are specialized imaging devices that can capture detailed information about a crop's spectral properties by imaging in hundreds or even thousands of narrow spectral bands across the electromagnetic spectrum. This means that they can capture very detailed and precise spectral signatures of objects. HSI imaging has many practical applications, including identifying different types of vegetation, mapping geological features, and detecting changes in land use patterns.

Figure 2. Selected camera types. **A)** (RGB) Canon EOS 1300D (from Canon Inc. [©]), **B)** (NIR) Canon EOS Rebel T6 (from Canon Inc. [©]), **C)** (Thermal), FLIR one pro-LT (from FLIR Systems Inc. [©]) **D)** (MSI) MicaSense Altum (from Micasense, Inc. [©]), **E)** (HSI) Specim FX10 (from SPECIM, SPECTRAL IMAGING LTD [©]).

2.4   Abiotic and biotic stresses

Abiotic and biotic stresses are the two major types of environmental stresses that can affect the growth, development, and survival of plants, animals, and microorganisms. They can also interact with one-another and with other environmental factors, which greatly complicates their management in agriculture, forestry, and ecosystem conservation.

2.4.1   Abiotic stresses

Abiotic stresses are stresses resulting from non-living environmental factors such as temperature, drought, salinity, heavy metal toxicity, radiation, and atmospheric pollutants that can negatively impact organisms' physiology and metabolism. For instance, high temperatures can cause protein denaturation, membrane lipid peroxidation, and oxidative damage, leading to reduced growth and yield in plants (Wahid and Close, 2007). Similarly, drought stress can reduce photosynthesis, transpiration, and nutrient uptake, resulting in stomatal closure, leaf wilting, and plant death (Chaves et al., 2003). Meanwhile, salinity stress can increase ion toxicity, osmotic stress, and nutrient imbalance, leading to ion imbalance, water stress, and oxidative damage in plants (Munns and Tester, 2008).

- **Heat stress** occurs when plants are exposed to high temperatures outside their optimal range for growth and metabolism. Heat can cause a range of physiological and biochemical changes in plants, resulting in damage to membranes, protein denaturation, and oxidative stress. These changes may in turn reduce photosynthesis, impair water uptake, and reduce yield. Different plant species have different thresholds for heat stress, with some being more tolerant than others. However, even heat-tolerant species may experience negative effects on growth and yield under prolonged or extreme heat stress. Heat stress can be managed in various ways, including by breeding for heat tolerance, using shading or mulching to reduce temperature, and regulating plant transpiration through irrigation management (Wahid and Close, 2007).

- **Drought stress** occurs when plants experience a lack of water or a shortage of available water in the soil. This can cause plants to close their stomata to conserve water, which reduces photosynthesis and growth. A lack of water can also damage cell membranes and proteins, leading to oxidative stress and reduced yield. Plants have evolved various mechanisms to cope with drought stress, such as root growth, osmotic adjustment, and stomatal regulation. These mechanisms can help plants maintain water uptake and reduce water loss. However, prolonged drought stress can cause irreversible damage to plants, leading to reduced yield and even death. Management strategies for drought stress include selecting drought-tolerant crop varieties, using drought-tolerant crop rotations, and optimizing irrigation and water management practices (Chaves et al., 2003).

- **Nutrient stress** occurs when plants experience a deficiency or excess of essential nutrients such as nitrogen, phosphorus, and potassium, or micronutrients like iron or zinc. This can cause reduced plant growth, stunted development, and yield losses. For example, nitrogen deficiency can cause chlorosis and reduced leaf size, while phosphorus deficiency can cause reduced root growth and poor fruit development. Excess nutrients (particularly excess nitrogen or phosphorus) can also cause problems such as reduced root growth, increased disease susceptibility, and environmental pollution resulting from leaching or runoff. Plants have developed various mechanisms to cope with nutrient stress, including root elongation, nutrient uptake mechanisms, and nutrient storage. Management strategies for nutrient stress include selecting crop varieties with better nutrient use efficiency, optimizing fertilizer treatments, and using integrated nutrient management practices to reduce nutrient losses and improve nutrient uptake efficiency (Kumari et al., 2022).

2.4.2 Biotic stresses

Biotic stresses are stresses caused by living organisms such as pests, diseases, and weeds that can cause damage or harm to other organisms. For example, insects, mites, nematodes, and rodents can feed on crops, causing physical

damage and transmitting diseases that can reduce yield and quality (Koul et al., 2004). Fungal, bacterial, and viral pathogens can infect plants, causing necrosis, chlorosis, and defoliation, leading to plant death or yield loss (Savary et al., 2019). Weeds can compete with crops for water, nutrients, and light, reducing crop yield and quality (Oerke, 2006). Some notable biotic agents that threaten food production are Fusarium Head Blight (FHB) affecting wheat, and Common Scab (CS), affecting potatoes.

- **Fusarium Head Blight (FHB)** is a devastating disease affecting wheat caused by the fungus *Fusarium graminearum*. FHB can cause significant yield losses and reduce grain quality by producing mycotoxins that are hazardous to human and animal consumption. The disease is characterized by the bleaching and shriveling of infected grain heads, which can lead to significant yield loss. FHB is favored by warm and humid weather conditions during the flowering and grain development stages of wheat growth. The fungus infects the wheat plant via the flowers and colonizes the developing grain. It can also infect the stem and leaves of the wheat plant, leading to additional damage. Once the fungus colonizes the grain, it produces mycotoxins that can accumulate in the grain and reduce its quality. The mycotoxin produced by FHB is called deoxynivalenol (DON) and can cause several digestive issues in humans and animals that consume contaminated grain (Polak-Śliwińska and Paszczyk, 2021; Del Ponte et al., 2022). FHB management measures for wheat include planting resistant varieties, rotating crops with non-host crops, and applying fungicides. Some cultural practices such as reducing plant density and avoiding excessive nitrogen fertilizer application can also reduce the incidence and severity of FHB (Gilbert and Haber, 2013).

- **Common Scab (CS)**: is a disease of potatoes caused by the bacterium in Europe *Streptomyces turgidiscabies* and *S. europaeiscabiei*. It is characterized by the formation of rough, scabby lesions on the surface of the potato tubers, which can significantly reduce yield and quality. Common Scab is favored by alkaline soil conditions and dry weather during tuber development. The bacterium infects the potato tubers through wounds or natural openings and colonizes the surface of the tuber. The scabby lesions that develop on the tuber can reduce the

29

marketability of the potato and make it more susceptible to other diseases and pests (Tsror et al., 1999; Oppenheim et al., 2019). Common Scab management practices for potatoes include planting resistant varieties, reducing soil pH, and applying biological or chemical control measures. Cultural practices such as avoiding excessive irrigation and applying organic matter to the soil can also help to reduce its incidence and severity (Al-Mughrabi et al., 2016).

2.5   Image Processing

Image processing is the manipulation of digital images using mathematical algorithms and computer software to extract information, enhance images, or convert them into different formats. It is an interdisciplinary field that combines computer science, mathematics, and engineering. Image processing has many applications in areas including medical imaging, remote sensing, and computer vision. Some common techniques used in image processing are filtering, segmentation, edge detection, image compression, morphological operators, feature extraction, and object recognition (Gonzalez, 2009; Szeliski, 2010).

2.5.1   Image

An image is a visual representation of something. A digital image is created by dividing a two-dimensional image into a grid of small squares, known as pixels (short for "picture elements"), which are the basic units of digital images. Each pixel is a tiny square or dot that represents a single point in an image and is characterized by specifying its color, brightness, and location.

2.5.2   Image resolution

The resolution of an image is measured in pixels per inch (PPI) or dots per inch (DPI) and determines the image's quality, sharpness, and level of detail. A higher-resolution image contains more pixels per inch and appears clearer and sharper than a lower-resolution one. Several image formats may be used, including RAW, JPEG, PNG, GIF, BMP, and TIFF.

- **RAW** image files contain minimally processed data directly from a digital camera's image sensor. They include all information captured by the camera's sensor, including details such as brightness, contrast, color temperature, and white balance.

- **JPEG (Joint Photographic Experts Group)** is a common format used for photographs and other complex images. It uses compression to reduce the file size while maintaining relatively high quality.

- **PNG (Portable Network Graphics)** is used for images that require transparency or higher quality than JPEG can provide. It does not use compression and can therefore give rise to relatively large files.

- **GIF (Graphics Interchange Format)** is used for simple animations and images with limited colors. It uses compression and can support transparency.

- **BMP (Bitmap)** is used for Windows-based systems and does not use compression. It supports both color and black-and-white images.

- **TIFF (Tagged Image File Format)** is commonly used in professional photography and printing. It supports high-quality images and can be used for both color and black-and-white images.

2.5.3   Color Spaces

In image processing, a color space is a mathematical representation of colors that allows us to describe and manipulate the colors in an image. Several color spaces are used in image processing, each of which has its own characteristics and advantages (Gonzalez, 2009; Poynton, 2012).

- **RGB (Red, Green, and Blue)** is the most commonly used color space in digital imaging. It represents colors using a combination of red, green, and blue intensities, which are typically represented as integer values ranging from 0 to 255. RGB is an additive color model, meaning that colors are created by adding different intensities of red, green, and blue light.

- **CMYK** (**Cyan, Magenta, Yellow, and Key/Black)** is used primarily for printing. It represents colors using a combination of cyan, magenta, yellow, and black values. CMYK is a subtractive color model, meaning that the colors are created by subtracting different amounts of cyan, magenta, yellow, and black ink from a white background.

- **HSL (Hue, Saturation, and Lightness) and HSV (Hue, Saturation, and Value)** are based on the idea of a color wheel. They represent colors using three values: hue, saturation, and brightness. HSL and HSV are often used in image editing software to adjust an image's color balance and tone.

- **Lab** is a device-independent color space that is used to represent all visible colors. It separates color information into a luminance (L) channel and two color channels ('a' and 'b'). The Lab color space is used in color correction and color management applications.

2.5.4   Image processing techniques

- **Filtering** is the process of modifying or enhancing an image by applying a set of mathematical operations. Several different types of filters are used in image processing, including spatial filters, frequency filters, and time filters.

- **Segmentation** is the process of dividing an image into multiple segments or regions. It is used to identify objects or features in an image and separate them from the background.

- **Edge detection** is the process of identifying the edges or boundaries of objects in an image. It is used to enhance the visual appearance of an image or to identify the edges of objects for further analysis.

- **Image compression** is the process of reducing an image's size without losing important information. It is used to store and transmit images efficiently.

- **Morphological operations** are mathematical operations used to process images based on their shape. They are used to extract features or remove noise from an image.

- **Feature extraction** is the process of identifying and extracting relevant information or features from an image. It is used in computer vision and pattern recognition.

- **Object recognition** is the process of identifying and classifying objects in an image. It is used in many fields including robotics, surveillance, and medical imaging.

2.5.5   Machine learning and Deep learning

- **Machine learning (ML):** is a subset of artificial intelligence (AI) that involves teaching computers to learn from data without being explicitly programmed. This allows computers to automatically improve their performance at specific tasks by learning from data. Machine learning has greatly improved the efficiency and accuracy of image-based plant phenotyping, which can help researchers better understand plant growth and development, and ultimately contribute to improving crop yields and food security. Machine learning may be either supervised or unsupervised (Bishop and Nasrabadi, 2006; Murphy, 2012; van Dijk et al., 2021).

    - **Unsupervised learning** is a type of machine learning in which the algorithm is trained on an unlabeled dataset, meaning that there are no corresponding target variables. The goal of unsupervised learning is to find patterns and structures in the data without using predefined labels. For example, in an unsupervised learning task involving clustering customers based on their purchasing behavior, the algorithm would be trained on a dataset of customer purchases without labels indicating which customers belong to which cluster. The algorithm would then group customers into clusters based on similarities in their purchasing behavior (Hinton and Sejnowski, 1999; Celebi et al., 2013).

- **Supervised learning** is a type of machine learning in which the algorithm is trained on a labeled dataset, meaning that each data point is associated with a corresponding label or target variable. The goal of supervised learning is to learn a mapping between the input features (or independent variables) and the target variable. This mapping can then be used to make predictions based on previously unseen data. For example, in a supervised learning task of predicting symptoms of plant disease, the algorithm would be trained on a dataset of symptoms with their corresponding features and other relevant features. It would then use this training data to learn a model that can predict the presence of disease in new material based on its features (Bishop and Nasrabadi, 2006; Murphy, 2012).

- **Deep learning (DL):** is a subfield of machine learning that involves training artificial neural networks with many layers to learn and make predictions from large amounts of data. Deep learning algorithms are modeled on the human brain, where interconnections between neurons enable the processing and transmission of information. Some of the most popular deep learning frameworks include TensorFlow, PyTorch, and Keras. Deep learning algorithms such as deep convolutional neural networks (CNNs) have been used to automate and improve the accuracy of image processing in plant phenotyping. For example, researchers have developed CNN-based models for detecting and segmenting plant leaves from images, and for predicting plant growth and yield based on visual traits. One study used a CNN-based model to extract plant growth and architecture traits from images of tomato plants, achieving high accuracy in predicting yield-related traits. Another study used a CNN-based model to detect and segment individual leaves from images of maize plants, enabling accurate measurement of leaf area and plant biomass (Pound et al., 2017; Ubbens and Stavness, 2017).

3. Objectives

3.1 General objective

Global agricultural production demand is growing in parallel with the world's population. Moreover, aggravating factors including climate change, soil degradation, and the increased virulence and resistance of pathogens represent additional threats to food safety. According to UNFAO, the production of energy food crops will have to double to meet future demand. Germplasm phenotyping and the identification of efficient genotypes under changing climate scenarios will be essential for increasing crop yields and climate resilience to meet these demands. Conventional phenotyping based on visual or manual assessments provides insights into plant development for the characterization and selection of individuals with tolerance to biotic and abiotic stress. However, these techniques suffer from subjectivity and limited reproducibility, in addition to being labor-intensive and time-consuming. They also require expertise in sample evaluation, which limits the scale on which experiments can be performed. Therefore, several methods have been developed for evaluating plant characteristics using simple solutions with RGB cameras or more advanced sensors in the VIS-NIR domain. Unfortunately, simpler approaches can generate somewhat inconsistent outputs, while more advanced ones are costly and often impractical or unsuitable for real-scale trials. The main objective of this thesis is thus to develop affordable phenotyping methods that avoid these problems and offer researchers and plant breeders cost-effective and reliable tools for monitoring and analyzing biotic and abiotic stresses in diverse plant material under controlled environments. New methods are presented for assessing important traits in different species (wheat, sugar beet, and potato), including biomass (wheat and sugar beet), and chemical processes that affect plant composition (e.g., gluten content and strength in wheat), providing valuable insights into plant development. The thesis also introduces new methods for analyzing morphological features that can be used to evaluate quality traits and/or disease severity (wheat and potato) in order to facilitate the development of more sustainable control strategies. This is important because current disease control strategies rely heavily on unsustainable practices. These methods

could thus facilitate and accelerate the characterization and selection of genotypes by enabling automated, non-destructive, low-cost, and high-throughput phenotyping with reliable and accurate results.

3.2   Specific objectives

1. Develop a low-cost, automated, and user-friendly, phenotyping system adapted for indoor facilities to monitor and measure important agronomic plant traits. (Paper I)
2. Compare the performance of two cost-benefit seed image analysis methods by assessing morphological traits in wheat grain to predict Fusarium head blight, (FHB). (Paper II)
3. Evaluate the potential of combining image analysis with gluten protein screening by size-exclusion high-performance liquid chromatography (SE-HPLC) to identify genotypes that are stable under and tolerant of adverse growth conditions (Paper III).
4. Develop an image processing approach combining color-morphology analysis with deep learning to estimate tuber quality traits and common scab (CS) severity by analyzing color images. (Paper IV).

4. Materials and Methods

4.1 Phenocave: Automate indoor phenotyping

4.1.1 Plant material

In the first part of the study, Phenocave was tested by conducting two experiments in a Biotron chamber, one focusing on wheat and another examining sugar beet. In the wheat experiment, spring wheat plants of a genotype provided by Lantmännen Lantbruk (Svalöv, Sweden) were grown under three environmental conditions: control (optimal conditions), drought during the stem-elongation and heading stage (no irrigation for five days), and high nutrient stress during the heading stage (double dosage of fertilizer). In the sugar beet experiment, sugar beet seeds of a single genotype were treated with different enhancing agents developed by DLF Beet Seed AB (then named MariboHilleshög; Landskrona, Sweden) and grown under optimal conditions to evaluate plant development. The seeds were divided into four groups: untreated (control); primed to accelerate germination and early seedling growth; pelleted and coated to improve seed drilling performance and establishment; and treated with all agents via priming, pelleting, and coating.

4.1.2 Methodology

Phenocave was custom-built for use in a Biotron chamber of four square meters. It consists of a gantry robot supplied by the Igus Company (Cologne, Germany), mounted on an aluminum structure designed and built by the

Eltech Automation Company (Lomma, Sweden). It supports three different imaging sensors, including digital DLSR RGB (Canon EOS 1300D), MSI (MicaSense Altum), and HSI (Specim FX10) cameras. The cameras have free linear movement in the XY plane and the RGB and MSI cameras can be used simultaneously or individually. The HSI camera, on the other hand, can only be used alone because it must be in constant motion when scanning the workplace. The system was tested by capturing RGB and thermal images of individual plant pots. Image analysis of digital biomass was performed using a pipeline written in the Java language, which was implemented as a plugin for ImageJ (Schneider et al., 2012). Each image was segmented into areas of interest to extract projected green and yellow areas. The imaged plants were then collected for destructive measurement of their real biomass, which was done by weighing the fresh matter and the dry matter obtained after oven drying, and the empirical measurements were compared to the estimates obtained by image analysis.

4.2 Prediction of FHB disease severity based on seed morphology

4.2.1 Plant material

To predict FHB disease in wheat, wheat kernels with FHB infections of differing severity were studied (Paper II). The kernels were collected from a previous experiment (Zakieh et al., 2021) using winter wheat genotypes from two different sources. One source consisted of a breeding set of 338 genotypes provided by the Swedish agricultural cooperative Lantmännen Lantbruk (Svalöv, Sweden). The second source consisted of a genebank set of 181 germplasm genotypes provided by the Nordic Genetic Resource Center, Nordgen. This set represents highly diverse plant material including old cultivars and landraces (Paper II).

4.2.2 Methodology

Two different grain phenotyping methods were used to measure kernel morphology parameters: the free software package SmartGrain (Tanabata et

al., 2012) and the Cgrain Value™ (Cgrain_AB) automated imaging and cost-benefit analysis system, which includes both software and hardware.

For SmartGrain, image capture was done using a low-cost protocol from a top-view angle using an RGB digital camera (Canon EOS 1300D). Kernels of each genotype were placed manually on a blue background alongside a scale tool. Following an established protocol (Tanabata et al., 2012), seven morphological traits were extracted for each kernel: area seed (AS), perimeter length (PL), length (L), width (W), length-to-width ratio (LWR), the circularity of the seed (CS), the distance between the intersection of length and width, and the center of gravity (DS). For Cgrain Value™, image capture, and analysis were done using the same instrument with the hardware and software supplied by the manufacturer. The capture process generates a 3D view of each kernel by using a special mirror system that captures around 90% of the kernel's surface. Nine morphological traits are then extracted for individual kernels and kernel groups (depending on the properties of the placed in the instrument): length (L), width (W), thickness (T), average width (AVG.W), volume (V), weight (WT), and HSL color space values (hue, saturation, and light). Three multiple linear regression models were built using the free software package R (R Development Core Team, 2010), one for each tool individually and one based on their combined results.

4.3 Identification of climate stress (heat and drought) tolerant genotypes for wheat breeding targeting stability by image processing and SE-HPLC analysis

4.3.1 Plant material

For the third part of the study, eight spring wheat genotypes (Diskett, Happy, Bumble, SW1, SW2, SW3, SW4, and SW5) provided by Lantmännen Lantbruk (Svalöv, Sweden) were exposed to four environmental conditions at the heading stage in the Biotron (Paper III): control (optimal growth conditions), heat, drought (no irrigation for five days), and combined heat and drought. The growing conditions including the temperature, humidity, and day length (hours) were based on the five-year average (2016–2020) of the weather data for the growing period from the 22nd of April to the 11th of August (Supplementary file S3, paper III) in Malmö, Sweden. Weather data

were obtained from the Swedish Meteorological and Hydrological Institute 119 (SMHI) (www.smhi.se).

4.3.2 Methodology

Plants were placed in two different chambers to induce different stresses: one chamber was used for the heat and heat plus drought treatments, while the second was used for the drought and control treatments. Three different assessments were then performed in each chamber - one to extract digital biomass data based on RGB image analysis, one designed to extract phenotypic trait data, and one to extract gluten protein parameters based on SE-HPLC analysis. For the first assessment, image acquisition was done using a digital camera (Canon EOS 1300D) by capturing views of the plant pots from the top, front, back, left, and right (Armoniene et al., 2018) before, during, and after eight days of stress treatment. The projected leaf area was automatically extracted for each view using the EasyLeaf software (Easlon and Bloom, 2014). The average of the five views was then taken as the digital biomass estimate for the pot. In addition, seven phenotypic traits were measured: height, spike length, spike width, number of spikes, fresh biomass weight (after harvesting), thousand kernel weight (TKW), and grain yield. Finally, SE-HPLC was performed to assess the gluten protein parameters of the harvested grains. The following parameters were determined following a previously established protocol (Lama et al., 2022): total extractable protein (TOTE), total SDS-unextractable proteins (TOTU), percentage of total unextractable polymeric proteins in total polymeric proteins (%UPP), and percentage of large unextractable polymeric proteins in total large polymeric proteins (%LUMP). Total polymeric proteins (TPP) and total monomeric proteins (TMP) were also calculated.

4.4 Evaluation of CS disease severity using deep learning and estimation of tuber quality based on morphological traits

4.4.1 Plant material

To detect and quantify CS, artificially inoculated potato tubers were studied. The tubers with CS infections of differing severity were supplied by Graminor (Ridabu-Norway). The samples were taken from the company's core collection grown in field experiments from 2019 to 2022, and 2) from a greenhouse inoculation experiment (Paper IV). The material comprised red and yellow tubers and their symptoms had emerged naturally in the field. For analytical purposes, the tubers were manually categorized into five classes of increasing infection severity, with class one comprising completely or mostly healthy tubers and class five representing the maximum severity. The percentages used for categorization were based on data generated using a semi-automated method.

4.4.2 Methodology

Before image acquisition, tubers were washed and manually placed on a blue background in groups of six. Images were then captured using a digital camera (Canon PowerShot G9 X Mark II) and stored for further analysis. All image analysis was performed using two software modules written in the Python programming language: one for assessing morphological parameters and one for estimating CS disease severity. Both modules were linked to a graphical user interface (GUI) (Shipman, 2013; Schimansky, 2022). Morphological parameters for individual tubers were extracted by using the OpenCV package to assess the length, width, area, length-to-width ratio, circularity, and color values (in the CIELab color space, for which the color values are lightness and a* and b* chromaticity values for the green-red and yellow-blue axes, respectively). The skin color of the tuber (red or yellow) was then identified. For the analysis of CS disease severity, a convolutional neural network (CNN) was built using the Keras (Gulli and Pal, 2017) and TensorFlow (Developers, 2021) packages. Initially, tubers were classified into five categories according to the severity of the symptoms visible on their surfaces: healthy (category 1) and infected (categories 2, 3, 4, and 5). Data were obtained in a semi-automated way using Trainable Weka Segmentation

(TWS) (Arganda-Carreras et al., 2017), applying the default settings for a random-forest supervised classifier with four classes (background, red tuber, yellow tuber, and scab). The results obtained were percentage values representing the extent of disease symptoms on the tuber surface and were manually validated. In some cases, corrections were performed, after which the tubers were categorized into the five previously mentioned classes. Each potato detected in a previously segmented image was automatically isolated and reduced to a tile size of 172*172 pixels for inclusion in a training set. Six deep learning architectures (VGG16, VGG19, ResNet50V2, ResNet 101V2, InceptionV3, and Xception) were then trained using this dataset, applying two training strategies (transfer learning and fine-tuning) to identify the approach with the best performance. The robustness of the resulting model was then tested using two standard metrics: loss and accuracy.

5. Results and Discussion

5.1 Phenocave: Automate indoor phenotyping

An affordable, automated, and user-friendly system named Phenocave was developed. Phenocave can be used to monitor and evaluate plant characteristics with different imaging technologies (Figure 3). The system was tested by using it to measure wheat growth under controlled conditions and when subjected to stresses resulting from drought and a double dosage of fertilizer. The wheat plants in this experiment were evaluated in three groups, with the first group consisting of control plants and the second comprising those subjected to abiotic stresses. Growth development was assessed from the seedling stage (seven days post-sowing) three times per week until the end of the grain-filling stage (58 days post-sowing), covering all six growth stages. The digital biomass extracted from the images correlated significantly and positively with the biomass measured using conventional destructive methods involving measurement of fresh and dry weight ($r = 0.96$, $p < 0.01$, $r^2 = 0.92$ for dry weight; $r = 0.97$, $p < 0.01$, $r^2 = 0.94$ for fresh weight). The groups subjected to drought stress during two growth stages were evaluated with an RGB camera to extract digital biomass and with a thermal camera to verify the stress by measuring canopy temperatures. For the second experiment using sugar beet, the speed of germination was quantified by leaf area projection for eighteen days. During this period, seeds treated with enhancing agents exhibited accelerated growth. Specifically, seeds enhanced with priming agents in treatments B and D (primed, pelleted, and coated) exhibited the fastest germination, emerging just four days of sowing. Conversely, seeds not exposed to

priming, i.e., those in treatments A (control) and C (pelleted and coated) exhibited delayed germination.

These results show that the Phenocave system can be a useful tool for non-destructively evaluating and monitoring diverse plant characteristics under various growth conditions over extended periods of time. One limitation encountered during this work is that the lens's proximity to the object made band alignment of the multispectral camera impossible. This problem will be solved as the system is refined in the future.

Figure 3. The Phenocave system installed in a Biotron chamber with two mounted imaging sensors: an RGB camera (Canon EOS 1300D), and an MSI camera (MicaSense Altum). Image reproduced with permission from (Leiva et al., 2021).

5.2 Prediction of FHB disease severity based on seed morphology

To determine how FHB affects kernel morphology, the traits of five FHB-infected susceptible and resistant genotypes from breeding and genebank sets were measured with the SmartGrain and Cgrain Value ™ systems. Based on the severity of the symptoms visible on the spikes, resistant genotypes were assigned visual scores of 0% (indicating no visible evidence of infection) while susceptible genotypes were assigned scores of 100% (unambiguous visible evidence of infection). These results showed that FHB affects the kernels of susceptible genotypes more severely than resistant ones, as expected. Analysis of variance (two-way ANOVA) was then used to identify morphological traits significantly associated with disease severity. This revealed that length, width, thickness, and color parameters including light, and hue were significantly ($P< 0.001$) associated with disease severity, while volume, CS, and saturation ($P< 0.01$) were also clearly associated with FHB severity. Other parameters that were not significantly associated nevertheless exhibited differences between infected and non-infected kernels. A principal component analysis was also performed to investigate the responses of the seed traits to infection and their correlations with one-another. The hue and light color parameters measured with Cgrain Value ™ were found to have a moderate to high positive correlation ($r = 0.65$) and a low positive correlation ($r = 0.36$), respectively. In addition, the length-to-width ratio measured with SmartGrain had a low positive correlation ($r = 0.27$). Some negative correlations of varying significance were also identified based on the visual assessments of symptoms and other characteristics. Finally, to predict disease severity, a multiple linear regression model was generated to identify the contributions of the 16 different morphological traits measured by Cgrain Value™ and SmartGrain. Good predictive accuracy ($R2 = 0.58$) was achieved by combining the trait information provided by both tools. In addition, moderate predictive accuracy was achieved using only trait information provided by Cgrain Value™ ($R2 = 0.52$), while medium to low accuracy was achieved using trait data obtained with SmartGrain ($R2 = 0.30$). These methods for predicting FHB infection severity are proposed as alternatives to expensive and time-consuming conventional analysis. This use is supported by the good agreement between the phenotype-genotype associations predicted by both techniques and the traits assigned based on

visual inspection. Moreover, previous studies found a strong association between symptoms visible on wheat head spikes and the frequency of kernel damage (Góral et al., 2018). The methodology developed in this work could thus be used to compare estimated visual disease severity scores and identify possible associations between symptoms visible on wheat head spikes and grain traits.

This work focused on the characteristics of whole spike kernels rather than the damage to a small number of spikes caused by Fusarium colonization at the site of inoculation. This is expected to reduce the cost, time, and labor needed for disease resistance assessment. Additionally, visual scorings of FHB disease severity based on discoloration, bleaching, and spike stunting (Zakieh et al., 2021) were previously verified by the identification of several loci in genome-wide association studies (GWAS) (Appendix 1 of paper II). Because the plant material examined in this work was identical to that used in the GWAS study, the results presented here can also be considered to be supported by the GWAS findings.

5.3 Identification of climate stress (heat and drought) tolerant genotypes for wheat breeding targeting stability by image processing and SE-HPLC analysis

Digital biomass measurements were used to evaluate the impact of different stresses on wheat plant development. This revealed that combined heat-drought stress had the most severe impact, followed by drought stress alone; the impact of heat stress alone was comparatively modest. The results obtained under controlled conditions showed that the SW3 and SW4 genotypes had the highest and lowest digital biomass production of the studied genotypes, respectively. Drought stress reduced digital biomass in all genotypes when compared to the control set. Heat stress had a mild effect on all plants but its effect was strongest in the Bumble, SW2, and SW5 genotypes. Combined heat-drought stress significantly reduced digital biomass in all genotypes, but Happy was the most resistant genotype and Diskett was the most susceptible.

The analysis of gluten protein parameters revealed that the SW3 and Happy genotypes gave the highest yield, SW1, and Happy gave the highest TKW, SW2 and Bumble gave the highest %UPP, and Diskett and SW1 gave the

highest protein concentration (TOTE) and were thus most promising in terms of performance and stability under the studied conditions. To identify genetic material suitable for use in breeding programs targeting extreme climate resistance, the superior performance of these genotypes should be verified in field trials including analyses of their phenotypic and gluten protein characteristics using the advanced tools developed in this work.

Significant positive correlations were observed between grain yield and digital biomass under all stress treatments, and between yield and actual biomass under the heat and combined stress treatments. These results indicate that RGB imaging is an effective tool for identifying stress indicators in wheat plants. Drought stress also induced significant changes in gluten concentration (%UPP and %LUPP). The majority of the gluten protein parameters and the digital grain biomass (biomass) were found to be negatively correlated, indicating that maintaining high wheat grain quality under field conditions may be very challenging. The spike number is a measure of yield and could thus be a useful trait to monitor in addition to traits directly related to gluten protein quality when screening for high yield and gluten protein production under climate change.

5.4 Detection of CS disease severity using deep learning and estimation of tuber quality based on morphological traits

The ScabNet pipeline developed in this work proved to be a capable and reliable tool for assessing tuber size characteristics such as length, width, area, length-to-width ratio, circularity, and values of each channel in the HSL color space. The morphological trait data obtained with ScabNet were compared to manual measurements and data obtained using a method implemented in ImageJ, revealing a strong association ($r>0.83$) with the manual measurements and a strong correlation ($r>0.88$) with the ImageJ results. Six deep-learning model architectures were evaluated to develop a module for CS detection. In all cases, the models exhibited conventional learning behavior characterized by increasing accuracy combined with decreasing loss at each epoch. The fine-tuning strategy achieved significantly better performance than the transfer learning strategy for the ResNet, Inception, and Xception architectures with both the training and validation

datasets. Conversely, the simpler VGG networks performed better when using the fine-tuning strategy. Four of the six models generated using fine-tuning (InceptionV3, Xception, ResNet50V2, and ResNet101V2) achieved accuracy above 90%. However, only InceptionV3 and Xception provided consistent outputs; the behavior of ResNet when applied to the validation set differed significantly from that seen with the training set. Similarly, InceptionV3 and Xception achieved stable results in terms of validation accuracy and loss without overfitting (for more detailed information, see Appendix 1, manuscript IV). The most accurate and stable model was obtained using the Xception architecture with the fine-tuning learning strategy, so this model was selected for further evaluation. Xception had a stable accuracy above 95% after 10 epochs and its accuracy improved consistently to a maximum of 99% when applied to the validation set. Moreover, its loss values remained low, as shown by the confusion matrix included with the test results. With the exception of InceptionV3 trained with the fine-tuning strategy, all other architectures delivered poor performance.

Instead of basing classes on infected area categories, the model could be improved by aligning it with breeders' evaluation standards. Unfortunately, our results cannot be compared to any literature data because to our knowledge, no other studies have addressed the problem of scoring CS potato tubers using RGB image analysis. However, methods based on spectrometric data captured using hyperspectral imaging have been reported (Dacal-Nieto et al., 2011). Such approaches could offer new perspectives on the disease's development or help identify early symptoms before they appear but their output cannot be directly compared to the results presented here.

The results obtained in this study show that the ScabNet pipeline is a powerful and flexible tool for quickly and efficiently analyzing images of potato tubers with a wide range of sizes, shapes, colors (red and yellow), and degrees of CS severity. Correlations with manual measurements and (in the case of morphological features) two other image analysis methods showed that the pipeline can reliably and accurately measure tuber length and width. To improve the precision and accuracy of tuber identification in the future, the deep learning element of the pipeline could be expanded to include semantic segmentation.

6. Conclusions

This thesis presents affordable and user-friendly methods using RGB imaging to assist the process of HTPP. The methods were developed to maximize selection efficiency and accuracy and thus represent a major step towards practically useful methods that can be used on large scales without excessive cost, usage complexity, or manpower requirements. As such, these methods make state-of-the-art approaches accessible in the context and at the scale of the breeding industry.

The four methods developed in this work successfully captured diverse plant characteristics ranging from characteristics relating to growth and development to those important for detecting and predicting disease.

The Phenocave system automatically collects image data in a user-friendly manner under controlled conditions. This makes it possible to rapidly gather data on a wide range of key agronomic traits under different growth conditions. Additionally, it is compatible with or adaptable to many different imaging sensors including RGB, MSI, and HSI cameras, enabling the evaluation of a very wide range of plant characteristics. These findings indicate that Phenocave is a powerful tool for improving the accuracy and consistency of data collection for phenotyping.

The combination of image analysis with grain nutrient composition analysis revealed the impact of different stress factors on plant development while simultaneously providing insights into the metabolic changes occurring in plants in response to stress. These results thus deepen our understanding of plant traits and their relationship with abiotic stresses.

The ability to use imaging techniques to predict FHB based on seed phenotyping is a promising development in plant disease detection and prevention. FHB was shown to alter seeds' morphological parameters such as length and width. In addition, these changes correlated strongly with visual scorings of wheat spikes. As such, this method could be used to identify and

eliminate contaminated seeds, helping to prevent the spread of the FHB and minimize crop losses.

The deep learning-based ScabNet pipeline was shown to be a reliable, accurate, and consistent tool for diagnosing CS and measuring the resulting disease lesion areas. Its predictions were shown to correlate strongly with visual scorings, indicating that ScabNet could help to reduce economic losses by identifying genotypes that can tolerate CS and thus produce tubers with high market value even when challenged by this disease.

Although the methods presented here were evaluated using wheat, sugar beet, and potato as model plants, they could easily be adapted to other crops. However, some challenges remain to be addressed in order to unleash their full potential. For instance, it would be very desirable to incorporate additional imaging sensors such as MSI and HSI to enable stress diagnosis before the appearance of visible symptoms. It will also be important to evaluate the performance of each method with a wider range of wheat and potato varieties under diverse abiotic stresses to validate the accuracy and reliability of their predictions. Both of these issues will be addressed in future work.

Overall, these methods offer a wide range of ways to evaluate the effect of biotic and abiotic stress. In addition, they represent important steps towards more accessible, user-friendly, and affordable imaging technologies for plant research and agriculture, which is especially important for users who may lack the resources and expertise needed to implement advanced imaging technologies. With careful planning and thoughtful execution, these methods could be a powerful tool for driving innovation and achieving outcomes that were previously beyond the reach of most breeding programs. As such, there is a clear justification for further work to develop and refine these imaging systems in order to make them even more affordable, user-friendly, and accessible to a wider range of users.

7. Future perspectives

The methods presented in this thesis were developed with the aim of increasing the adoption of imaging-based technology for plant phenotyping. While they already offer good performance, they could be refined and optimized further to improve their accuracy, efficiency, and applicability to diverse plant species under other environmental conditions.

The automated Phenocave imaging system for capturing plant trait data was developed to support regular and advanced imaging technologies, such as RGB, MSI, and HSI cameras. However, evaluations were only performed using the RGB camera and the thermal infrared sensor of the MSI camera. Therefore, future work on this system should investigate the use of MSI or HSI imaging to predict numerous biophysical parameters including those related to photosynthetic systems. In addition, there is a need to develop user-friendly pipelines for the analysis of the resulting data. This will make the Phenocave platform even more robust and reliable for evaluating important agronomic traits that could be relevant in genotype selection.

Plant responses to abiotic stresses based on image and grain nutrient composition analysis were evaluated under heat and drought stress, both individually and in combination. To further evaluate the benefits of the imaging-based approach, future studies could examine its performance when applied to other abiotic stresses such as salinity or flooding. In addition, the image capture process could be adapted for compatibility with Phenocave. This would enable automatic image acquisition and the use of other imaging sensors to provide a deeper understanding of plants' response to stress and enable the evaluation of more agronomic traits.

Linear regression analysis revealed that evaluations of grain morphology can be powerful tools for detecting and predicting FHB infection. However, it is possible that their performance could be improved by developing more sophisticated models that take into account a wider range of morphological

features such as texture. Additionally, a system like Phenocave could be adapted to capture high-resolution images that provide detailed information about the structure and composition of grains, which may be useful for identifying other morphological traits associated with FHB resistance or susceptibility.

CS infection severity in potato tubers was estimated using a deep learning-based method. Although the results revealed a high correlation between the predictions and the visual scores, only two potato varieties were studied. Therefore, a larger study examining more potato varieties should be conducted to verify the method's potential for detecting and preventing this disease. In addition, instead of using individual tubers as tiles, semantic segmentation could be used to enable the identification of specific objects or regions showing signs of CS infection.

Overall, the methods presented herein represent important steps towards more efficient, sustainable, and resilient agricultural practices and could be adapted to other crops that may present similar symptoms to those observed in this work.

References

Al-Mughrabi, K.I., Vikram, A., Poirier, R., Jayasuriya, K., and Moreau, G. (2016). Management of common scab of potato in the field using biopesticides, fungicides, soil additives, or soil fumigants. *Biocontrol Science and Technology* 26(1)**,** 125-135.

Altieri, M.A., and Nicholls, C.I. (2017). The adaptation and mitigation potential of traditional agriculture in a changing climate. *Climatic Change* 140**,** 33-45.

Araus, J.L., and Cairns, J.E. (2014). Field high-throughput phenotyping: the new crop breeding frontier. *Trends in plant science* 19(1)**,** 52-61.

Araus, J.L., Kefauver, S.C., Zaman-Allah, M., Olsen, M.S., and Cairns, J.E. (2018). Translating high-throughput phenotyping into genetic gain. *Trends in plant science* 23(5)**,** 451-466.

Arganda-Carreras, I., Kaynig, V., Rueden, C., Eliceiri, K.W., Schindelin, J., Cardona, A., et al. (2017). Trainable Weka Segmentation: a machine learning tool for microscopy pixel classification. *Bioinformatics* 33(15)**,** 2424-2426. doi: 10.1093/bioinformatics/btx180.

Armoniene, R., Odilbekov, F., Vivekanand, V., and Chawade, A. (2018). Affordable Imaging Lab for Noninvasive Analysis of Biomass and Early Vigour in Cereal Crops. *Biomed Res Int* 2018**,** 5713158. doi: 10.1155/2018/5713158.

Arvidsson, S., Perez-Rodriguez, P., and Mueller-Roeber, B. (2011). A growth phenotyping pipeline for Arabidopsis thaliana integrating image analysis and rosette area modeling for robust quantification of genotype effects. *New Phytol* 191(3)**,** 895-907. doi: 10.1111/j.1469-8137.2011.03756.x.

Berger, B., de Regt, B., and Tester, M. (2012). High-throughput phenotyping of plant shoots. *Methods Mol Biol* 918**,** 9-20. doi: 10.1007/978-1-61779-995-2_2.

Bishop, C.M., and Nasrabadi, N.M. (2006). *Pattern recognition and machine learning.* Springer.

Breseghello, F., and Coelho, A.S.G. (2013). Traditional and modern plant breeding methods with examples in rice (Oryza sativa L.). *Journal of agricultural and food chemistry* 61(35)**,** 8277-8286.

Brown, J., and Caligari, P. (2011). *An introduction to plant breeding.* John Wiley & Sons.

Caraza-Harter, M.V., and Endelman, J.B. (2020). Image-based phenotyping and genetic analysis of potato skin set and color. *Crop Science* 60(1)**,** 202-210.

Casadesús, J., Kaya, Y., Bort, J., Nachit, M., Araus, J., Amor, S., et al. (2007). Using vegetation indices derived from conventional digital cameras as selection criteria for wheat breeding in water-limited environments. *Annals of applied biology* 150(2)**,** 227-236.

Celebi, M.E., Kingravi, H.A., and Vela, P.A. (2013). A comparative study of efficient initialization methods for the k-means clustering algorithm. *Expert systems with applications* 40(1)**,** 200-210.

Cgrain_AB *Cgrain Value TM, The new standard for analysis grain quality* [Online]. Available: www.cgrain.se.

Chaves, M.M., Maroco, J.P., and Pereira, J.S. (2003). Understanding plant responses to drought—from genes to the whole plant. *Functional plant biology* 30(3)**,** 239-264.

Chawade, A., van Ham, J., Blomquist, H., Bagge, O., Alexandersson, E., and Ortiz, R. (2019). High-throughput field-phenotyping tools for plant breeding and precision agriculture. *Agronomy* 9(5)**,** 258.

Dacal-Nieto, A., Formella, A., Carrión, P., Vazquez-Fernandez, E., and Fernández-Delgado, M. (Year). "Common scab detection on potatoes using an infrared hyperspectral imaging system", in: *Image Analysis and Processing–ICIAP 2011: 16th International Conference, Ravenna, Italy, September 14-16, 2011, Proceedings, Part II 16*: Springer), 303-312.

Del Ponte, E.M., Moreira, G.M., Ward, T.J., O'Donnell, K., Nicolli, C.P., Machado, F.J., et al. (2022). Fusarium graminearum Species Complex: A Bibliographic Analysis and Web-Accessible Database for Global Mapping of Species and Trichothecene Toxin Chemotypes. *Phytopathology®* 112(4)**,** 741-751.

Developers, T. (2021). TensorFlow. *Zenodo*.

Dhondt, S., Wuyts, N., and Inzé, D. (2013). Cell to whole-plant phenotyping: the best is yet to come. *Trends in plant science* 18(8)**,** 428-439.

Easlon, H.M., and Bloom, A.J. (2014). Easy Leaf Area: Automated digital image analysis for rapid and accurate measurement of leaf area. *Applications in plant sciences* 2(7)**,** 1400033.

Fahlgren, N., Gehan, M.A., and Baxter, I. (2015). Lights, camera, action: high-throughput plant phenotyping is ready for a close-up. *Current opinion in plant biology* 24**,** 93-99.

Fasoula, D.A., Ioannides, I.M., and Omirou, M. (2020). Phenotyping and plant breeding: overcoming the barriers. *Frontiers in plant science* 10**,** 1713.

Femenias, A., Llorens-Serentill, E., Ramos, A.J., Sanchis, V., and Marín, S. (2022). Near-infrared hyperspectral imaging evaluation of Fusarium damage and DON in single wheat kernels. *Food Control* 142**,** 109239.

Fu, X., and Jiang, D. (2022). "High-throughput phenotyping: the latest research tool for sustainable crop production under global climate change scenarios," in *Sustainable Crop Productivity and Quality Under Climate Change*. Elsevier), 313-381.

Garcia, S.M., Ryckewaert, M., Abdelghafour, F., Metz, M., Moura, D., Feilhes, C., et al. (2021). Combination of multivariate curve resolution with factorial discriminant analysis for the detection of grapevine diseases using hyperspectral imaging. A case study: flavescence dorée. *Analyst* 146(24)**,** 7730-7739.

Gilbert, J., and Haber, S. (2013). Overview of some recent research developments in Fusarium head blight of wheat. *Canadian Journal of Plant Pathology* 35(2)**,** 149-174.

Gonzalez, R.C. (2009). *Digital image processing.* Pearson education india.

Góral, T., Wiśniewska, H., Ochodzki, P., Nielsen, L.K., Walentyn-Góral, D., and Stępień, Ł. (2018). Relationship between Fusarium head blight, kernel damage, concentration of Fusarium biomass, and Fusarium toxins in grain of winter wheat inoculated with Fusarium culmorum. *Toxins* 11(1)**,** 2.

Großkinsky, D.K., Svensgaard, J., Christensen, S., and Roitsch, T. (2015). Plant phenomics and the need for physiological phenotyping across scales to narrow the genotype-to-phenotype knowledge gap. *Journal of experimental botany* 66(18)**,** 5429-5440.

Gulli, A., and Pal, S. (2017). *Deep learning with Keras.* Packt Publishing Ltd.

Hinton, G., and Sejnowski, T.J. (1999). *Unsupervised learning: foundations of neural computation.* MIT press.

Joalland, S., Screpanti, C., Gaume, A., and Walter, A. (2016). Belowground biomass accumulation assessed by digital image based leaf area detection. *Plant and soil* 398(1-2)**,** 257-266.

Komyshev, E., Genaev, M., and Afonnikov, D. (2017). Evaluation of the SeedCounter, a mobile application for grain phenotyping. *Frontiers in plant science* 7**,** 1990.

Koul, O., Dhaliwal, G.S., and Cuperus, G.W. (2004). *Integrated pest management potential, constraints and challenges.* CABI.

Kumari, V.V., Banerjee, P., Verma, V.C., Sukumaran, S., Chandran, M.A.S., Gopinath, K.A., et al. (2022). Plant nutrition: An effective way to alleviate abiotic stress in agricultural crops. *International Journal of Molecular Sciences* 23(15)**,** 8519.

Lama, S., Vallenback, P., Hall, S.A., Kuzmenkova, M., and Kuktaite, R. (2022). Prolonged heat and drought versus cool climate on the Swedish spring wheat breeding lines: Impact on the gluten protein quality and grain microstructure. *Food and Energy Security* 11(2)**,** 1-17. doi: 10.1002/fes3.376.

Leiva, F., Vallenback, P., Ekblad, T., Johansson, E., and Chawade, A. (2021). Phenocave: An Automated, Standalone, and Affordable Phenotyping System for Controlled Growth Conditions. *Plants (Basel)* 10(9). doi: 10.3390/plants10091817.

Miller, M.D., Schmitz Carley, C.A., Figueroa, R.A., Feldman, M.J., Haagenson, D., and Shannon, L.M. (2022). TubAR: an R Package for Quantifying Tuber Shape and Skin Traits from Images. *American Journal of Potato Research***,** 1-11.

Mortensen, A.K., Gislum, R., Jørgensen, J.R., and Boelt, B. (2021). The use of multispectral imaging and single seed and bulk near-infrared spectroscopy to characterize seed covering structures: methods and applications in seed testing and research. *Agriculture* 11(4)**,** 301.

Munns, R., and Tester, M. (2008). Mechanisms of salinity tolerance. *Annu. Rev. Plant Biol.* 59**,** 651-681.

Murphy, K.P. (2012). *Machine learning: a probabilistic perspective.* MIT press.

Neilson, J.A., Smith, A.M., Mesina, L., Vivian, R., Smienk, S., and De Koyer, D. (2021). Potato tuber shape phenotyping using RGB imaging. *Agronomy* 11(9)**,** 1781.

Oerke, E.-C. (2006). Crop losses to pests. *The Journal of Agricultural Science* 144(1)**,** 31-43.

Oppenheim, D., Shani, G., Erlich, O., and Tsror, L. (2019). Using deep learning for image-based potato tuber disease detection. *Phytopathology* 109(6)**,** 1083-1087.

Phillips, R.L. (2010). Mobilizing science to break yield barriers. *Crop Science* 50**,** S-99-S-108.

Pieruschka, R., and Schurr, U. (2019). Plant phenotyping: past, present, and future. *Plant Phenomics*.

Polak-Śliwińska, M., and Paszczyk, B. (2021). Trichothecenes in food and feed, relevance to human and animal health and methods of detection: A systematic review. *Molecules* 26(2)**,** 454.

Pound, M.P., Atkinson, J.A., Wells, D.M., Pridmore, T.P., and French, A.P. (Year). "Deep learning for multi-task plant phenotyping", in: *Proceedings of the IEEE International Conference on Computer Vision Workshops*), 2055-2063.

Poynton, C. (2012). *Digital video and HD: Algorithms and Interfaces.* Elsevier.

Qi, C., Sandroni, M., Westergaard, J.C., Sundmark, E.H.R., Bagge, M., Alexandersson, E., et al. (2023). In-field classification of the asymptomatic biotrophic phase of potato late blight based on deep learning and proximal hyperspectral imaging. *Computers and Electronics in Agriculture* 205**,** 107585.

R Development Core Team (2010). "R: A language and environment for statistical computing". (Vienna, Austria: R Foundation for Statistical computing).

Rangarajan, A.K., Whetton, R.L., and Mouazen, A.M. (2022). Detection of fusarium head blight in wheat using hyperspectral data and deep learning. *Expert Systems with Applications* 208**,** 118240.

Ryckewaert, M., Héran, D., Simonneau, T., Abdelghafour, F., Boulord, R., Saurin, N., et al. (2022). Physiological variable predictions using VIS–NIR spectroscopy for water stress detection on grapevine: Interest in combining climate data using multiblock method. *Computers and Electronics in Agriculture* 197**,** 106973.

Savary, S., Willocquet, L., Pethybridge, S.J., Esker, P., McRoberts, N., and Nelson, A. (2019). The global burden of pathogens and pests on major food crops. *Nature ecology & evolution* 3(3)**,** 430-439.

Schimansky, T. (2022). *CustomTkinter* [Online]. Github. Available: https://github.com/TomSchimansky/CustomTkinter.

Schneider, C.A., Rasband, W.S., and Eliceiri, K.W. (2012). NIH Image to ImageJ: 25 years of image analysis. *Nat Methods* 9(7)**,** 671-675. doi: 10.1038/nmeth.2089.

Shipman, J.W. (2013). Tkinter 8.5 reference: a GUI for Python. *New Mexico Tech Computer Center* 54.

Si, Y., Sankaran, S., Knowles, N.R., and Pavek, M.J. (2017). Potato tuber length-width ratio assessment using image analysis. *American journal of potato research* 94**,** 88-93.

Si, Y., Sankaran, S., Knowles, N.R., and Pavek, M.J. (2018). Image-based automated potato tuber shape evaluation. *Journal of Food Measurement and Characterization* 12**,** 702-709.

Solgi, S., Ahmadi, S.H., and Seidel, S.J. (2023). Remote sensing of canopy water status of the irrigated winter wheat fields and the paired anomaly analyses on the spectral vegetation indices and grain yields. *Agricultural Water Management* 280**,** 108226.

Szeliski, R. (2010). Computer vision: algorithms and applications Springer Science & Business Media.

Tanabata, T., Shibaya, T., Hori, K., Ebana, K., and Yano, M. (2012). SmartGrain: High-Throughput Phenotyping Software for Measuring Seed Shape through Image Analysis *Plant Physiology* 160(4)**,** 1871-1880. doi: 10.1104/pp.112.205120.

Tsror, L., Erlich, O., and Hazanovsky, M. (1999). Effect of Colletotrichum coccodes on potato yield, tuber quality, and stem colonization during spring and autumn. *Plant disease* 83(6)**,** 561-565.

Ubbens, J.R., and Stavness, I. (2017). Deep plant phenomics: a deep learning platform for complex plant phenotyping tasks. *Frontiers in plant science* 8**,** 1190.

van Dijk, A.D.J., Kootstra, G., Kruijer, W., and de Ridder, D. (2021). Machine learning in plant science and plant breeding. *Iscience* 24(1)**,** 101890.

Wahid, A., and Close, T. (2007). Expression of dehydrins under heat stress and their relationship with water relations of sugarcane leaves. *Biologia Plantarum* 51**,** 104-109.

Walter, A., Liebisch, F., and Hund, A. (2015). Plant phenotyping: from bean weighing to image analysis. *Plant methods* 11(1)**,** 1-11.

Whan, A.P., Smith, A.B., Cavanagh, C.R., Ral, J.-P.F., Shaw, L.M., Howitt, C.A., et al. (2014). GrainScan: a low cost, fast method for grain size and colour measurements. *Plant methods* 10(1)**,** 1-10.

Wiwart, M., Koczowska, I., and Borusiewicz, A. (Year). "Estimation of Fusarium Head Blight of Triticale Using Digital Image Analysis of Grain": Springer Berlin Heidelberg), 563-569.

Yang, W., Duan, L., Chen, G., Xiong, L., and Liu, Q. (2013). Plant phenomics and high-throughput phenotyping: accelerating rice functional genomics using multidisciplinary technologies. *Current opinion in plant biology* 16(2)**,** 180-187.

Yipeng, L., Wenbing, L., Kaixuan, H., Wentao, T., Ling, Z., Shizhuang, W., et al. (2022). Determination of wheat kernels damaged by Fusarium head blight using monochromatic images of effective wavelengths from hyperspectral imaging coupled with an architecture self-search deep network. *Food Control* 135**,** 108819.

Zakieh, M., Gaikpa, D.S., Leiva Sandoval, F., Alamrani, M., Henriksson, T., Odilbekov, F., et al. (2021). Characterizing Winter Wheat Germplasm for Fusarium Head Blight Resistance Under Accelerated Growth Conditions. *Frontiers in Plant Science* 12. doi: 10.3389/fpls.2021.705006.

Popular science summary

Phenotyping, the process of measuring plants' physical and biochemical traits, has become increasingly important in plant breeding and agricultural research. Traditional phenotyping methods involve expensive and time-consuming procedures. However, recent advances in digital imaging technology have made it possible to perform cost-effective phenotyping using RGB (red, green, and blue) imaging.

RGB imaging uses a standard camera to capture images of plants and extract data on traits such as leaf area, shape, and color. The images are then analyzed using computer vision algorithms to obtain quantitative measurements that can be used to identify desirable traits and select plant varieties tolerant of abiotic and biotic stresses. One advantage of RGB imaging is its affordability compared to other phenotyping methods: it requires only a standard camera and basic image analysis software, making it accessible to researchers with limited resources.

The work in this thesis started by developing an affordable imaging system to collect imaging data with imaging sensors such as RGB, thermal, MSI, and HSI cameras to provide a comprehensive understanding of plant health and performance. Paper I presents a blueprint of this system and a pipeline for analyzing the RGB and thermal images. This may help researchers interested in cost-efficiently monitoring plant growth and complex traits such as drought tolerance, disease resistance, and nutrient use efficiency. Paper III shows that affordable phenotyping based on RGB imaging could also help improve crop yield and quality because it was successfully used in conjunction with analysis of gluten parameters to identify wheat genotypes that maintain stable gluten production when exposed to abiotic stresses such as heat and drought. Finally, imaging-based evaluation of morphological parameters was successfully used to predict FHB in kernels and measure

quality parameters in tubers (Papers II and VI). The resulting morphological data was used to build a training model to estimate CS disease symptoms in potato tubers (Paper IV). This model is valuable because it enables evaluation of disease symptoms without subjectivity or the need for deep expertise. The methods here presented could thus revolutionize plant breeding and agricultural research by providing fast, accurate, and cost-effective data on plant traits.

Populärvetenskaplig sammanfattning

Fenotypning, processen att mäta växters fysiska och biokemiska egenskaper, har blivit allt viktigare inom växtförädling och jordbruksforskning. Traditionella fenotypningsmetoder kan innebära dyra och tidskrävande procedurer men de senaste framstegen inom digital bildteknik har gjort det möjligt att genomföra kostnadseffektiv fenotypering med hjälp av RGB (röd, grön och blå) bildtagning.

Inom RGB-bildtagning används en vanlig kamera för att ta bilder av växter och extrahera data för egenskaper som bladyta, form och färg. Bilderna analyseras sedan med hjälp av datorseendealgoritmer för att få kvantitativa mätningar som kan användas för att identifiera önskvärda egenskaper och välja växtvarianter som är toleranta mot abiotiska och biotiska stressfaktorer. En fördel med RGB-bildtagning är dess prisvärdhet jämfört med andra fenotypningsmetoder: den kräver endast en vanlig kamera och grundläggande bildanalysprogram, vilket gör den tillgänglig för forskare med begränsade resurser.

Arbetet i denna avhandling inleddes med att utveckla ett prisvärt bildsystem för att samla in bilddata med bildsensorer som RGB, termisk, MSI och HSI-kameror för att ge en omfattande förståelse av växternas hälsa och prestanda. Artikel I presenterar en översikt av detta system och en pipeline för att analysera RGB- och termiska bilder. Detta kan underlätta för forskare som är intresserade av kostnadseffektiv övervakning av växters tillväxt och komplexa egenskaper som torktolerans, sjukdomsresistens och näringsanvändningseffektivitet. Artikel III visar att prisvärd fenotypning baserad på RGB-bildtagning även kan hjälpa till att förbättra grödans avkastning och kvalitet då den framgångsrikt användes i kombination med analys av glutenparametrar för att identifiera vete-genotyper som bibehåller

stabil glutenproduktion när de utsätts för abiotiska stressfaktorer som värme och torka. Slutligen användes bildbaserad utvärdering av morfologiska parametrar för att förutsäga angrepp av svampsjukdomen Fusarium head blight (FHB) i vetekärnor och för att mäta kvalitetsparametrar i potatisknölar (artikel II och VI). Den morfologiska datan användes för att bygga en träningsmodell för att uppskatta sjukdomssymptom för potatisskabb (CS) i potatisknölar (artikel IV). Modellen är högst användbar då den möjliggör utvärdering av symptomen för potatisskabb utan subjektivitet eller behov av expertis inom området. De metoder som presenteras här kan revolutionera växtförädling och jordbruksforskning genom att tillhandahålla snabb, noggrann och kostnadseffektiv data om växtegenskaper som är kritiska för framtida odlingsmöjligheter.

Acknowledgments

MDPI

Article

Phenocave: An Automated, Standalone, and Affordable Phenotyping System for Controlled Growth Conditions

Fernanda Leiva [1], **Pernilla Vallenback** [2], **Tobias Ekblad** [3], **Eva Johansson** [1] and **Aakash Chawade** [1,*]

[1] Department of Plant Breeding, Swedish University of Agricultural Sciences, SE-23422 Lomma, Sweden; fernanda.leiva@slu.se (F.L.); eva.johansson@slu.se (E.J.)

[2] Lantmännen Lantbruk, SE-26881 Svalöv, Sweden; Pernilla.vallenback@lantmannen.com

[3] MariboHilleshög Research AB, SE-26191 Landskrona, Sweden; tobek79@gmail.com

[*] Correspondence: aakash.chawade@slu.se

Abstract: Controlled plant growth facilities provide the possibility to alter climate conditions affecting plant growth, such as humidity, temperature, and light, allowing a better understanding of plant responses to abiotic and biotic stresses. A bottleneck, however, is measuring various aspects of plant growth regularly and non-destructively. Although several high-throughput phenotyping facilities have been built worldwide, further development is required for smaller custom-made affordable systems for specific needs. Hence, the main objective of this study was to develop an affordable, standalone and automated phenotyping system called "Phenocave" for controlled growth facilities. The system can be equipped with consumer-grade digital cameras and multispectral cameras for imaging from the top view. The cameras are mounted on a gantry with two linear actuators enabling XY motion, thereby enabling imaging of the entire area of Phenocave. A blueprint for constructing such a system is presented and is evaluated with two case studies using wheat and sugar beet as model plants. The wheat plants were treated with different irrigation regimes or high nitrogen application at different developmental stages affecting their biomass accumulation and growth rate. A significant correlation was observed between conventional measurements and digital biomass at different time points. Post-harvest analysis of grain protein content and composition corresponded well with those of previous studies. The results from the sugar beet study revealed that seed treatment(s) before germination influences germination rates. Phenocave enables automated phenotyping of plants under controlled conditions, and the protocols and results from this study will allow others to build similar systems with dimensions suitable for their custom needs.

Keywords: affordable; phenotyping; drought; image analysis; automated

1. Introduction

One of the most important factors in functional plant biology and growth analysis is plant biomass [1,2]. This parameter is the basis to obtain the net primary production and growth rate in every crop at different growth stages [3,4]. Conventional methods for estimating plant biomass, however, require destructive harvests and are labor-intensive and expensive. Thus, conventional methods for variety evaluation are often based on the final yield for replicated plots under different environments [5]. Since conventional methods to measure plant biomass are destructive, it is challenging to assess the process of development of individual plants at different growth stages. In addition, certain measurements are generally obtained from individual plants that are randomly selected from a plot. Therefore, there is a need to develop more efficient, precise, and accurate methods to assess key agronomical traits for crop monitoring [6]. Another type of seed study is "seed priming and coating", a pre-sowing technology to treat seeds with one or various agents before germination [7]. These technologies help plants prepare their defense metabolism against certain stress factors [8,9]. Thus, coating and priming can improve seed performance, resulting in faster and better germination and improving plant growth [10–12].

Conventional methods and X-ray analysis have been used to measure the growth rate in sugar beet. However, a reliable, quick, and automated method to estimate the early growth of seeds treated with different treatments would make it easier to evaluate new treatments more efficiently.

The current emergence of imaging techniques and recent advances in technology have contributed to further advances in plant phenotyping for the field and controlled conditions. These new image-based systems evaluate genotype-environment interaction through tracking plant growth and health performance in a non-destructive, automated, and high-throughput way [13]. Another advantage of such systems is that they allow the evaluation of a large number of individuals over time, raising the possibility of identifying traits that cannot be tracked by conventional measurements [14] and reducing crop production losses [15,16].

Plant phenotyping systems designed to analyze projected leaf area or canopy biomass over plant development time using a single camera in the visible light range (RGB) have proven to be helpful for the estimation of growth rate, health status, drought or salinity stress, and early vigor [17–21]. Other systems use more sophisticated commercial optical sensors like hyperspectral or multispectral imaging [22]. Hundreds of images can be taken within a short period and have proven to provide reliable information related to foliar and moisture nutrient content, plant health, water content composition parameters for seeds, and leaf area index, applying different vegetation indexes [3,15,23]. Other sensors, such as thermal and chlorophyll fluorescence, can also be integrated to detect abiotic and biotic stresses and photosynthetic performance [24–27]. The choice of optical sensors mainly depends on the phenotypic variation of interest and image acquisition conditions [26].

Some examples of high-throughput plant phenotyping platforms are the "WIWAM" platforms in Belgium [28], which are systems based on non-invasive automated imaging and precise irrigation of plants. Another similar system is Plant PhenoLab in Denmark, a fully automated high-throughput phenotyping robot that allows rotating, irrigation, fertilization, weighing, and measuring plants, equipped with thermal and multispectral cameras. In the same light, the National Plant Phenotyping Infrastructure NaPPI in Finland is another example of an automated platform. Such infrastructure enables studying a large number of plants for various agronomic traits. In the category of systems using XY motion is Phenovator, a system for measuring the photosynthesis, growth, and multispectral reflectance of small plants such as Arabidopsis [29]. A more advanced system is presented by PSI (Photon Systems Instruments, Brno, Czechia), named PlantScreenTM XYZ, which works with small and mid-size plants. Such platforms acquire RGB, kinetic chlorophyll fluorescence, hyperspectral, and thermal data through XYZ motion of a robotic arm.

Platforms that acquire images in closed stations require complex conveyor systems, translated into great investments in facilities, hardware, and software. On the other hand, platforms that acquire images in place usually have relatively low efficiency in data acquisition. Another limitation is the requirement of specialized knowledge to control and monitor the systems. Several custom-made affordable systems have recently emerged, broadly categorized based on the type of plant species to study. For instance, "Phenotiki" [30] is an affordable system that analyzes the growth, color, and leaf area of Arabidopsis plants based on a Raspberry Pi single-board computer. Another example is Phenoscope [31], a platform that provides watering and zenithal imaging to monitor plant size and expansion rate during the vegetative stage. An image processing pipeline was also developed to analyze rosette area modeling [32]. These approaches have been developed for rosette-shaped plants, especially Arabidopsis. Other solutions of affordable systems applied on different plant sizes are MVS-Pheno [33] and LCP lab [18], which are portable, low-cost platforms for individual plants. Both platforms work with regular RGB cameras, obtaining a multiview image using a rotatory console. The analysis of data differs with the software; MVS-Pheno developed its software while LCP lab works with freely available software.

Image acquisition and processing are pivotal for the right estimation of plant traits. Plants thus need to be segmented successfully from other objects, such as the back-

ground [4,34,35]. However, many of the pipelines available are developed for a narrow range of plant species and, in some cases, require manual work. Solutions are thus needed to enable the phenotypic evaluation of different species under highly controlled conditions, systems that are cost-effective, automated, and that can improve the intensity and accuracy of germplasm selection [3].

In this work, we propose an automated plant phenotyping system called Phenocave built for highly controlled plant growth conditions and regular greenhouses. Instructions to build a similar system and image analysis protocols are provided. The results obtained from the evaluation of Phenocave on wheat (*Triticum aestivum* L.) and sugar beet *(Beta vulgaris* L.) are presented.

2. Materials and Methods

2.1. Phenocave

Phenocave has a workspace of 2 × 2 m and 0.5 mm of precision in positioning the camera over the object of interest. It is based on a programmable logic controller (PLC) in conjunction with a programmable motor controller. The system consists of a gantry robot from Igus company (Cologne, Germany) mounted on an aluminum frame structure constructed by Eltech automation (Lomma, Sweden) (Figure 1A). The structural support incorporates two pairs of rigid aluminum legs with reinforcing, attachment points for the gantry, the cabling network with carrier system (Igus, e-chain Black Cable Chain), and an electronic box mounted at the right side of the frame, which contains all the electronic components and the user control system. The gantry robot comprises two linear axis actuators with belt transmission connected to two stepper motors (NEMA23) for XY linear motion.
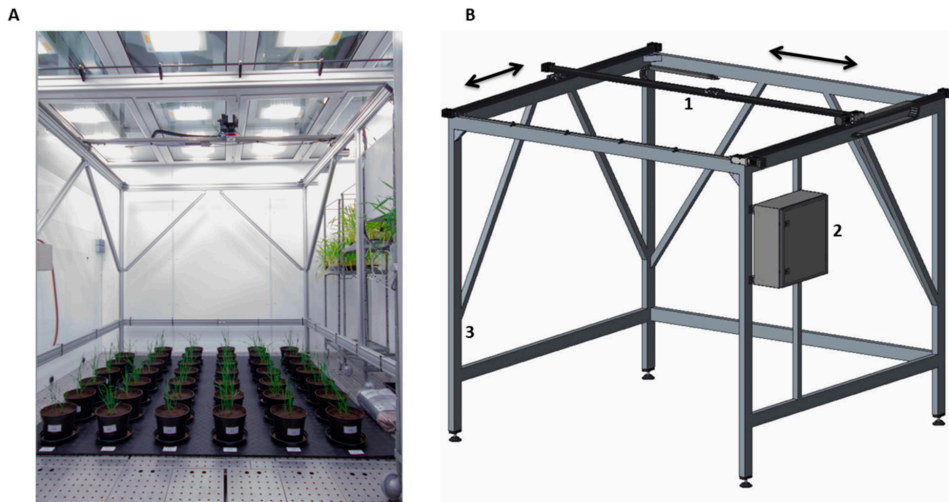
Figure 1. (**A**) Phenocave installed in the Biotron chamber with two imaging sensors mounted, a DSLR Canon EOS and a multispectral MicaSense Altum; (**B**) schematic Phenocave model. The gray arrows indicate the movement on the XY coordinates.

Engine configuration (camera position, image acquisition speeds, and operating times) is performed with a controller (Drylin Dryve D1). These settings can be configured in the Igus web-based control system for Drylin from any internet browser. All connections and the two motor drivers are connected to a PLC (CPU Siemens S7-1200) that implements a control system over the number of steps (image to acquire) that would be carried out using the XY coordinates and a timer to execute a desirable loop. These parameters can be

set up on the display panel (Siemens KTP400 Basic PN) included in the electronic box [36]. To determine the efficiency, reliability, and quality of the obtained results, two case studies were conducted, which included wheat and sugar beet as model plants. The Phenocave parameters were set up based on the position of pots with XY coordinates in mm, the motor speed for image acquisition, and the operating times were fixed for the whole experiment.

2.2. Image Acquisition with Phenocave

Individual plant pot images were acquired from top-view using three different imaging sensors attached to the central aluminum plate (Drylin W bearing and mounting plate) from 1.8 m above ground. One RGB digital single-lens reflex (DSLR) camera, a Canon EOS 1300D (Canon U.S.A. Inc., Huntington, NY, USA) with a resolution of 18 megapixels, was mounted with a Canon EF-S 50 mm f/1.8 STM lens. The optimal exposure settings for imaging based on the growth conditions were F-Stop 1/160, exposure time 1/10, AF AI-Servo, and ISO 400. All pictures were saved in 5184 × 3456 pixel JPG format. The second sensor was the MicaSense Altum multispectral camera (MicaSense Inc., Seattle, WA, USA) with an image resolution of 2064 × 1544 pixels and storage in TIF format. The MicaSense Altum has one thermal and five multispectral bands (blue, green, red, red edge, and NIR). As the distance from the top of the plant to the camera lens was less than two meters, it was not possible to align the five multispectral bands perfectly (personal communication with MicaSense support). Thus only the thermal images from the MicaSense Altum were used for analysis. The third sensor was the Canon DSLR Rebel T6 NDVI conversion. Aiming to avoid light reflection and obtain a good background separation from the object of interest (plant leaves) during image processing, a dark floor (interlocking rubber sheets floor) was placed over the original floor of the chamber. Pots were labeled with two identifier numbers according to the position (i.e., row and column). Images were taken every second day to follow the growth conditions (Figure 1B).

2.3. Image Acquisition with LCP Lab (Comparative Method)

The results for the wheat case study from Phenocave were compared with a previously published LCP lab system [18]. Pots were individually photographed at every time point from one top-view angle and four side views using two DSLR cameras, Canon EOS 1300D and the 18–55 mm kit lens. Both cameras were tethered to the software digiCamControl [37] with slightly different settings (side view: focal length of 35 mm, F-Stop f/9, and top view: focal length of 30 mm, F-Stop f/10, and both with ISO 400 and exposure time of 1/160 s). The side-view camera was mounted on a tripod 1.5 m away from the target (i.e., plant pots), whereas the top-view camera was maintained at the height of 1 m above the plants. Pots were placed manually on a top-quality Intelligent 360 Photography turntable platform (Shenzhen Comxim Technology Co., Ltd., Shenzhen, Guangdong, China).

2.4. Image Processing
2.4.1. Color Images

Green leaf area projection of the plant color images obtained from the Phenocave and the rotatory system was extracted using an image-processing algorithm developed and written in Java as a plugin for ImageJ software (National Institutes of Health, Bethesda, MD, USA). First, a region of interest ROI (plant pot) was selected for each image, and everything outside of it was converted to zero value pixels (black). This was done to minimize the overlapping and non-plant objects in the images. Subsequently, the image was split into red, green, and blue bands to apply a color difference mask obtained by subtracting one color channel from another [18]. For this case, two masks were created, one by subtracting the red channel from the green channel (green minus red), which contrasted most of the plant from other objects. The other mask was obtained by subtracting the green channel from the blue channel (blue minus green) for isolating the leaves missing in the first mask. In both masks and for all time points, a fixed threshold was applied considering that the illumination was always the same and even with values above the pixels belonging to the plant (threshold

values (30, 255) and (3, 255)) and discarding the rest of the pixels. This threshold was selected using the option threshold by default of ImageJ and manually adjusted until it reached the desired result. Subsequently, a median filter from the ImageJ toolbox "Remove Outliers" was applied, a filter that replaces a pixel if the median of the surrounding pixels deviates from the median by more than one threshold value (radius = 10 threshold = 50 which = Bright). Finally, both created masks were joined by OR logical operator to be used as a mask to the original image. The resulting image consisted of data of green and yellow leaf pixels and, in some cases, soil. Therefore, a K-means classifier was applied. However, the results were not satisfactory, especially for wheat plants in the maturity stage. Thus, to segment these areas further, a Bayesian classifier was implemented. This machine-learning approach works with a training set of samples previously labeled (green leaves and yellow leaves) which will be the different classes to classify. From them, it creates probability density functions per class, and this way determines the belonging of each new pixel to the class previously defined.

The resulting image is grayscale with pixel values '0' (black) for the background regions, '1' (gray) for the green leaves, and '2' (white) for the yellow leaves. The number of pixels of the green leaves was extracted from the histogram. A work flow is presented in Figure 2. For the images of the rotatory method, the scale was selected for every image (one top view and four side views) by using the reference calibration (ruler 300 mm) and calculating pixels/mm, to give a total green area of the plant. The results of the five images were summed.
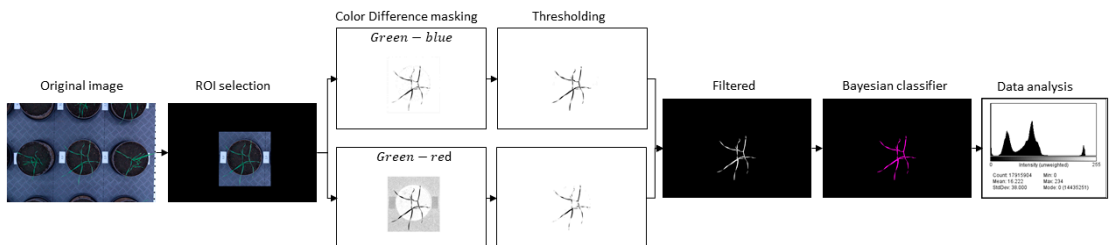
Figure 2. Work flow of image analysis pipeline performed for the extraction of the projected plant biomass from top-view digital images.

2.4.2. Thermal Images

Thermal images were processed using the free and open-source software QGIS (QGIS Geographic Information System) [38]. First, a set of images was selected after five days of inducing drought, one at stem elongation and one at the heading stage, and another one after two days of normal irrigation for all the plants. The processing steps included the changing of the band rendering, from single-band gray to single-band pseudo color with discrete values from 29,200 (18.85 °C) representing cold (blue) to 29,350 (20.35 °C) hot (red). Afterward, the plant regions to analyze were selected using the option of a circle shape in the polygon tool of the QGIS toolbox, then applying zonal statistics to each shape feature to obtain the mean thermal value for each plant (Figure 3).
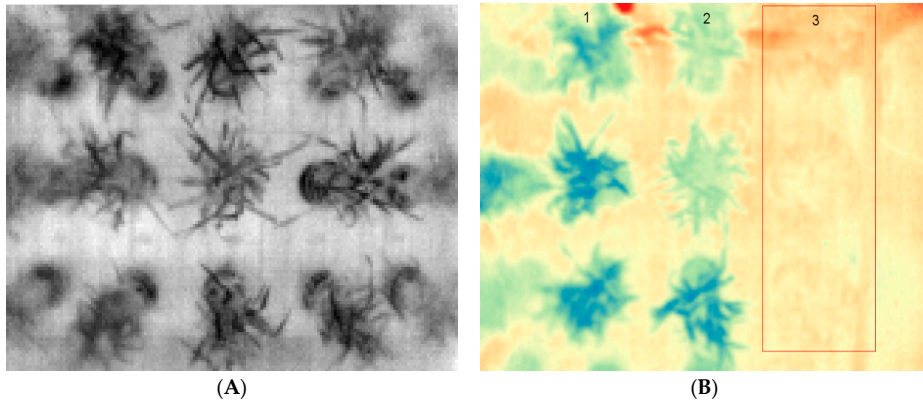
Figure 3. Visualization of a thermal image using the software QGIS (QGIS Geographic Information System): (**A**) left side original image: (**B**) image with pseudocolor, plants in the first and second column (1, 2) show lower near infrared values (color blue), while plants in the third column (3) (red and yellow color) marked with the red frame show higher values (plants under drought conditions).

2.5. Case Studies

Phenocave was evaluated using three different case studies on wheat and sugar beet.

2.5.1. Case Study: Wheat

The experiment was conducted in the Biotron chamber at temperature 23 °C/19 °C (day/night), humidity 50%, and 400 μmol m^{-2} s^{-1} of uniform light intensity with LED lights. A total of 123 seeds of a single spring wheat genotype (provided by Lantmännen Lantbruk) were sown in 41 pots of 3 L (three seeds per pot) with 1.7 kg of soil (Exclusive Flower and Plant Soil with Osmocote). Three treatments were set up with four replicates in two different groups. Group 1 consisted of the control set (28 pots, set 1), while group 2 consisted of three subsets with three types of treatments, namely drought stress at stem elongation (4 pots, set 2), drought stress at the heading stage (4 pots, set 3), and high nitrogen at the heading stage (4 pots, set 4). Plants were placed randomly in the 4 sq m area of the Phenocave workspace. All pots were supplied with 24.99 mg N dosage of ammonium nitrate diluted in 100 mL of water (liquid fertilizer NH_4NO_3) before drought treatments were induced.

Digital biomass measurements were obtained across the different growth stages, seedling, tillering, stem elongation, booting, heading, and grain filling [39], in the control set (see image processing section). At the end of each growth stage, four pots were randomly selected (total 24 pots), first to acquire images with the comparative rotatory system (see image acquisition section), then for the conventional process of determining biomass. In this process, shoots were cut and immediately weighed using a precision balance (Sauter RE 3012). Thereafter, shoots were wrapped in aluminum foil and oven-dried at 100 °C, for a period of 24 h. Finally, the dry matter was weighed using the same balance.

Drought stress conditions in sets 2 and 3 were induced by stopping the irrigation in eight pots at two different time points, four pots at the stem elongation stage (D_SE), 38 days after sowing (set 2), and the other four at the beginning of the heading stage, 45 days after sowing (set 3). Finally, plants were re-watered in both cases after six days of drought, days 44 and 51 after sowing, respectively. At the heading stage, another four pots (set 4) were supplied with 24.99 mg N dosage of ammonium nitrate diluted in 100 mL of water (liquid fertilizer NH_4NO_3). The remaining five pots from the control set were allowed to grow until the maturity stage for grain yield determinations. Pots (not under drought treatment) were irrigated every second day with 500 mL of water until the tillering stage, and thereafter the irrigation was increased to 1000 mL. Imaging was continued every

second day until the end of the maturity stage (grain filling). Finally, the conventional measurement of biomass was performed for all remaining plants.

- Phenotyping with Handheld Sensors for Wheat

Handheld sensor phenotyping was done from the stem elongation stage (28 plants) until the maturity stage (12 plants), by sampling three times per week and taking three measurements per plant. NDVI measurements were taken with a PlantPen NDVI-300 (Photon Systems Instruments PSI, Drásov, Czech Republic) using three leaves randomly selected from each plant. Then, chlorophyll concentration measurements were taken on the same leaves with an MC-100 chlorophyll concentration meter (Apogee Instruments, Inc., North Logan, UT, USA). Thereafter, QY (PSII Maximum Quantum Efficiency, (Fv/Fm) measurements were taken with a FluorPen FP 100-MAX (Photon Systems Instruments PSI, Drásov, Czech Republic) with detachable blade clips. On each one of the three leaves of the plant, a clip was placed, creating a dark adaptation for 15 min before measurement.

Plant height and leaf area were other parameters measured, but only in the final maturity stage of treatment of plant sets (12 plants). Plant height was measured manually with a ruler from the surface of the soil to the tip of the plant spike. The leaf area was measured in the flag leaf using an LI-3000C Portable Leaf Area Meter (LI-COR Biosciences, Inc., Lincoln, NE, USA). In both cases, three measurements were performed for each pot, and the average of them was considered the final value.

- Analysis of Grain Protein Concentration and Composition

Similarly, as in previous studies [40], the grain protein concentration was evaluated through nitrogen combustion using a nitrogen/carbon analyzer (Flash 2000NC Analyzer, Thermo Scientific, Waltham, MA, USA). The total protein content was calculated by multiplying the total nitrogen content by a conversion factor of 5.7 [41].

Quality of the wheat grain was evaluated following previously described methods [42], determining %UPP (percentage of SDS-unextractable polymeric protein in total polymeric protein) correlating with gluten strength, and TOTE (total SDS-extractable protein) correlating with grain protein concentration [43,44]. Thus, the amount and size distribution of polymeric and monomeric proteins were determined by size-exclusion high-performance liquid chromatography (SE-HPLC) in a two-step extraction procedure [45] with modifications by Johansson et al. [46], extracting SDS-extractable proteins in the first step, and SDS-unextractable proteins by sonication in the second step. SE-HPLC analyses were carried out with the Waters HPLC system (Milford, NH, USA) with a Phenomenex BIOSEP SEC-4000 column (Torrance, CA, USA). The area under the chromatogram was used to calculate %UPP and TOTE following previous methodology [47–50]. Samples were extracted and run in triplicates.

2.5.2. Case Study: Sugar Beet

The trial was conducted using seeds of a single sugar beet genotype (material provided by MariboHilleshög) exposed to different treatments. As a control, one of the sets consisted of completely untreated seeds (A), while a second set were naked seeds that had undergone a priming procedure (B) to accelerate germination. The proprietary priming process was developed at MariboHilleshög with the specific purpose of enhancing germination speed and early seedling growth. The third set of seeds was pelleted and coated (C), which is common practice for commercially sold sugar beet seeds in most markets. The pellets improve seed drilling performance while the coating contains fungicides and insecticides. The last set of seeds were primed, pelleted, and coated (D) with the purpose to have all the treatments and benefits in one.

The experiment was organized in a randomized complete block design with four treatments and three replicates. Thirty-six seeds of each treatment (144 seeds) were sown in plastic pots (5 × 5 and 10 cm high) filled with standard garden soil. The 144 plants were evenly distributed per treatment in 12 trays (3 trays per treatment). Then, trays were placed in the Phenocave workspace (4 sq m) in four columns and three rows. Thereafter,

plants were allowed to grow in Biotron at 22 °C/18 °C (day/night) temperature, humidity 50%, 350 μmol m^{-2} s^{-1} of uniform light intensity with LED light conditions.

2.6. Statistical Analysis

Statistical analyses were conducted using R [51], analyses of Pearson's correlations were performed with the conventional biomass measurements and the results obtained from Phenocave. Analysis of variance (ANOVA) was performed with post hoc Tukey's honest significant difference (HSD) test (*p*-value < 0.05), to evaluate the different effects of treatments and traits measured. For HPLC analysis, Duncan's multiple range test (DMRT) was performed to estimate specific differences between treatment means.

3. Results

3.1. Phenocave

The Phenocave automated phenotyping platform comprises an aluminum gantry that can be mounted with various optical sensors as required. In addition, depending on the number of targets, the platform acquires top-view images sequentially with a speed of 0.5–1.5 m/s. Furthermore, it is possible to set up different positions on the XY coordinate with a precision of 0.5 mm in a single cycle per line. A total of 25 pots of 3 L equally distributed in the 2 × 2 m workspace, can take 10 min for imaging and can be repeated in a loop. It is also possible that the camera moves continuously on the *x*-axis, which can be achieved by selecting the home position and a target (used for hyperspectral imaging). The images are stored in the camera for further analysis.

To evaluate Phenocave, two case studies were undertaken using spring wheat and sugar beet.

3.1.1. Case Study: Spring Wheat
Group 1

- Image Analysis Results

The image acquisition started when plants reached the seedling stage (seven days post-sowing) and continued three times per week until the end of the grain-filling stage (58 days post-sowing), i.e., during six growth stages, for a total of 360 images. Image segmentation was performed to separate the background and foreground (plant) pixels and segment yellow and green plant material. The RGB images of the plants representing the six time points are presented in Figure 4 and the biomass measurements from digital and conventional methods are presented in Figure 5. There was a progressive development of plants in the six growth stages. The grain filling growth stage had the highest fresh and dry weight values. Whereas for the digital biomass measurements, the highest canopy green cover was at the heading growth stage and it decreased in the grain filling stage.

The digital biomass obtained during the six growth stages was correlated with the conventional biomass measurements results (weight of fresh and dry matter), giving a significant correlation (r = 0.96, *p* < 0.01, r^2 = 0.92 for dry weight; and r = 0.97, *p* < 0.01, r^2 = 0.94, for fresh weight). The results of the rotatory system were correlated with the conventional biomass measurements (weight of fresh and dry matter), giving as result a high correlation (r = 0.78, *p* < 0.01, r^2 = 0.61 for dry weight; and r = 0.88, *p* < 0.01, r^2 = 0.79, for fresh weight, Table 1).

Table 1. Pearson correlation coefficient between digital biomass, fresh weight, and dry weight at different growth stages.

Wheat Growth Stage According to Zadok Scale	Phenocave		Rotatory System	
	Digital Biomass (Pixels) vs. Fresh Leaves (g)	Digital Biomass (Pixels) vs. Dry Leaves (g)	Digital Biomass (Pixels) Fresh vs. Leaves (g)	Digital Biomass (Pixels) vs. Dry Leaves (g)
Seedling	0.82	0.82	0.95	0.93
Tillering	0.99	0.99	0.92	0.91
Stem Elongation	0.52	0.84	0.67	0.62
Booting	0.90	0.87	0.96	0.97
Heading	0.89	0.85	0.85	0.57
Grain Filling	0.89	0.62	0.95	0.67

Figure 4. Representative red–green–blue (RGB) images from Phenocave before processing. Spring wheat plants at various growth stages: (**A**) seedling, (**B**) tillering, (**C**) stem elongation, (**D**) booting, (**E**) heading, and (**F**) grain filling.
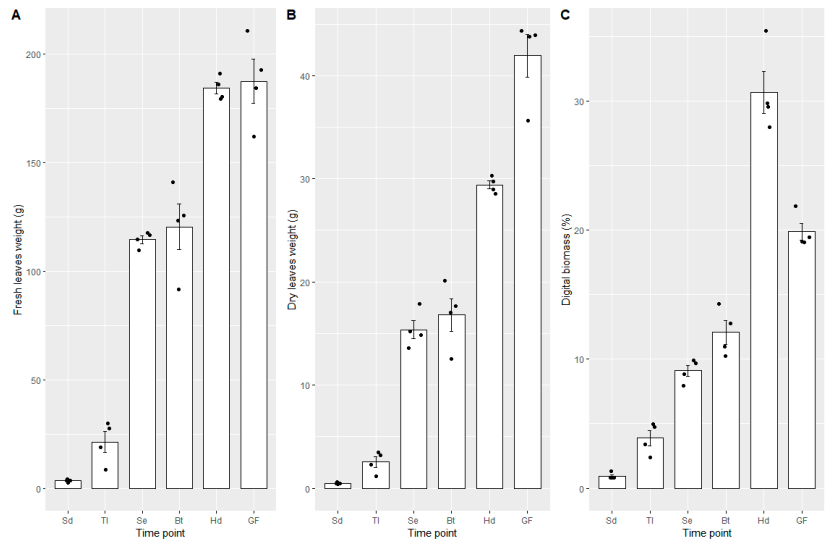
Figure 5. Fresh leaves (**A**), dry leaves (**B**), and digital biomass (**C**) obtained from different growth stages, namely, seedling (Sd), tillering (TI), stem elongation (Se), booting (Bt), heading (Hd), and grain filling (GF). Error bars are standard error.

Furthermore, to estimate time efficiency over conventional biomass measurements and a semi-automatic lab LCP method [18], working time was recorded for wheat plants at the heading stage. The time for conventional biomass measurements took 13 h, distributed in shoot cutting, weighing, oven drying, and weighing. Time with the LCP lab for placing each pot on the platform took around 40 s, setting up the software to acquire images manually and save images took 60 s, finally acquiring a single image took 10 s, thus totaling 2 min per pot. Using the Phenocave system took 15 s to set the number of images and about 15 s to take one image, a total of 0.5 min per image/pot.

Group 2

- Image Analysis Results

There was a strong impact of the induced treatments on plant growth rates. As shown in Figure 6, plants under control conditions grew well, showing a high level of green canopy biomass compared to the plants under stress. Significant improvements were observed in plant performance after the second application of nitrogen fertilizer at the heading stage (marked with a dark cyan arrow). Plants under drought treatment showed lower growth once drought treatment was induced (marked with rose and dark cyan arrows). Even though irrigation was withheld for the same amount of time in the two drought treatment sets, drought impacted differently during the two growth stages. There was a greater reduction in the plant biomass during the drought at the heading stage compared to the stem elongation stage. Significant differences in canopy cover were observed in the drought-stressed and control plants also based on thermal imaging (Figure 7). The differences were reduced once the plants were allowed to recover from stress. Likewise, significant differences ($p < 0.05$) were found in the digital biomass among plants under different treatments four days after the treatments were induced (Table 2).
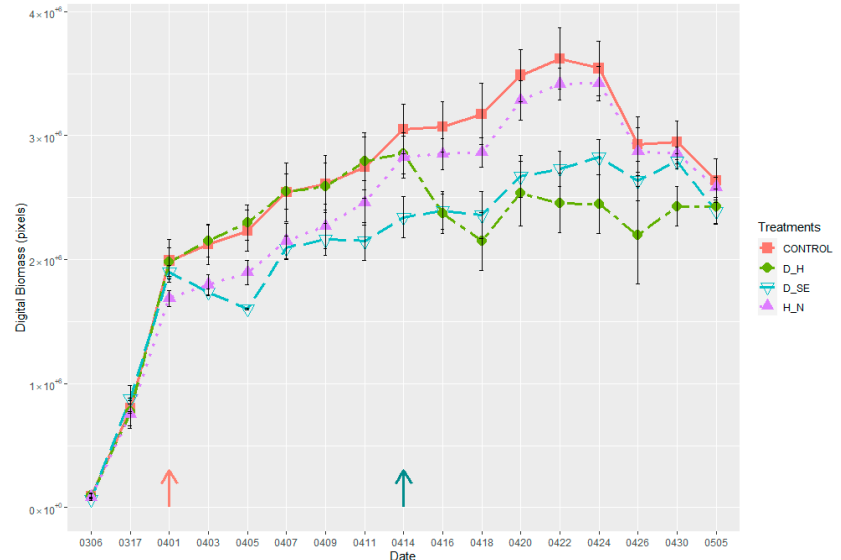
Figure 6. Plant growth pattern under different treatments, (control, drought at stem elongation (D_SE), drought at heading (D_H), and high nitrogen content (H_N)), from sowing to grain development. Pink arrow indicates when drought stress was induced, D_SE; dark cyan arrow indicates when drought stress was induced, D_H, and second nitrogen dosage was applied, H_N. The *Y*-axis represents the time points when the digital biomass was sampled and the *X*-axis represents the mean values of the obtained digital biomass. Error bars are standard error.
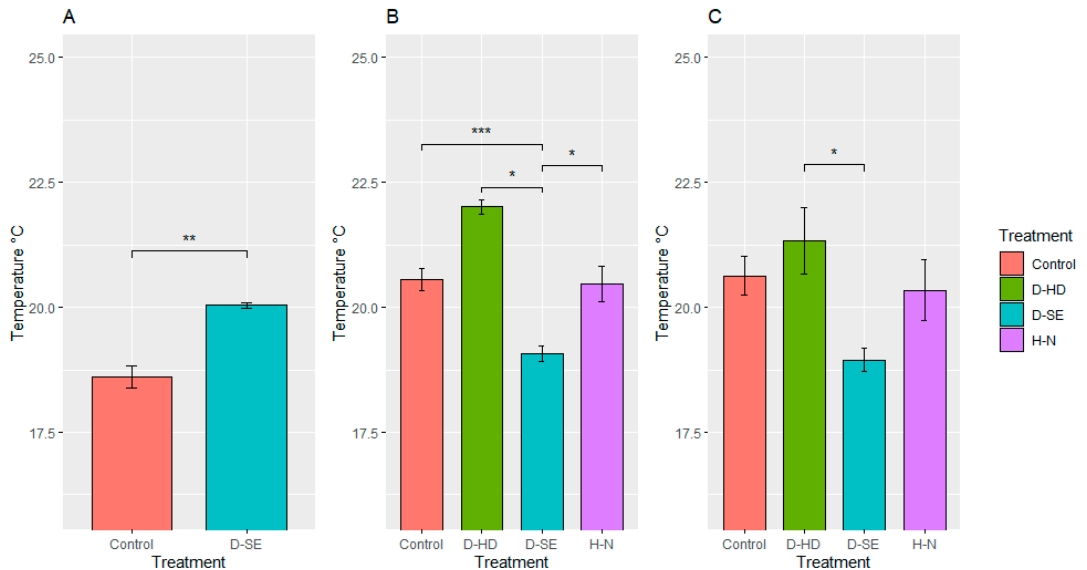
Figure 7. Surface temperature of plants under different treatments, (control, drought at stem elongation (D-SE), drought at heading (D-HD), and high nitrogen content (H-N)). The *X*-axis represents the treatments and the *Y*-axis represents the mean temperature values obtained with QGIS software. Statistically significant differences (Tukey's HSD *** $p < 0.001$, ** $p < 0.01$ and * $p < 0.05$) are denoted by the stars above the bars. Error bars are standard error. Temperature measurements (**A**) after five days of inducing drought stress at stem elongation, D_SE and (**B**) after five days of inducing drought stress at heading, D_HD, and second dosage of liquid nitrogen fertilizer was applied, H-N. (**C**) Temperature measurements when all plants were irrigated.

Table 2. Differences among the four treated plant groups after treatment effect: drought at stem elongation (D_SE), drought at heading (D_H), and high nitrogen (H_N). Significant differences marked with asterisk (* $p < 0.05$, ** $p < 0.01$).

Treatment		Pr(>|t|) Significant Value of Projected Green Area after Treatment	
		Treatment D_SE	Treatments D_H and H_N
Control	D_H	0.71	0.001 **
Control	D_SE	0.003 **	0.008 **
D_H	D_SE	0.002 **	0.37
Control	H_N	0.07	0.483
D_H	H_N	0.04 *	0.006 **
D_SE	H_N	0.14	0.04 *

- Handheld Sensor Measurements

The parameters measured with the handheld sensors—NDVI, chlorophyll content (CC), and quantum yield (QY) showed statistically significant differences among the different treatments along the measured time points. Plants showed normal values (NDVI = 0.75, CC = 30, QY = 0.84) during the first two growth stages (seedling and tillering), then values increased (NDVI = 0.78, CC = 35, QY = 0.84) in the next two growth stages (stem elongation and booting); in the last two time points (heading and grain filling), values decreased again to the initial values. In the case of plants exposed to drought at stem elongation, values were lower (NDVI = 0.73, CC = 27, QY = 0.69). Plants set under drought at heading also showed lower values (NDVI = 0.68, CC = 20, QY = 0.75), while for the plants with high nitrogen content values increased (NDVI = 0.72, CC =34, QY = 0.82) (Figure 8).
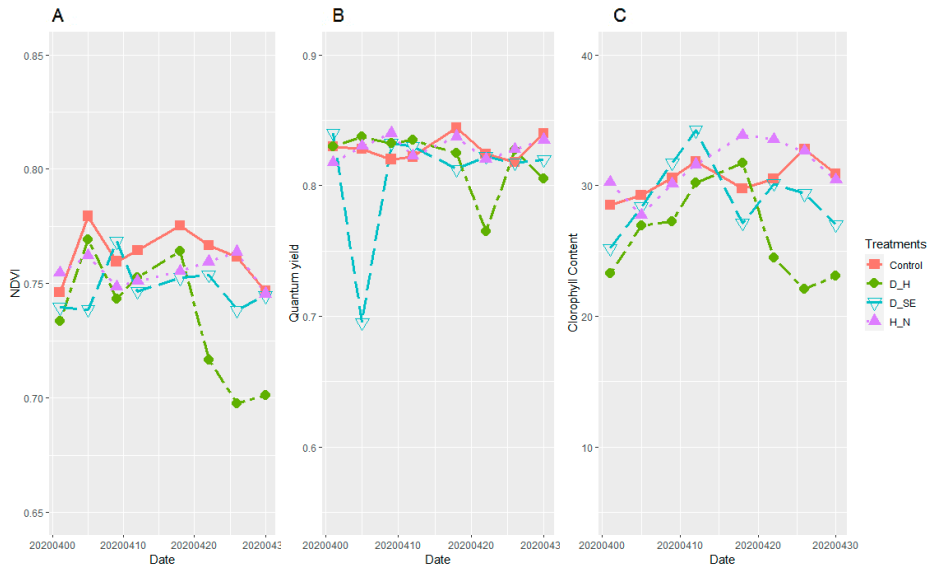
Figure 8. Plants development curves obtained with handheld sensors versus sampling dates (from stem elongation to grain filling stage), clustered based on their treatment forming four groups (control, drought at stem elongation (D_SE), drought at heading (D_H), and high nitrogen content (H_N). (**A**) Normalized difference vegetation index (NDVI); (**B**) quantum yield (QY); (**C**) chlorophyll content index (CC).

- Protein Content and Quality

As described in the methods, grain protein concentration was measured using combustion, while grain protein quality was obtained from TOTE and %UPP values measured with SE-HPLC. The grain protein concentration in the wheat was generally low (Table 3), ranging from 7.7% to 13%. The highest grain protein concentration was found in samples that were drought treated at heading, with a mean protein concentration of 11.7%. The control samples and those subjected to drought under stem elongation showed the lowest grain protein concentrations of 8.4% and 8.0%, respectively, and did not differ significantly. The high nitrogen treatment resulted in samples differing from those of the other treatments and with a mean grain protein concentration of 9.4% (Table 3). The grain protein concentration measured through combustion correlated significantly ($p < 0.01$) with TOTE values obtained from the SE-HPLC. Thus, similarly as for grain protein concentration, the highest TOTE values were found for samples subjected to drought at heading, followed by samples subjected to high nitrogen treatment, and significantly lower values were seen for the control samples and the samples subjected to drought at stem elongation (Table 3). Significantly, the highest %UPP values, indicating the highest gluten strength among samples, were obtained for those samples subjected to drought stress at heading, while for the other treatments, no significant differences were revealed for %UPP (Table 3).

The clearest correlation ($p < 0.005$ for mean values) between grain protein concentration and any of the above described Phenocave parameters was (positive) for the surface temperature at watering after drought treatment (Figure 7C). Drought at heading, which was the treatment mainly affecting the grain quality (Table 3, %UPP), was also the treatment that most clearly showed an effect on several of the Phenocave parameters, including plant growth (Figure 6), surface temperature after drought treatment at regular watering (Figure 7C), NDVI (Figure 8A), and chlorophyll content index (Figure 8C).

Table 3. Mean values of grain protein concentration, as well as of total SDS-extractable proteins (TOTE) and percentage of SDS-unextractable polymeric protein in total polymeric protein (%UPP) obtained from size exclusion-high performance liquid chromatography for wheat subjected to different treatments; control, drought at heading (DH), drought at stem elongation (DSE), and with high nitrogen application (HN). Numbers within the same column followed by the same letter do not differ significantly at $p < 0.05$ by Duncan post hoc test.

Treatment	Grain Protein Concentration (%)	TOTE (10^7)	%UPP
CONTROL	8.4 c	6.72 c	64.5 b
DH	11.7 a	9.05 a	70.7 a
DSE	8.0 c	6.46 c	61.7 b
HN	9.4 b	7.75 b	60.3 b

3.1.2. Case Study: Sugar Beet

The projected leaf area trait in the 12 trays was quantified three times a week during the early growth stage (seedling) for 18 days (Figure 9). During this time, a different germination speed was observed among the sugar beet treatment sets (Figure 10). Two of the treatments, B (primed) and D (pelleted, primed, and coated), had the fastest germination, which could be observed in the majority of samples after four days of sowing. However, the seeds that were not exposed to priming treatment, namely treatment A (control) and C (pelleted and coated), showed a delay in germination, where only half of the samples showed germination after four days. Nonetheless, the germination was 100% in all the treatment sets ten days post-sowing.
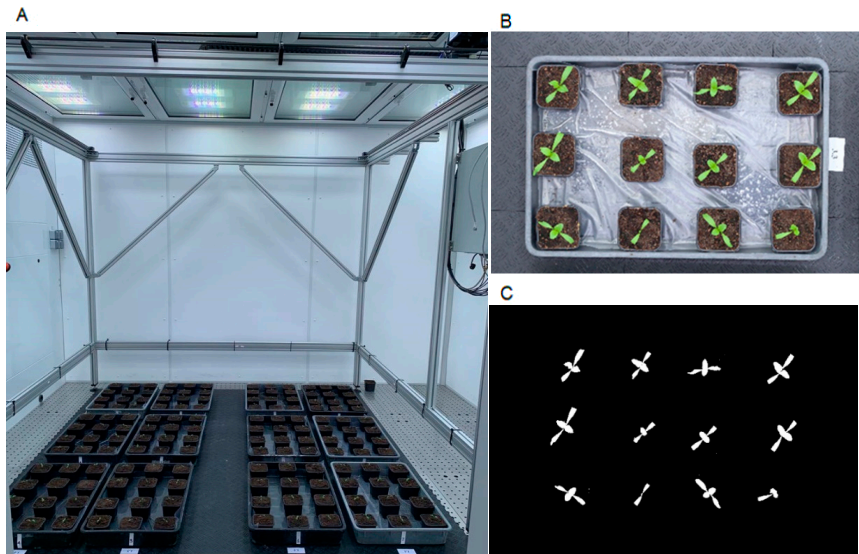
Figure 9. (**A**) Sugar beet experiment installed in Phenocave; (**B**) individual image of sugar beet plants per tray; (**C**) image after processing with the developed pipeline.

Statistically significant differences in plant development by canopy measurement were obtained in four time points of measurement, 5, 8, 12, and 15 days after sowing for all sets of treatment, $p < 0.01$ ** and $p < 0.05$ * in the first and second time points, respectively (Table 4). The differences decreased in the next two time points, $p < 0.05$ *, between treatments B and

C. There were no significant differences in the next time points, 18, 21, and 24 days after sowing, when plants grew under optimal conditions.
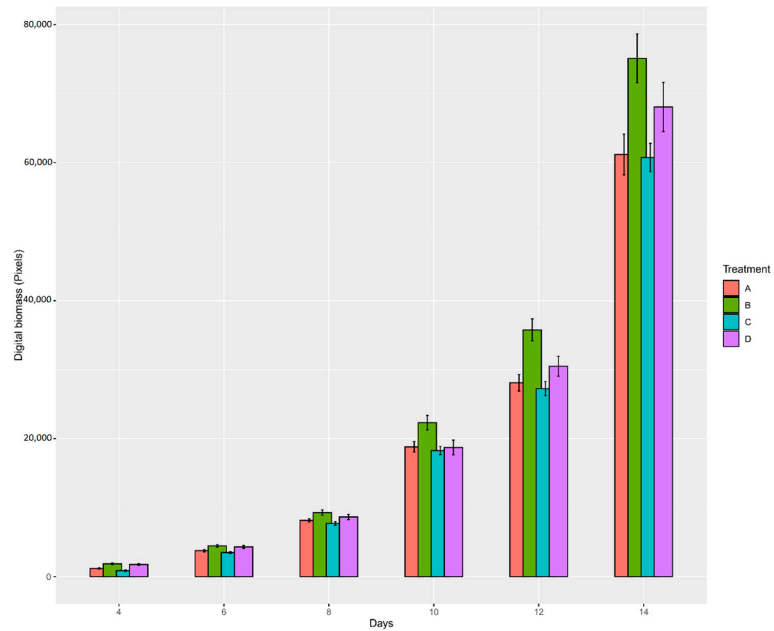
Figure 10. Plant germination and development of plants from seeds with different treatments: (**A**) control; (**B**) primed; (**C**) pelleted and coated; and (**D**) primed, pelleted, and coated; from sowing to 15 days after sowing. The *Y*-axis represents the digital biomass in pixels and the *X*-axis represents sampling days.

Table 4. *p*-Value analysis of the plant germination rate of plants' seeds with different treatments: (**A**) control (intercept); (**B**) primed; (**C**) pelleted and coated; and (**D**) primed, pelleted, and coated; during the different days sampled. Significant differences marked with asterisk (* $p < 0.05$, ** $p < 0.01$ and *** $p < 0.001$).

Treatment	Pr(>|t|) Significant Value of Germination after Sampling					
	1 Day	3 Days	5 Days	7 Days	9 Days	10 Days
(Intercept)	1.01×10^{-5} ***	1.94×10^{-8} ***	2.97×10^{-8} ***	1.26×10^{-7} ***	1.17×10^{-7} ***	1.39×10^{-6} ***
B	0.003 **	0.02 *	0.04 *	0.0567	0.01 *	0.11
C	0.12	0.21	0.61	0.724	0.50	0.87
D	0.009 **	0.06.	0.13	0.4474	0.24	0.35

4. Discussion

Phenocave is a platform highly automated for plant phenotyping, and once the program is set up, it requires minimal human intervention. Image acquisition for different types of plants is one of the issues presented in some low-cost phenotyping platforms [30,31,34,52], while Phenocave can be used with any type of plant size. In addition, the acquisition efficiency of the platform is another advantage over other similar platforms. Approximately 10 min are required to acquire a set of 25 big plant images using Phenocave and they can be analyzed in less than 15 min, whereas the semi-automated LCP lab [18] requires 30 min and labor to implement one of the suggested free software packages. The Phenocave system is user-friendly, which facilitates its application for researchers with different scientific expertise. Furthermore, Phenocave can be set up in a controlled growth

environment. Nonetheless, a resulting limitation of Phenocave is that the workspace is only 2×2 m, allowing the assessment of up to 25 large plant pots of 3 to 5 L and about 150 small ones of less than 2 L. Despite the fact that the workspace makes it difficult to handle more than 30 big plants, the pots remain static without causing any possible mechanical damage to the plant leaves or any secondary effect on the expression of the phenotype. Another advantage of this setup is that plants can be analyzed by different sensors in the same run, reducing the amount of time between data acquisition for the same individual.

Experiments carried out under controlled environments are often difficult to associate in terms of yield performance under field conditions. The flexibility of specific environmental conditions and the control of the exposure of the plants by modifying those conditions is one of the biggest advantages of growing plants under controlled environmental conditions [53]. Many experiments in indoor controlled environments evaluate different parameters of plant growth under different conditions. However, many of them imply high costs, a lot of labor, specialized knowledge, and not all of them work for all types of plants. Thus, to improve the speed, accuracy, costs, and reliability of this process Phenocave was developed as an automated phenotyping system to evaluate visual traits from top-view plant images. Phenocave provides easy accessibility, especially because of its good cost-performance ratio; moreover, the pipeline developed is in ImageJ, an open-source software, and its architecture is flexible, which allows it to be unmounted and mounted in other indoor environments, and the interface is user-friendly.

Positive correlations were observed between projected green area obtained from imaging and destructively harvested green and yellow leaf biomass in all the growth stages (Table 1). The correlation had a slight decrease at the stem elongation stage because of the number of overlapping leaves (Figure 4C). Plants with overlapping leaves evaluated with image analysis can cause underestimation of the projected area [54,55]. Despite this correlation reduction, the results generally were highly correlated. Studies in controlled greenhouse conditions have found similar correlations between areas estimated by image analysis and harvested biomass [4,35,54,55] which indicates the applicability of top imaging with Phenocave for non-destructive evaluation of germplasm.

Understanding the impact of drought at different growth stages contributes to the efficiency of breeding drought-tolerant wheat varieties. Important factors such as the intensity and frequency of drought affect the performance of any crop. The plant developmental stage at which drought events occur is equally important [56]. While testing Phenocave to identify the response of plants to drought at two growth stages, we found negative effects in wheat, such as reduction of leaf biomass production and grain yield. Nonetheless, the duration, intensity, and timing of certain stresses differ in how and which yield components are affected [57–59]. In the present study, the stress was imposed over six days of stopping the irrigation, resulting in visual differences in shoot biomass in the plants (Figure 6). The occurrence of drought stress at the stem elongation stage led to a significant reduction in leaf biomass and fewer spikes. Previous studies have shown that drought stress at the stem elongation stage greatly decreased the grain yield compared to booting and grain filling stages [60]. Results of drought stress at the heading stage showed a significant decrease in the number of grains per head, grain weight, and leaf biomass which was even more severe than in the early stage.

As for the wheat case study, the HPLC analysis revealed a low grain protein yield (7.7–13%) compared to field-grown wheat (normally 11–14% in Swedish field conditions), which indicates the need to fertilize wheat to a level around the high nitrogen treatment conditions used in the present experiment. Despite the generally low grain protein concentrations obtained here, the present results corresponded with those previously reported [61,62]; for example, that reduced green biomass is a major effector on grain protein concentration. Thus, a drought at heading resulted in a severe decrease of plant biomass and thereby a reduction of carbohydrate transportation to the grain, which resulted in a high grain protein concentration. The negative correlation between TOTE and %UPP reported in several studies [43,44,50] was not seen for samples with different treatments

in the present study. The relatively high gluten strength, verified by correlating %UPP values [43,44], found in the samples subjected to drought at heading, is most likely due to an increase in hydrogen and disulfide bond formation, previously reported as an outcome of decreased precipitation and increased temperature [48,61,62].

The second case study was the effect of sugar beet seed treatments on germination and plant growth. The results indicated that seeds under priming treatment were positively influenced in terms of germination ability and speed, especially during the first four days. This is the effect of priming seeds, which causes an acceleration of germination and the acceleration of seedling growth [63]. On the other hand, pelleting and coating treatment reduced germination rates, especially in the early stages. The delayed seed germination can be explained by the slow water flow from the germination medium through the pellet and pericarp to the seed [64]. Hence, although necessary from an agricultural perspective, pelleting and coating may slightly delay germination, while priming may compensate for this delay. Previous research showed that primed seeds with a lower level of vigor showed a faster and higher germination ability than non-primed seeds with higher vigor [64]. Despite this effect caused by both treatments, after 14 days of germination, the differences in seed germination and plant growth development diminished.

An advantage of using Phenocave is the free choice of the use of the imaging sensors supported by Phenocave (RGB, multispectral, NDVI, multispectral) and the space (2 sq m) within which plants can be placed anywhere in the imaging region as required by the experimental design. While the current setup of Phenocave is limited to manual data transfer and manual irrigation, this might be included in the automatic system in future modifications. Multispectral bands from the Micasense Altum sensor were not available in Phenocave since the short distance between the lens and the object was problematic for band alignment. Several algorithms have been developed to identify keypoint feature descriptors for band alignment [65]. Keypoint descriptors assist in better alignment when the alignment bands have nearly uniform reflectance profiles and unique patterns in the scene [66]. Thus, in future work, an automated work flow will be developed for the alignment of bands from the Micasense Altum camera for pictures taken in close range. An additional improvement could be regular radiometric calibration of the thermal sensor of the Micasense Altum camera. A previous study showed that radiometric calibration of thermal sensors produces more accurate results [67]. Thus, a similar calibration of sensors could be beneficial for experiments requiring higher measurement accuracy. Nonetheless, this study demonstrates that the Phenocave system is a useful tool for the non-destructive estimation of plant shoot biomass under different growth conditions and at various time points.

5. Conclusions

In order to adapt to climate change, unexpected agronomical diseases, and other factors that affect plant performance, it is of utmost importance to assess plants under different environmental conditions in a fast, accurate, friendly, and affordable manner. Phenocave offers the opportunity to assess the visual traits of the plants under highly controlled environments. In addition, the platform reduces manual work for the users because of a high level of automation. It moves in XY direction acquiring high-quality individual photographs of plants with different imaging sensors (RGB, thermal, NDVI, and hyperspectral), which allows the extraction of different characteristics of plants.

One of the advantages of Phenocave is that it evaluates small- to mid-size plants, such as sugar beet and small-grain cereals. Besides, it can be unmounted and mounted to be used in other environments. This study highlights the potential of developing systems similar to Phenocave which promote work time efficiency, cost efficiency, and flexibility. In future work, data transfer and management will be further improved, and broader applications such as plant diseases and automatic irrigation will be studied, which can further contribute to allowing faster evaluation of plant responses to various treatments.

References

1. Cornelissen, J.; Lavorel, S.; Garnier, E.; Díaz, S.; Buchmann, N.; Gurvich, D.; Reich, P.; Ter Steege, H.; Morgan, H.; Van Der Heijden, M. A handbook of protocols for standardised and easy measurement of plant functional traits worldwide. *Aust. J. Bot.* **2003**, *51*, 335–380. [CrossRef]
2. Poschlod, P.; Kleyer, M.; Tackenberg, O. Databases on life history traits as a tool for risk assessment in plant species. *Z. Okol. Nat.* **2000**, *9*, 3–18.
3. Reynolds, D.; Baret, F.; Welcker, C.; Bostrom, A.; Ball, J.; Cellini, F.; Lorence, A.; Chawade, A.; Khafif, M.; Noshita, K.; et al. What is cost-efficient phenotyping? Optimizing costs for different scenarios. *Plant Sci.* **2019**, *282*, 14–22. [CrossRef]
4. Tackenberg, O. A New Method for Non-destructive Measurement of Biomass, Growth Rates, Vertical Biomass Distribution and Dry Matter Content Based on Digital Image Analysis. *Ann. Bot.* **2007**, *99*, 777–783. [CrossRef]
5. Duan, L.; Yang, W.; Huang, C.; Liu, Q. A novel machine-vision-based facility for the automatic evaluation of yield-related traits in rice. *Plant Methods* **2011**, *7*, 44. [CrossRef] [PubMed]
6. Furbank, R.T.; Tester, M. Phenomics—Technologies to relieve the phenotyping bottleneck. *Trends Plant Sci.* **2011**, *16*, 635–644. [CrossRef]
7. Savvides, A.; Ali, S.; Tester, M.; Fotopoulos, V. Chemical priming of plants against multiple abiotic stresses: Mission possible? *Trends Plant Sci.* **2016**, *21*, 329–340. [CrossRef] [PubMed]
8. Conrath, U. Molecular aspects of defence priming. *Trends Plant Sci.* **2011**, *16*, 524–531. [CrossRef] [PubMed]
9. Paparella, S.; Araújo, S.; Rossi, G.; Wijayasinghe, M.; Carbonera, D.; Balestrazzi, A. Seed priming: State of the art and new perspectives. *Plant Cell Rep.* **2015**, *34*, 1281–1293. [CrossRef] [PubMed]
10. Gamir, J.; Sánchez-Bel, P.; Flors, V. Molecular and physiological stages of priming: How plants prepare for environmental challenges. *Plant Cell Rep.* **2014**, *33*, 1935–1949. [CrossRef] [PubMed]
11. Ibrahim, E.A. Seed priming to alleviate salinity stress in germinating seeds. *J. Plant Physiol.* **2016**, *192*, 38–46. [CrossRef] [PubMed]
12. Lutts, S.; Benincasa, P.; Wojtyla, L.; Kubala, S.; Pace, R.; Lechowska, K.; Quinet, M.; Garnczarska, M. Seed priming: New comprehensive approaches for an old empirical technique. *New Chall. Seed Biol.-Basic Transl. Res. Driv. Seed Technol.* **2016**, 1–46. [CrossRef]
13. Fahlgren, N.; Gehan, M.A.; Baxter, I. Lights, camera, action: High-throughput plant phenotyping is ready for a close-up. *Curr. Opin. Plant Biol.* **2015**, *24*, 93–99. [CrossRef] [PubMed]
14. Richards, R.A.; Rebetzke, G.J.; Watt, M.; Condon, A.G.; Spielmeyer, W.; Dolferus, R. Breeding for improved water productivity in temperate cereals: Phenotyping, quantitative trait loci, markers and the selection environment. *Funct. Plant Biol.* **2010**, *37*, 85–97. [CrossRef]
15. Chawade, A.; van Ham, J.; Blomquist, H.; Bagge, O.; Alexandersson, E.; Ortiz, R. High-throughput field-phenotyping tools for plant breeding and precision agriculture. *Agronomy* **2019**, *9*, 258. [CrossRef]
16. Chawade, A.; Armoniene, R.; Berg, G.; Brazauskas, G.; Frostgard, G.; Geleta, M.; Gorash, A.; Henriksson, T.; Himanen, K.; Ingver, A.; et al. A transnational and holistic breeding approach is needed for sustainable wheat production in the Baltic Sea region. *Physiol. Plant.* **2018**, *164*, 4, 442–451. [CrossRef]

17. Humplik, J.F.; Lazar, D.; Husickova, A.; Spichal, L. Automated phenotyping of plant shoots using imaging methods for analysis of plant stress responses—A review. *Plant Methods* **2015**, *11*, 29. [CrossRef] [PubMed]

18. Armoniene, R.; Odilbekov, F.; Vivekanand, V.; Chawade, A. Affordable Imaging Lab for Noninvasive Analysis of Biomass and Early Vigour in Cereal Crops. *Biomed. Res. Int.* **2018**, *2018*, 5713158. [CrossRef]

19. Golzarian, M.R.; Frick, R.A.; Rajendran, K.; Berger, B.; Roy, S.; Tester, M.; Lun, D.S. Accurate inference of shoot biomass from high-throughput images of cereal plants. *Plant Methods* **2011**, *7*, 2. [CrossRef]

20. Menzel, M.I.; Tittmann, S.; Buhler, J.; Preis, S.; Wolters, N.; Jahnke, S.; Walter, A.; Chlubek, A.; Leon, A.; Hermes, N.; et al. Non-invasive determination of plant biomass with microwave resonators. *Plant Cell Environ.* **2009**, *32*, 368–379. [CrossRef]

21. Kumar, D.; Kushwaha, S.; Delvento, C.; Liatukas, Ž.; Vivekanand, V.; Svensson, J.T.; Henriksson, T.; Brazauskas, G.; Chawade, A. Affordable Phenotyping of Winter Wheat under Field and Controlled Conditions for Drought Tolerance. *Agronomy* **2020**, *10*, 882. [CrossRef]

22. Stuart, M.B.; McGonigle, A.J.S.; Willmott, J.R. Hyperspectral Imaging in Environmental Monitoring: A Review of Recent Developments and Technological Advances in Compact Field Deployable Systems. *Sensors* **2019**, *19*, 3071. [CrossRef] [PubMed]

23. Römer, C.; Wahabzada, M.; Ballvora, A.; Pinto, F.; Rossini, M.; Panigada, C.; Behmann, J.; Léon, J.; Thurau, C.; Bauckhage, C. Early drought stress detection in cereals: Simplex volume maximisation for hyperspectral image analysis. *Funct. Plant Biol.* **2012**, *39*, 878–890. [CrossRef] [PubMed]

24. Fortier, J.; Truax, B.; Gagnon, D.; Lambert, F. Abiotic and biotic factors controlling fine root biomass, carbon and nutrients in closed-canopy hybrid poplar stands on post-agricultural land. *Sci. Rep.* **2019**, *9*, 6296. [CrossRef]

25. Baker, N.R. Chlorophyll fluorescence: A probe of photosynthesis in vivo. *Annu. Rev. Plant Biol.* **2008**, *59*, 89–113. [CrossRef]

26. Li, L.; Zhang, Q.; Huang, D. A review of imaging techniques for plant phenotyping. *Sensors* **2014**, *14*, 20078–20111. [CrossRef]

27. Odilbekov, F.; Armonienė, R.; Koc, A.; Svensson, J.; Chawade, A. GWAS-Assisted Genomic Prediction to Predict Resistance to Septoria Tritici Blotch in Nordic Winter Wheat at Seedling Stage. *Front. Genet.* **2019**, *10*, 1224. [CrossRef]

28. Skirycz, A.; Vandenbroucke, K.; Clauw, P.; Maleux, K.; De Meyer, B.; Dhondt, S.; Pucci, A.; Gonzalez, N.; Hoeberichts, F.; Tognetti, V.B. Survival and growth of Arabidopsis plants given limited water are not equal. *Nat. Biotechnol.* **2011**, *29*, 212–214. [CrossRef] [PubMed]

29. Flood, P.J.; Kruijer, W.; Schnabel, S.K.; van der Schoor, R.; Jalink, H.; Snel, J.F.; Harbinson, J.; Aarts, M.G. Phenomics for photosynthesis, growth and reflectance in Arabidopsis thaliana reveals circadian and long-term fluctuations in heritability. *Plant Methods* **2016**, *12*, 1–14. [CrossRef]

30. Minervini, M.; Giuffrida, M.V.; Perata, P.; Tsaftaris, S.A. Phenotiki: An open software and hardware platform for affordable and easy image-based phenotyping of rosette-shaped plants. *Plant J.* **2017**, *90*, 204–216. [CrossRef]

31. Tisne, S.; Serrand, Y.; Bach, L.; Gilbault, E.; Ben Ameur, R.; Balasse, H.; Voisin, R.; Bouchez, D.; Durand-Tardif, M.; Guerche, P.; et al. Phenoscope: An automated large-scale phenotyping platform offering high spatial homogeneity. *Plant J.* **2013**, *74*, 534–544. [CrossRef]

32. Arvidsson, S.; Pérez-Rodríguez, P.; Mueller-Roeber, B. A growth phenotyping pipeline for Arabidopsis thaliana integrating image analysis and rosette area modeling for robust quantification of genotype effects. *New Phytol.* **2011**, *191*, 895–907. [CrossRef]

33. Wu, S.; Wen, W.; Wang, Y.; Fan, J.; Wang, C.; Gou, W.; Guo, X. MVS-Pheno: A Portable and Low-Cost Phenotyping Platform for Maize Shoots Using Multiview Stereo 3D Reconstruction. *Plant Phenomics* **2020**, *2020*, 1848437. [CrossRef] [PubMed]

34. Granier, C.; Aguirrezabal, L.; Chenu, K.; Cookson, S.J.; Dauzat, M.; Hamard, P.; Thioux, J.J.; Rolland, G.; Bouchier-Combaud, S.; Lebaudy, A. PHENOPSIS, an automated platform for reproducible phenotyping of plant responses to soil water deficit in Arabidopsis thaliana permitted the identification of an accession with low sensitivity to soil water deficit. *New Phytol.* **2006**, *169*, 623–635. [CrossRef] [PubMed]

35. Rajendran, K.; Tester, M.; Roy, S.J. Quantifying the three main components of salinity tolerance in cereals. *Plant Cell Environ.* **2009**, *32*, 237–249. [CrossRef] [PubMed]

36. Darrow, R.D.; Dumoulin, C.L. Automatic Gantry Positioning for Imaging Systems. U.S. Patent 5,255,680, 26 October 1993.

37. Istvan, D. DigiCamControl Software, Version 2.1.2. 2014. Available online: http://digicamcontrol.com/ (accessed on 30 November 2019).

38. QGIS Development Team. *QGIS Geographic Information System*; Version 3.12.3; Open Source Geospatial Foundation: Beaverton, OR, USA, 2009.

39. Zadoks, J.C.; Chang, T.T.; Konzak, C.F. A decimal code for the growth stages of cereals. *Weed Res.* **1974**, *14*, 415–421. [CrossRef]

40. Mukamuhirwa, A.; Persson Hovmalm, H.; Bolinsson, H.; Ortiz, R.; Nyamangyoku, O.; Johansson, E. Concurrent drought and temperature stress in rice—A possible result of the predicted climate change: Effects on yield attributes, eating characteristics, and health promoting compounds. *Int. J. Environ. Res. Public Health* **2019**, *16*, 1043. [CrossRef]

41. Mariotti, F.; Tomé, D.; Mirand, P.P. Converting nitrogen into protein—Beyond 6.25 and Jones' factors. *Crit. Rev. Food Sci. Nutr.* **2008**, *48*, 177–184. [CrossRef]

42. Husenov, B.; Asaad, S.; Muminjanov, H.; Garkava-Gustavsson, L.; Johansson, E. Sustainable Wheat Production and Food Security of Domestic Wheat in Tajikistan: Implications of Seed Health and Protein Quality. *Int. J. Environ. Res. Public Health* **2021**, *18*, 5751. [CrossRef]

43. Malik, A.H.; Kuktaite, R.; Johansson, E. Combined effect of genetic and environmental factors on the accumulation of proteins in the wheat grain and their relationship to bread-making quality. *J. Cereal Sci.* **2013**, *57*, 170–174. [CrossRef]

44. Malik, A.H.; Prieto-Linde, M.L.; Kuktaite, R.; Andersson, A.; Johansson, E. Individual and interactive effects of cultivar maturation time, nitrogen regime and temperature level on accumulation of wheat grain proteins. *J. Sci. Food Agric.* **2011**, *91*, 2192–2200. [CrossRef] [PubMed]

45. Gupta, R.B.; Khan, K.; Macritchie, F. Biochemical Basis of Flour Properties in Bread Wheats. I. Effects of Variation in the Quantity and Size Distribution of Polymeric Protein. *J. Cereal Sci.* **1993**, *18*, 23–41. [CrossRef]

46. Johansson, E.; Prieto-Linde, M.L.; Jönsson, J.Ö. Effects of wheat cultivar and nitrogen application on storage protein composition and breadmaking quality. *Cereal Chem.* **2001**, *78*, 19–25. [CrossRef]

47. Johansson, E.; Kuktaite, R.; Andersson, A.; Prieto-Linde, M.L. Protein polymer build-up during wheat grain development: Influences of temperature and nitrogen timing. *J. Sci. Food Agric.* **2005**, *85*, 473–479. [CrossRef]

48. Johansson, E.; Prieto-Linde, M.L.; Gissén, C. Influences of weather, cultivar and fertiliser rate on grain protein polymer accumulation in field-grown winter wheat, and relations to grain water content and falling number. *J. Sci. Food Agric.* **2008**, *88*, 2011–2018. [CrossRef]

49. Kuktaite, R.; Larsson, H.; Johansson, E. Variation in protein composition of wheat flour and its relationship to dough mixing behaviour. *J. Cereal Sci.* **2004**, *40*, 31–39. [CrossRef]

50. Vazquez, D.; Berger, A.; Prieto-Linde, M.L.; Johansson, E. Can nitrogen fertilization be used to modulate yield, protein content and bread-making quality in Uruguayan wheat? *J. Cereal Sci.* **2019**, *85*, 153–161. [CrossRef]

51. R Development Core Team. *R: A Language and Environment for Statistical Computing*; R Foundation for Statistical Computing: Vienna, Austria, 2010.

52. James, R.A.; Sirault, X.R.R. Infrared Thermography in Plant Phenotyping for Salinity Tolerance. In *Plant Salt Tolerance: Methods and Protocols*; Shabala, S., Cuin, T.A., Eds.; Humana Press: Totowa, NJ, USA, 2012; pp. 173–189.

53. Araus, J.L.; Cairns, J.E. Field high-throughput phenotyping: The new crop breeding frontier. *Trends Plant Sci.* **2014**, *19*, 52–61. [CrossRef]

54. Fanourakis, D.; Briese, C.; Max, J.F.; Kleinen, S.; Putz, A.; Fiorani, F.; Ulbrich, A.; Schurr, U. Rapid determination of leaf area and plant height by using light curtain arrays in four species with contrasting shoot architecture. *Plant Methods* **2014**, *10*, 1–11. [CrossRef] [PubMed]

55. Joalland, S.; Screpanti, C.; Gaume, A.; Walter, A. Belowground biomass accumulation assessed by digital image based leaf area detection. *Plant Soil* **2016**, *398*, 257–266. [CrossRef]

56. Sarto, M.V.M.; Sarto, J.R.W.; Rampim, L.; Rosset, J.S.; Bassegio, D.; da Costa, P.F.; Inagaki, A.M. Wheat phenology and yield under drought: A review. *Aust. J. Crop Sci.* **2017**, *11*, 941–946. [CrossRef]

57. Demotes-Mainard, S.; Doussinault, G.; Meynard, J. Effects of low radiation and low temperature at meiosis on pollen viability and grain set in wheat. *Agronomie* **1995**, *15*, 357–365. [CrossRef]

58. Foulkes, M.; Scott, R.; Sylvester-Bradley, R. The ability of wheat cultivars to withstand drought in UK conditions: Formation of grain yield. *J. Agric. Sci.* **2002**, *138*, 153–169. [CrossRef]

59. Weldearegay, D.; Yan, F.; Jiang, D.; Liu, F. Independent and combined effects of soil warming and drought stress during anthesis on seed set and grain yield in two spring wheat varieties. *J. Agron. Crop Sci.* **2012**, *198*, 245–253. [CrossRef]

60. Keyvan, S. The effects of drought stress on yield, relative water content, proline, soluble carbohydrates and chlorophyll of bread wheat cultivars. *J. Anim. Plant Sci.* **2010**, *8*, 1051–1060.

61. Johansson, E.; Branlard, G.; Cuniberti, M.; Flagella, Z.; Hüsken, A.; Nurit, E.; Peña, R.J.; Sissons, M.; Vazquez, D. Genotypic and environmental effects on wheat technological and nutritional quality. In *Wheat Quality for Improving Processing and Human Health*; Igrejas, G., Ikeda, T.M., Guzmán, C., Eds.; Springer: Berlin/Heidelberg, Germany, 2020; pp. 171–204.

62. Johansson, E.; Malik, A.H.; Hussain, A.; Rasheed, F.; Newson, W.R.; Plivelic, T.; Hedenqvist, M.S.; Gällstedt, M.; Kuktaite, R. Wheat gluten polymer structures: The impact of genotype, environment, and processing on their functionality in various applications. *Cereal Chem.* **2013**, *90*, 367–376. [CrossRef]

63. Khan, A.A. Preplant physiological seed conditioning. *Hortic. Rev.* **1992**, *13*, 131–181.

64. Orzeszko-Rywka, A.; Podlaski, S. The effect of sugar beet seed treatments on their vigour. *Plant Soil Environ.* **2018**, *49*, 249–254. [CrossRef]

65. Hassaballah, M.; Alshazly, H.A.; Ali, A.A. Analysis and Evaluation of Keypoint Descriptors for Image Matching. In *Recent Advances in Computer Vision*; Springer: Berlin/Heidelberg, Germany, 2019; pp. 113–140.

66. Banerjee, B.P.; Raval, S.A.; Cullen, P.J. Alignment of UAV-hyperspectral bands using keypoint descriptors in a spectrally complex environment. *Remote Sens. Lett.* **2018**, *9*, 524–533. [CrossRef]

67. Kelly, J.; Kljun, N.; Olsson, P.-O.; Mihai, L.; Liljeblad, B.; Weslien, P.; Klemedtsson, L.; Eklundh, L. Challenges and Best Practices for Deriving Temperature Data from an Uncalibrated UAV Thermal Infrared Camera. *Remote Sens.* **2019**, *11*, 567. [CrossRef]

II

Check for updates

Phenotyping Fusarium head blight through seed morphology characteristics using RGB imaging

Fernanda Leiva[1]*, Mustafa Zakieh[1], Marwan Alamrani[1],
Rishap Dhakal[1], Tina Henriksson[2], Pawan Kumar Singh[3]
and Aakash Chawade[1]

[1]Department of Plant Breeding, Swedish University of Agricultural Sciences, Lomma, Sweden,
[2]Lantmännen Lantbruk, Svalöv, Sweden, [3]International Maize and Wheat Improvement Center
(CIMMYT), Texcoco, Mexico

Fusarium head blight (FHB) is an economically important disease affecting wheat and thus poses a major threat to wheat production. Several studies have evaluated the effectiveness of image analysis methods to predict FHB using disease-infected grains; however, few have looked at the final application, considering the relationship between cost and benefit, resolution, and accuracy. The conventional screening of FHB resistance of large-scale samples is still dependent on low-throughput visual inspections. This study aims to compare the performance of two cost–benefit seed image analysis methods, the free software "SmartGrain" and the fully automated commercially available instrument "Cgrain Value™" by assessing 16 seed morphological traits of winter wheat to predict FHB. The analysis was carried out on a seed set of FHB which was visually assessed as to the severity. The dataset is composed of 432 winter wheat genotypes that were greenhouse-inoculated. The predictions from each method, in addition to the predictions combined from the results of both methods, were compared with the disease visual scores. The results showed that Cgrain Value™ had a higher prediction accuracy of $R^2 =$ 0.52 compared with SmartGrain for which $R^2 = 0.30$ for all morphological traits. However, the results combined from both methods showed the greatest prediction performance of $R^2 = 0.58$. Additionally, a subpart of the morphological traits, namely, width, length, thickness, and color features, showed a higher correlation with the visual scores compared with the other traits. Overall, both methods were related to the visual scores. This study shows that these affordable imaging methods could be effective to predict FHB in seeds and enable us to distinguish minor differences in seed morphology, which could lead to a precise performance selection of disease-free seeds/grains.

KEYWORDS

Fusarium head blight, seed phenotyping, seed morphological characters, wheat, visual scores, SmartGrain, Cgrain Value™

Introduction

In the countries of the Baltic Sea region, the most widely cultivated crop is winter wheat (*Triticum aestivum L.*), (Shiferaw et al., 2013; Chawade et al., 2018). While efforts are made to achieve sustainable intensification of high grain yields in wheat production, the emergence and increase in the virulence of plant pathogens conversely leave the nutritional integrity and production of wheat grains at risk (Castro Aviles et al., 2020). The decrease in grain quality and protein content negatively impacts the use of the grains and therefore affects food security and safety (Asseng et al., 2019). Fusarium head blight (FHB), mainly caused by the fungus *Fusarium graminearum* Schwabe [teleomorph: *Gibberella zeae* (Schwein) Petch], is one of the wheat diseases with a major impact on wheat grain yield and quality. FHB can dramatically reduce grain quality and yield through the formation of sterile and wizened florets. FHB-infected grains suffer from major marketing, consumption, and processing constraints, which is the buildup of mycotoxins— mainly deoxynivalenol (DON) (Del Ponte et al., 2022). DON inhibits protein synthesis, cutting off normal cell function, which is hazardous for the consumption of humans and animals (Polak-Śliwińska and Paszczyk, 2021). FHB disease management strategies rely on integrating several cultural practices such as fungicide treatment, crop rotation, mixed culture, and tillage (Gilbert and Haber, 2013). However, growing FHB-resistant cultivars is seen as a more sustainable and durable strategy for mitigating disease epidemics, thus avoiding large economic losses. Hence, identifying sources of novel resistance is a key component in pre-breeding activities that can be introgressed to develop commercial FHB-resistant cultivars.

The resistance components for FHB, commonly known as resistance types, have been defined into type I to type V (Mesterhazy, 2020): type I is resistance to initial infection, type II is resistance to disease spread (Schroeder and Christensen, 1963), type III is resistance to damage of Fusarium-damaged kernels (FDK), type IV is resistance to the buildup of DON toxins, and type V is tolerance. Traditionally, studies on FHB resistance have relied on measuring the symptoms in spikes and kernels (resistance types II and III). Type II is assessed by rating the visual symptoms on the spikes, which appear as bleached, yellowish or discolored, and stunted (Zakieh et al., 2021; Steed et al., 2022). FDK is quantified traditionally by estimating the amount of visibly damaged kernels, which appear smaller, shriveled, and in a range of colors from pale pink to brown (Delwiche et al., 2010), according to a predetermined scale for visual assessments or by employing manual tools (Ackerman et al., 2022). Comparisons between both types of resistance (resistance types II and III) have revealed that it would be more efficient and consistent to estimate FHB than the degree of colonization on the spike (Agostinelli, 2009; Balut et al., 2013; Khaeim et al., 2019; Ackerman et al., 2022). However, screening

by either manual or visual assessments is a labor- and time-consuming process for rating genotypes, is biased due to the subjectivity of visual assessments, and has low reproducibility among experiments (Barbedo et al., 2015; Khaeim et al., 2019). As a result of the previously cited limitations, the use of image analysis approaches has been investigated to evaluate FDK, particularly in estimating morphological characteristics. However, the existing different imaging approaches have their disadvantages and trade-off in terms of costs, time expenses, resolution, and precision when considering an application (Saccon et al., 2017).

Among the investigated methods, Iwata and Ukai (2002) and Iwata et al. (2010) investigated changes in grain shape using elliptic Fourier descriptors of two- and three-dimensional features from vertically and horizontally located seed images. Despite the accuracy reached, there are limitations in terms of image resolution and regarding the manual handling of samples during the procedure. Menesatti et al. (2009) presented a method to classify FHB in wheat-infected kernels—according to the shape criteria—into the following groups: chalky, shriveled, or healthy. The method proved to be functional to categorize kernels as chalky or healthy, but not for shriveled or gravely affected samples. Jirsa and Polišenská (2011) developed a model for the identification of Fusarium-damaged wheat kernels using image analysis. The characterization of healthy or damaged kernels based on color parameters revealed a high accuracy compared with the shape and DON content parameters. However, image processing was done with manual selections and comparing only 40 kernels—either heavily damaged or healthy—without considering any halfway stage. Similarly, the use of hyperspectral imaging for detecting Fusarium sp. in seeds has been previously investigated (Delwiche et al., 2010; Shahin and Symons, 2011; Bauriegel and Herppich, 2014; Barbedo et al., 2015; Femenias et al., 2022; Rangarajan et al., 2022; Yipeng et al., 2022). The methods have been shown to be accurate and have identified more factors involved in FDK. A more advanced technique based on X-ray computed tomography has been implemented for evaluating seed shape in finer detail (Gomes and Duijn, 2017; Liu et al., 2020). Nevertheless, inconsistencies because of specular reflection, correct wavelength selection, kernel orientation, selection of reference parameter, costs of acquisition devices, and the storage requirement for highly dimensional and massive data sets may be limiting the application of these methods (Dissing et al., 2013; Lu et al., 2020).

In the face of the constraints cited earlier, automated and light-weight free software for grain image analysis have been developed (Wang et al., 2009; Komyshev et al., 2017; Colmer et al., 2020; Zhu et al., 2021); some examples of them are GrainScan (Whan et al., 2014), which analyzes size and color features, and SmartGrain (Tanabata et al., 2012), which analyzes size and shape features. Both software are instantaneous in image recognition despite the position, overlapping, or the

number of seeds. Alternatively, commercially available imaging instruments for grain image analysis combine hardware and software, including WinSEEDLE (Regent Instruments Inc.), Seed Count (Next Instrument Pty Ltd.), Vibe QM3 Grain Analyzer (VIBE), and Cgrain Value™ (Cgrain AB). The instruments use optical or flatbed scanners to extract features such as size, shape, and color in the color representation hue, saturation, and light (HSL). However, SeedCount and Vibe QM3 Grain Analyzer only scan the top surface of the samples, thus omitting morphological characteristics that are not in the viewing area. A more advanced instrument is Videometer Lab (Videometer A/S, Denmark), which provides rapid color, shape, and texture measurements. Videometer Lab is ideal to use in analyzing kernel surfaces, but it requires certain expertise and allows the analysis of only a few samples at once.

In this context, this paper has three objectives; first is to investigate the applicability of low-cost digital image analysis to predict FHB infection in harvested grains through morphological traits. This will offer more insight into the traits that are correlated to the degree of FDK. The second objective is to compare the applicability of the two methods used for grain image analysis—SmartGrain, and Cgrain Value™—in terms of consistency and throughput. The third one is to illustrate the processing chain and result interpretation with a descriptive data analysis.

Materials and methods

Plant material

Wheat kernel samples were collected from an experiment under accelerated indoor growth conditions (Zakieh et al., 2021) using winter wheat genotypes from two different sources. The first source consisted of 338 genotypes (breeding set) provided by the Swedish agricultural cooperative (Lantmännen Lantbruk, Svalöv, Sweden). The second source consisted of 181 germplasm genotypes (genebank set) provided by the Nordic Genetic Resource Center (Nordgen), with highly diverse plant materials including landraces and old cultivars.

Experimental design/growth and inoculation protocol

Plants were grown following an augmented block design in a climate-controlled chamber. After germination, the plants were subjected to a vernalization period of 57 days at 3°C with 8 h of daily light at medium–high light intensity (LI) of 250 µmol m^{-2} s^{-1}. At the end of the vernalization period, the climatic conditions were adjusted with a gradual increase in temperature and LI for the acclimatization of the plants to the next phase of accelerated growth conditions. Once the acclimatization period was concluded, the

plants were left to grow at a constant temperature of 22°C. The accelerated growth conditions were adapted by exposing the plants to a prolonged daily light duration of 22 h, with LI at 400 µmol m^{-2} s^{-1} of uniform light intensity from LED light plates. Under these accelerated growth conditions, the plants were watered daily and fertilized weekly using first a combination of a high-phosphate and high-nitrogen soluble fertilizer SW-BOUYANT 7-1-5 + Mikro + KH$_2$PO$_4$, then only with a high-nitrogen fertilizer, and finally with a high-potassium soluble fertilizer Yara Tera Kristalon NPK 12-5-30 with S and Mikro.

After completing the anthesis stage, at 33 days post-acclimatization, the plants were moved to a glasshouse chamber with relative humidity (rh) of 60% and a constant temperature of 24°C for 24 h to allow their adaptation to the new growth conditions prior to inoculation. Thereafter, the winter wheat spikes were spray-inoculated with an inoculum suspension prepared from the harvested spore of *F. graminearum* and *F. culmorum*, with a concentration of 5 × 10^5 spore/ml. Subsequently, the plants were left to incubate at 90% rh with 16/8 h dark/light cycle at a constant temperature of 24°C for 48 h before adjusting the climatic conditions back to 60% rh. The plants were eventually left to grow under the latter conditions for 24 days before harvesting the seeds. Eight isolates from *F. graminearum* and *F. culmorum* species were used in inoculating the plants provided by the Swedish agricultural cooperative Lantmännen Lantbruk. An inoculum preparation was carried out by incubating the fungal spores at 24°C for 4 days in dark conditions to allow for mycelial growth on SNA media plates. Later, the fungal plates were exposed to near ultra-violet UV radiation for 10 h to induce macroconidia formation. Afterward, the fungal plates were incubated for 4 days at 24°C in dark conditions. Finally, macroconidia spores were collected to make the inoculation suspension with the provided concentration after adding the surfactant Tween®20 0.002% (v/v) final volume of the inoculum. A more detailed protocol is described in Zakieh et al. (2021).

FHB visual assessment

In order to evaluate FHB resistance on a large number of genotypes, a modified visual scoring of the FHB disease severity method was adopted. The method took into account the incidence of all FHB symptoms across the main tiller spike of each genotype. Therefore, disease severity was assessed as the percentage score of infected spikelets relative to all spikes, regardless of symptom continuity on the same spike. FHB development was scored at 6, 8, 10, and 12-days post-inoculation (dpi) (Stack and McMullen, 1998). The FHB disease severity scores varied between 100 to 5% for the most susceptible phenotypes and the most resistant ones, respectively. Finally, the results of the visual scores were validated by association mapping, thus identifying the quantitative trait loci of FHB resistance (Appendix 1).

Seed shape parameters

Two different grain phenotyping methods were employed in this study: an automated imaging instrument with software and hardware named Cgrain Value™ which is commercially available (Cgrain AB) and the free software named SmartGrain developed by Tanabata et al. (2012) and can be downloaded from the Quantitative Plant website (Lobet, 2017). The implementation of both methods is described in the following sections.

SmartGrain

For image acquisition, the seeds were captured with a low-cost image protocol acquisition from a top-view angle of 55 cm above the seeds and placed manually on a flat surface using a digital single-lens reflex camera Canon EOS 1300D (Canon U.S.A. Inc., Huntington, NY, USA), which has a resolution of 18 megapixels, mounted on a Kaiser RS-1 repro stand. The camera was tethered to the software digiCamControl (Istvan, 2014) with optimal exposure settings based on the best seed view, F-Stop 1/160, exposure time 1/10, and ISO 800. The seeds were placed manually per genotype uniformly on a blue cardboard that was used as a background on a stand aside from a 15-cm ruler for further analysis. Digital images were stored with $3,456 \times 2,304$-pixel resolution in JPEG format (Figure 1, top images).

The image analysis was thereafter carried out using SmartGrain software following its default protocol (Tanabata et al., 2012). Briefly, the image scale was set up by taking a known sample from the ruler and registering it on the software. Then, the segmentation method by color was chosen, the precision sensibility was set at the minimum value of "1", and the seed detection intensity was at a maximum value of "4" to obtain all possible shape details; the rest of the parameters were set to default. Finally, all the processed images were saved as TIFF files, and the results were saved in a CSV format. The software provides seven morphological characteristics: area seed (AS), perimeter length (PL), length (L), width (W), length-to-width ratio (LWR), circularity of the seed (CS), distance between the intersection of length and width, and the center of gravity (DS). **AS** corresponds to the total number of pixels of the segmented seed, this parameter estimates the seed size. **PL** refers to the length measurement of the seed outline. **L** corresponds to the major length measurement in the axis and **W** to the minor length axis measurement. **CS** estimates how round the region of interest is (seed), and it is calculated as $\frac{4\times\pi\times AS}{PL^2}$. **LWR** is calculated by $\frac{L}{W}$, and it provides an idea of the seed shape between rectangular and circular depending on the value. The distance between the transverse axis from the outline of the seed (IS) and the center of gravity (CG) is used to estimate **DS** [described in detail by Tanabata et al. (2012)].

Cgrain Value™

For single kernel analysis, seeds were scanned with Cgrain Value™, which is an analytical imaging instrument. The device
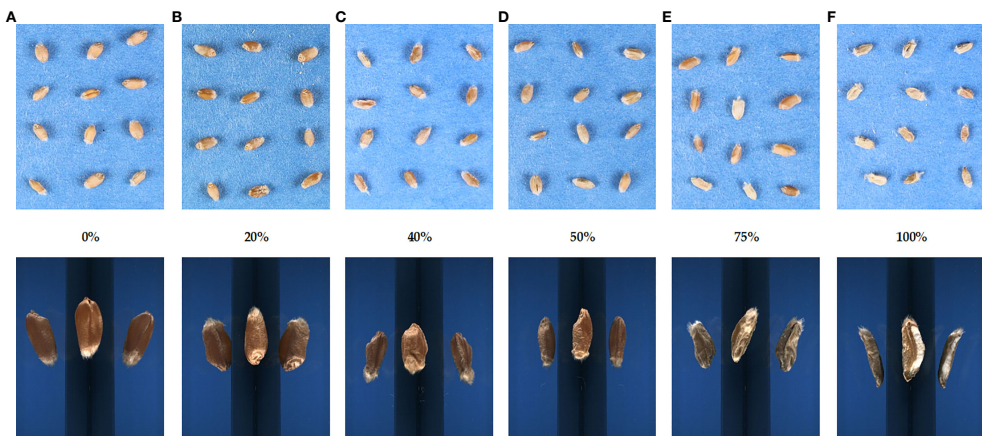
FIGURE 1
Images of the different levels of Fusarium head blight severity on winter wheat seeds. The rating of disease severity ranged from (**A**) 0 to (**F**) 100%. Scoring was based on the proportion of total infected spikes to the total amount of spikes. The top images were obtained for the SmartGrain analysis, and the bottom images were acquired using the Cgrain Value™ instrument.

inspects each kernel through a unique mirror design covering more than 90% of the grains' surfaces in every image. The analysis starts by pouring into the metal bowl of the Cgrain Value™ a batch of seeds per line and per genotype. The seeds rotate into the bowl and then, one by one, are photographed and analyzed simultaneously. After the analysis is completed, three different reports are created (result file, stat file, and image file). The result file consists of the morphological characteristics for each batch of seeds (seed count, thousand kernels, *etc.*), the stat file provides data per individual seed of a group (length, width, *etc.*), and the image file corresponds to the single seed images acquired (Figure 1, bottom images).

The instrument provides nine morphological attributes: length (L), width (W), thickness (T), average width (AVG.W), volume (V), weight (WT), light, hue, and saturation. Parameters such as L, W, and T are estimated by taking the longitudinal measurement of the axis major, higher minor, and minor, respectively. In the case of AVG.W, as the seed is received as a three-dimensional image, the measurement is referring to the mean of the average curvature. V corresponds to the seed volume obtained from the 3D image. For WT, the device has an internal balance, so while acquiring the image, it also weighs the grain. Color parameters, hue, saturation, and light are also determined by the instrument; it specifies the color base of a sample, how saturated it is, and how bright it is, respectively.

Statistical analysis

Statistical analyses were conducted using R (Team, R. C, 2013). The visual scorings of the last time-point on infected spikes, including cultivars with zero symptoms, were included in a file together with the mean values per genotype of the results given by Cgrain Value™ and SmartGrain. Each replicate of the data set was filtered by missing data (NA). Those with NA along the four replicates were removed and those with presence in more than one replicate were substituted using FactoMineR (Lê et al., 2008) and missMDA (Josse and Husson, 2016) packages. Then, using the Agricolae R package (De Mendiburu, 2014), the checks in each augmented block were used to adjust the means for each trait per replicate, the model of which is as follows:

$$y_{il} = u + G_{il} + \beta_1 + \epsilon_{il}$$

where y_{il} corresponds to the adjusted means of the ith wheat cultivar in the lth block, u is the general mean value, G_{il} is the effect of the ith wheat genotype in the lth block, β_1 is the lth block effect, and ϵ_{il} is the residual. Subsequently, using the adjusted means, the best linear unbiased estimates (BLUEs) was calculated using the randomized complete block design option in META-R 6.04 (Alvarado et al., 2015) based on the following model:

$$y_{ijm} = u + S_j + G_{ijm} + R_m + \epsilon_{ijm}$$

where y_{ijm} corresponds to the BLUE of the ith genotype from the jth population in the mth replicate, u is the general mean value, S_j is the effect of the jth source of material, G_{ijm} is the effect of the ith genotype in the mth replicate, R_m is the mth replicate of the effect, and ϵ_{ijm} is the residual effect. The source of wheat genotypes S_j was considered the grouping factor.

The BLUEs data previously centered were used to predict FHB using a multiple regression model:

$$y_i = \beta_0 + \beta_1 x_{i1} + \beta_2 x_{i2} + \dots + \beta_p x_{ip} + \epsilon$$

Where for i=n observations: y_i corresponds to the dependent variable, x_i to the explanatory variables, β_0 corresponds to y-intercept (constant term), β_p corresponds to the slope coefficients for each explanatory variable, and ϵ corresponds to the error of the model (also known as the residuals). Three models were created using the morphological traits provided by both methods (Cgrain Value™ and SmartGrain) as independent variables and visual scorings as the dependent variable. One model combines all the traits, and two others use the traits provided by each method. To build each model, the data set was partitioned employing the function "createDataPartition" of the caret package (Kuhn et al., 2020) into 70% for model training (training set) and the remaining 30% for evaluating model performance (test set). Subsequently, the model was fitted to the training set, and it predicted the responses using the test set. To evaluate the quality of the predictions and mitigate the possibility of errors due to the random data partitioning, the cross-validation was executed 100 times, which means resampling the data set, and the mean of the criterion was taken as the final result.

Results

This study examined a total of 16 morphological traits, including size, color, and shape of winter wheat grains from the genebank and breeding sets with different levels of FHB infection. Nine traits were obtained with the instrument Cgrain Value™ and seven traits with the software SmarGrain. The distribution of all the morphological traits measured by the two methods showed a Gaussian distribution (Figure 2). In order to understand the association between these traits and FHB resistance, a comparison with the traits measured of 80 FHB susceptible and resistant genotypes was performed. For this purpose, five genotypes per replicate (four replicates) from both sets, breeding and genebank, were selected based on the FHB severity scores on the spikes, genotypes scored as 0% (visually non-infected or resistant), and ones scored as 100% (visually infected or susceptible). Among the infected and non-infected selected groups, there was a 22.61% reduction in V and 11.32% in AS. Other parameters also showed a reduction, such as T_RAW at 10.60%, W at 8.30% in both methods, and WT at

22.63%. Additionally, L was reduced according to the results by 1.96% in Cgrain Value™ and 2.26% in SmartGrain. Similarly, CS and PL showed a decrease, but in less proportions with 4.60 and 3.25%, respectively. The minimum seed L measured was 4.59 mm for non-infected and 4.50 mm for infected genotypes. On the other hand, color parameters expressed major changes compared with all the other morphological traits. Hue and the light increased with the infection by 19.91 and 8.28%, respectively, while saturation decreased at about 15.52% (Table 1). According to the analysis of variance (two-way ANOVA), the morphological traits L, W, T_RAW, light, and hue were highly significant ($P < 0.001$), likewise with V, CS, and saturation ($P < 0.01$), indicating a clear association with FHB disease severity level. Meanwhile, the parameters WT, AS, LWR, PL, and DS did not indicate any significance but still showed slight differences between infected and non-infected grains.

Additionally, a principal component analysis (Figure 3) was performed to show the response of all the seed traits studied regarding the disease infection and how they correlate to each other. The proportion of total variance on the two first principal
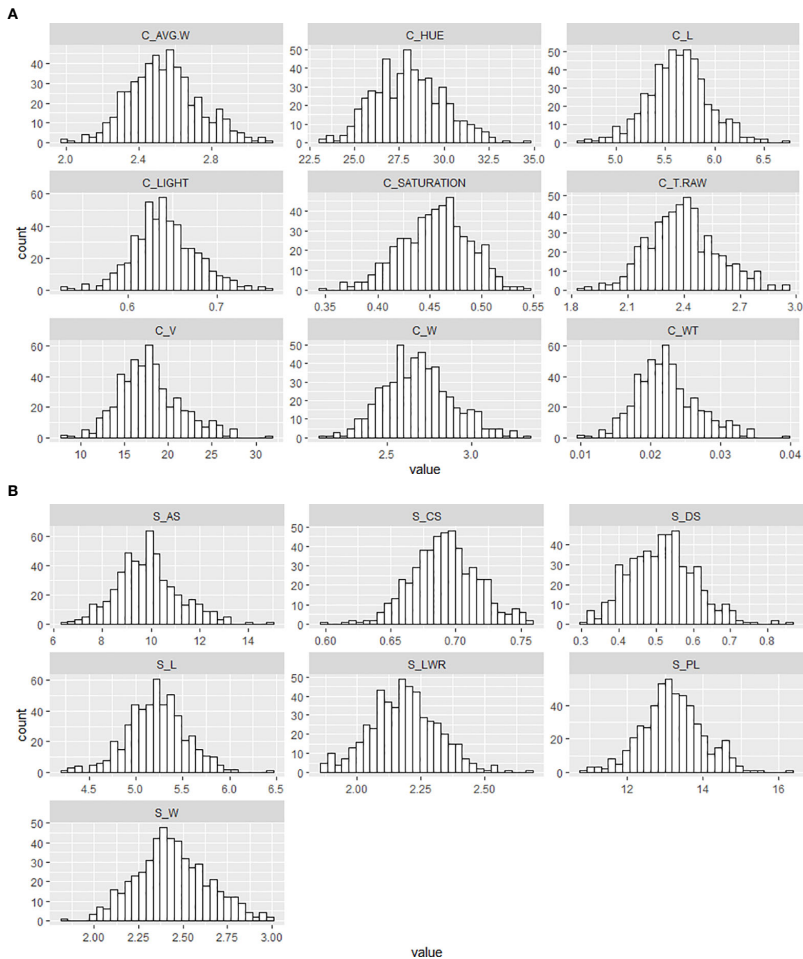
FIGURE 2
Frequency distribution of the different morphological traits of wheat genotypes seeds from the breeding and genebank sets collected with **(A)** the Cgrain Value™ instrument and **(B)** the SmartGrain software.

TABLE 1 Descriptive statistics showing differences between the seed shape characters of 80 genotypes from genebank and breeding set under non-infection (0%) and full infection (100%) FHB symptoms, with five genotypes of each one per replicate.

Description	Level	L	W	a) CGRAIN VALUE™ T.RAW	AVG.W	V	WT	HUE	SAT	LIGHT
Mean	Non_Infected	5.6	2.76	2.47	2.61	19.18	0.02	25.78	0.48	0.62
	Infected	5.49	2.53	2.2	2.36	14.84	0.01	30.81	0.4	0.68
% Reduction		1.96	8.29	10.6	9.41	22.61	25	-19.51	16.52	-9.67
Max	Non_Infected	6.88	3.7	3.245	3.41	38.9	0.04	30.46	0.55	0.715
	Infected	6.46	3.13	2.93	3.03	26.6	0.03	38.99	0.51	0.81
Min	Non_Infected	4.59	2.18	1.98	2.08	10.66	0.01	23.45	0.43	0.55
	Infected	4.5	2.05	1.88	1.96	7.1	0.008	24.88	0.3	0.58
SD	Non_Infected	0.52	0.36	0.3	0.32	6.74	0.008	1.32	0.02	0.04
	Infected	0.45	0.23	0.22	0.23	4.02	0.005	3.01	0.05	0.05
SE	Non_Infected	0.08	0.05	0.048	0.05	1.06	0.001	0.21	0.004	0.006
	Infected	0.07	0.04	0.036	0.04	0.63	0.0007	0.47	0.008	0.007
CV (%)		9.44	13.02	12.26	12.53	35.15	35.15	5.14	5.8	6.79

Description	Level	AS	PL	b) SMARTGRAIN L	W	LWR	CS	DS
Mean	Non_Infected	9.77	12.91	5.08	2.44	2.13	0.7	0.48
	Infected	8.66	12.49	4.97	2.23	2.25	0.67	0.51
% Reduction		11.32	3.25	2.26	8.27	-5.64	4.6	-6.9
Max	Non_Infected	17.36	17.15	6.57	3.71	2.53	0.8	0.85
	Infected	13.63	15.54	6.25	2.95	2.65	0.73	1.01
Min	Non_Infected	3.41	7.91	3.2	1.39	1.53	0.63	0.24
	Infected	3.01	7.31	2.88	1.36	1.88	0.61	0.23
SD	Non_Infected	3.21	2.16	0.81	0.48	0.17	0.03	0.13
	Infected	2.55	1.95	0.79	0.38	0.15	0.02	0.18
SE	Non_Infected	0.5	0.34	0.12	0.07	0.02	0.005	0.02
	Infected	0.4	0.3	0.12	0.06	0.02	0.004	0.02
CV (%)		32.85	16.72	16.11	19.72	8.41	4.76	28.27

a) Cgrain Value™ size, shape and color characteristics, (L) [mm], Width (W) [mm], Raw Thickness (T.RAW) [mm], Mean Width (AVG.W) [mm], Weight (WT) [g], Hue, Saturation, and Light; b) SmartGrain size and shape characteristics, Area size (AS) [mm2], Perimeter length (PL) [mm], Length (L) [mm], Width (W) [mm], Length to width ratio (LWR), Circularity (CS) Distance between IS and CG (DS) [mm].

components and correlations represents 60.50 and 19.90%, respectively, of the total variance. The LWR trait was shown to be the higher positive in the first principal component; similarly, hue was shown to be positive but in a lesser proportion. In the same component but with negative loading, we found CS as the variable with the highest contribution; the traits W from both methods, AVG.W, and T_RAW were also projected onto this component with a loading of a slightly lesser norm. Although saturation was also projected onto this component, it was shown to be the smallest loading. On the other hand, in the second principal component, the traits DS and L from both methods, PL, AS, V, and WT showed a high positive loading with similar proportions, whereas the trait light was the only one with a negative loading into the second principal component and the one with less projection among all the traits. In general, all the seed morphological traits assessed expressed variability and influence in the two principal components. In addition, as can be observed in the graph, the variation of LWR has an opposite

projection to the CS trait, expressing a good indicator to study the deformation of the grains caused by the disease infection.

Considering Table 1, the mean values for the same morphological traits measured by both methods (L and W) across the two sets, genebank and breeding, were similar. The difference between infected and non-infected seeds was 0.11 mm in L in both methods and between 0.21 and 0.25 mm in W and AVG_W. Both methods provide important parameters for seed morphology studies. Cgrain Value™ provides V and WT values and color information. Although these are important characteristics for different study purposes, mainly for identifying FHB-infected kernels, SmartGrain, in turn, provides information such as PL, AS, and CS that can show variabilities between infected and non-infected seeds. Here the BLUES for all the measured parameters were correlated with each other and in association with the visual scorings on the spikes (Figure 4). A moderate to high positive correlation was found with the color parameter hue, and a low positive
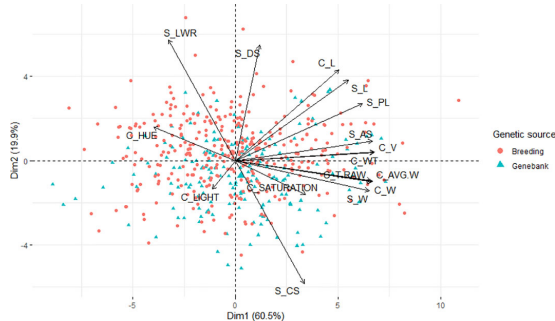
FIGURE 3
Principal component analysis biplot of the morphological traits collected with Cgrain Value™ and SmartGrain of the breeding and genebank seeds infected with different levels of Fusarium head blight.

correlation with light was given by Cgrain Value™ and LWR as well as given by SmartGrain ($r = 0.65$, $r = 0.36$, and $r = 0.27$, respectively). Negative correlations were also found between the visual evaluations of symptoms and the other characteristics in different levels of strength of association. There was no correlation between FHB visual scoring and DS ($r = 0.01$).

The multiple linear regression model developed to identify the contributions of the 16 different morphological traits provided by Cgrain Value™ and SmartGrain expressed a high moderate prediction ($R^2 = 0.58$), (Figure 5A). Aiming to identify which of both methods used in this study provides a higher prediction and also to identify the best morphological traits to predict FHB, two more models were constructed: one for the results given by Cgrain Value™ and another one for the results of SmartGrain. The model of Cgrain Value™ traits showed a moderate prediction ($R^2 = 0.52$), (Figure 5B). On the other hand, the model of SmartGrain traits showed medium–low prediction ($R^2 = 0.30$), (Figure 5C), clearly showing that the first model had
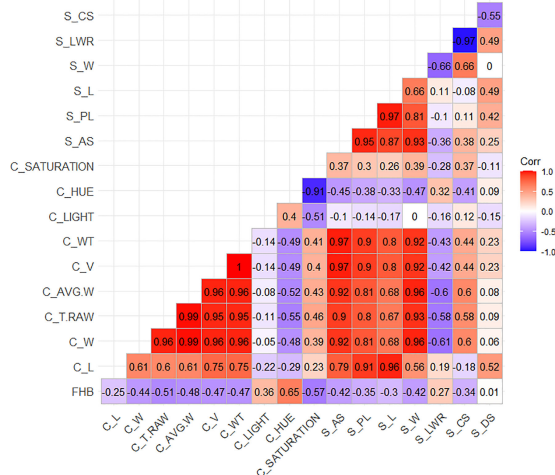
FIGURE 4
Sorted upper triangle correlation matrix among the morphological attributes of the wheat genotype seeds from the breeding and genebank sets collected with the Cgrain Value™ and the SmartGrain software.

FIGURE 5

Regression models for predicting Fusarium head blight in wheat: **(A)** all the characteristics obtained with Cgrain Value[TM] and SmartGrain, **(B)** Cgrain Value[TM] morphological traits, and **(C)** SmartGrain morphological traits.
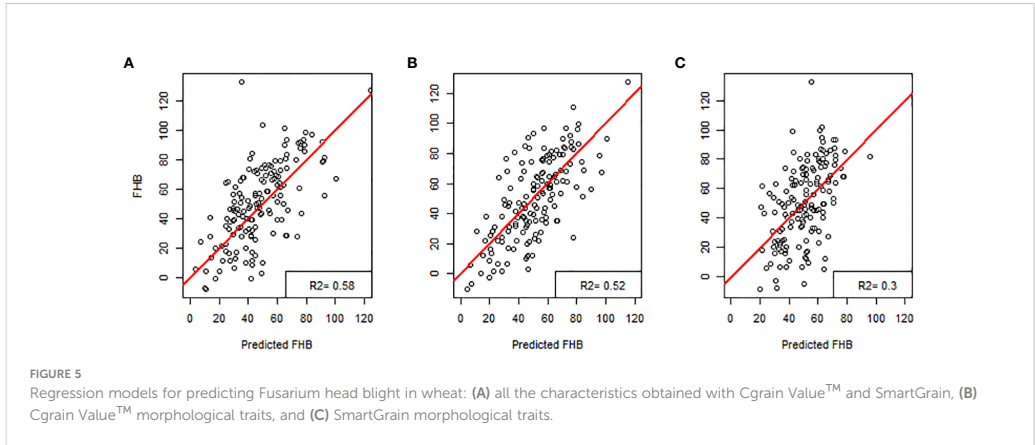
a higher prediction than separately. In addition, the morphological parameters that are the most suitable to assess FHB in grains above all the 16 evaluated were identified. According to the regression model and the ANOVA analysis, the parameters that provided more information about the disease are the length, width, thickness, average width, circularity, and the color parameters in the color representation HSL (Table 2). The sensitivity test showed that these variables provide the highest value of R-square, ($R^2 = 0.52$). These morphological traits are enumerated from most significant to least significant in Figure 6.

Discussion

This study compared the potential performances of two different image-based methods to predict FHB. The results of both indicated that morphological seed traits are functional for predicting FHB among two different sets of genotypes evaluated. Furthermore, a comparison of the applicability of the two methods was properly addressed by evaluating the cost, accuracy, and time efficiency—for instance, to extract dimension, shape, and color parameters, Cgrain Value[TM] utilizes a unique mirror design to inspect all possible angles of

TABLE 2 Summary of the multiple linear regression model combining all the 16 morphological characteristics provided by Cgrain Value[TM] and SmartGrain.

Model summary					
Morphological traits	**Sum sq**	**Mean sq**	**F-value**	**Pr (>F)**	
C_L	23,829	23,829	64.587	6.99E-15	***
C_W	51,079	51,079	138.446	< 2e-16	***
C_T.RAW	40,500	40,500	109.772	< 2e-16	***
C_AVG.W	2,013	2,013	5.456	0.0199	*
C_V	2,603	2,603	7.055	0.00816	**
C_WT	680	680	1.843	0.17526	
C_LIGHT	31,656	31,656	85.802	< 2e-16	***
C_HUE	39,386	39,386	106.752	< 2e-16	***
C_SATURATION	2,649	2,649	7.18	0.00762	**
S_AS	178	178	0.483	0.48734	
S_PL	624	624	1.691	0.1941	
S_L	3,027	3,027	8.204	0.00436	**
S_W	45	45	0.121	0.72828	
S_LWR	0	0	0.001	0.9802	
S_CS	1,651	1,651	4.476	0.03489	*
S_DS	539	539	1.461	0.22731	

The most significant characteristics concerning the Fusarium head blight disease infection according to the P-value has an *. (No significance P>0.05; *P≤0.05; **P≤0.01; ***P≤0.001).
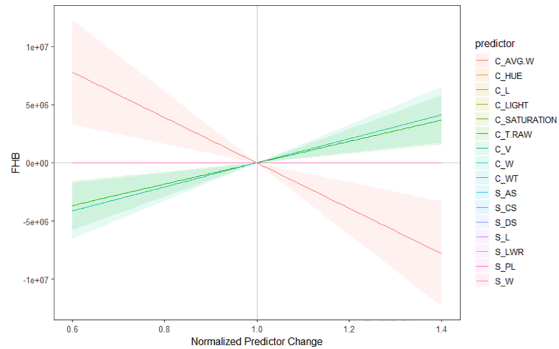
FIGURE 6
Sensitivity plot of the morphological characteristics to predict Fusarium head blight in wheat. The parameters are organized from the best predictors to the less significant to predict the disease. Color lines indicate the significance, considering red as the most important predictor and pink as the less important one. The highlighted regions reflect the correlation of the parameters among each other.

individual kernels in the sample. Additionally, image capture and processing are instantaneous, thanks to the hardware and software combination. Conversely, image acquisition using the SmartGrain system was carried out over a relatively long period, yet image processing was done relatively fast. However, compared with Cgrain Value™, the earlier approach is cheaper considering the cost of the tools used in image capture, requiring a simple RGB camera, a static frame, and the free software.

On the other hand, the morphological traits, based on the statistical analysis results, that showed significant correlations to the visual scores were color traits in the HSL color representation and thickness from Cgrain Value™, length and width, from both methods (Figures 5, 6). Although the other measured morphological traits were not significantly correlated to the visual scores, infected grains still expressed differences in these traits that may be ultimately informative about seed health and refine the prediction (Table 1). Nevertheless, DS was not correlated and did not express significant differences in infected seeds of FHB, but it could prove useful in other applications.

The evaluated visual scores of the symptoms associated with FHB—bleached, yellowish or discolored, and stunted spikes—were previously validated by the identification of several loci by genome-wide association studies (GWAS) (Appendix 1), in a previous study with the same plants and visual scorings (Zakieh et al., 2021). The proposed methods aim to replace costly and labor-intensive genetic analysis.

Therefore, the prediction of both methods studied here appears to be consistent for FHB with the assigned traits concerning the phenotype–genotype association. Previous investigations showed a high correlation between symptoms that are present on wheat heads and the rate of kernel damage (Góral et al., 2018). Therefore, it is feasible to reference the estimated visual scores of disease severity to establish similar results of association/disassociation with the corresponding assessments of grain traits following the methodology in this study.

An important aspect to highlight is that the percentage of disease severity can be assessed, where, in contrast to disease spread from the point of inoculation, it offers less intensive labor by spray inoculation of a larger number of wheat genotypes. Additionally, unlike point-inoculated wheat spikelets, spray-inoculated spikes allow for evaluating the degree of damage caused by the disease to all kernels of the infected spike. Within this work frame, whole spike kernels are investigated for their characteristics rather than the damage to a limited number of kernels caused by Fusarium colonization from the point of inoculation. This, in turn, is expected to shorten the period for disease resistance assessment, lower its cost, and be less labor demanding.

Conclusion

The results indicated that the traits with a higher correlation to FHB were length, width, thickness, and especially color values in HSL color representation. Moreover, Cgrain Value™ was advantageous to SmartGrain in terms of the time required for image capture and outperformed the latter when applied to a large number of samples, yet SmartGrain processes samples fast and is cheaper in comparison to Cgrain Value™. Although the disease prediction showed a low–moderate accuracy for SmartGrain and a high–moderate accuracy for Cgrain Value™ and the results of both methods combined, this is attributed to the prediction reference,

which corresponds to FHB disease severity scorings done on the spikes. However, the novelty of this study resides in the accuracy reached even with a different reference source, but which is directly related. Additionally, as the plant material genotypes and visual scores were validated by GWAS analysis, then the results presented here are phenotype–genotype-associated.

Data availability statement

The original contributions presented in the study are included in the article/supplementary material. Further inquiries can be directed to the corresponding author.

Author contributions

AC conceived the study. TH developed the breeding population set. MZ provided the material and the scores of the disease severity. MA performed the image and data acquisition with SmartGrain. RD performed the image and data acquisition with Cgrain Value[TM]. FL analyzed the data and wrote the draft. All authors contributed to the article and approved the submitted version.

Conflict of interest

The authors declare that the research was conducted in the absence of any commercial or financial relationships that could be construed as a potential conflict of interest.

Publisher's note

All claims expressed in this article are solely those of the authors and do not necessarily represent those of their affiliated organizations, or those of the publisher, the editors and the reviewers. Any product that may be evaluated in this article, or claim that may be made by its manufacturer, is not guaranteed or endorsed by the publisher.

References

Ackerman, A. J., Holmes, R., Gaskins, E., Jordan, K. E., Hicks, D. S., Fitzgerald, J., et al. (2022). Evaluation of methods for measuring fusarium-damaged kernels of wheat. *Agronomy* 12 (2), 532. doi: 10.3390/agronomy12020532

Agostinelli, A. M. (2009). *Phenotypic and genotypic selection for head scab resistance in wheat*. University of Kentucky Master's Theses. 582. Available at: https://uknowledge.uky.edu/gradschool_theses/582

Alvarado, G., López, M., Vargas, M., Pacheco, Á., Rodriguez, F., Burgueño, J., et al. (2015). META-R (Multi Environment Trail Analysis with R for Windows) Version 5.0. CIMMYT Research Data & Software Repository Network 23, 2015.

Asseng, S., Martre, P., Maiorano, A., Rötter, R. P., O'Leary, G. J., Fitzgerald, G. J., et al. (2019). Climate change impact and adaptation for wheat protein. *Global Change Biol.* 25 (1), 155–173. doi: 10.1111/gcb.14481

Balut, A. L., Clark, A. J., Brown-Guedira, G., Souza, E., and Van Sanford, D. A. (2013). Validation of Fhb1 and QFhs. nau-2DL in several soft red winter wheat populations. *Crop Sci.* 53 (3), 934–945. doi: 10.2135/cropsci2012.09.0550

Barbedo, J. G., Tibola, C. S., and Fernandes, J. M. (2015). Detecting fusarium head blight in wheat kernels using hyperspectral imaging. *Biosyst. Eng.* 131, 65–76. doi: 10.1016/j.biosystemseng.2015.01.003

Bauriegel, E., and Herppich, W. B. (2014). Hyperspectral and chlorophyll fluorescence imaging for early detection of plant diseases, with special reference to fusarium spec. infections on wheat. *Agriculture* 4 (1), 32–57. doi: 10.3390/agriculture4010032

Castro Aviles, A., Alan Harrison, S., Joseph Arceneaux, K., Brown-Guedira, G., Esten Mason, R., and Baisakh, N. (2020). Identification of qtls for resistance to fusarium head blight using a doubled haploid population derived from southeastern united states soft red winter wheat varieties ags 2060 and ags 2035. *Genes* 11 (6), 699. doi: 10.3390/genes11060699

Cgrain AB *Cgrain value TM, the new standard for analysis grain quality*. Available at: www.cgrain.se.

Chawade, A., Armonienė, R., Berg, G., Brazauskas, G., Frostgård, G., Geleta, M., et al. (2018). A transnational and holistic breeding approach is needed for sustainable wheat production in the Baltic Sea region. *Physiol. Plantarum* 164 (4), 442–451. doi: 10.1111/ppl.12726

Colmer, J., O'Neill, C. M., Wells, R., Bostrom, A., Reynolds, D., Websdale, D., et al. (2020). SeedGerm: a cost-effective phenotyping platform for automated seed imaging and machine-learning based phenotypic analysis of crop seed germination. *New Phytol.* 228 (2), 778–793. doi: 10.1111/nph.16736

Del Ponte, E. M., Moreira, G. M., Ward, T. J., O'Donnell, K., Nicolli, C. P., Machado, F. J., et al. (2022). Fusarium graminearum species complex: A bibliographic analysis and web-accessible database for global mapping of species and trichothecene toxin chemotypes. *Phytopathology*® 112 (4), 741–751. doi: 10.1094/PHYTO-06-21-0277-RVW

Delwiche, S. R., Kim, M. S., and Dong, Y. (2010). "Damage and quality assessment in wheat by NIR hyperspectral imaging," in *Sensing for agriculture and food quality and safety II: SPIE*, Vol.7676, 45–52.

De Mendiburu, F. (2014). Agricolae: statistical procedures for agricultural research. *R. Package Version* 1 (1), 1–4. doi: 10.7287/peerj.preprints.1404v1

Dissing, B. S., Papadopoulou, O. S., Tassou, C., Ersbøll, B. K., Carstensen, J. M., Panagou, E. Z., et al. (2013). Using multispectral imaging for spoilage detection of pork meat. *Food Bioprocess Technol.* 6 (9), 2268–2279. doi: 10.1007/s11947-012-0886-6

Femenias, A., Llorens-Serentill, E., Ramos, A. J., Sanchis, V., and Marin, S. (2022). Near-infrared hyperspectral imaging evaluation of fusarium damage and DON in single wheat kernels. *Food Control* 142, 109239. doi: 10.1016/j.foodcont.2022.109239

Gilbert, J., and Haber, S. (2013). Overview of some recent research developments in fusarium head blight of wheat. *Can. J. Plant Pathol.* 35 (2), 149–174. doi: 10.1080/07060661.2013.772921

Gomes, F. G. Jr, and Duijn, B. V. (2017). Three-dimensional (3-d) X-ray imaging for seed analysis. *Seed Testing Int.* 154), 48–52. Available at: https://www.scopus.com/inward/record.uri?eid=2-s2.0-85084478678&partnerID=40&md5=f95af32d6e967fe8630289cf7b49a4f0

Góral, T., Wiśniewska, H., Ochodzki, P., Nielsen, L. K., Walentyn-Góral, D., and Stępień, Ł. (2018). Relationship between fusarium head blight, kernel damage, concentration of fusarium biomass, and fusarium toxins in grain of winter wheat inoculated with fusarium culmorum. *Toxins* 11 (1), 2. doi: 10.3390/toxins11010002

Istvan, D. (2014). *"DigiCamControl software"*. 2.1.2. ed.

Iwata, H., Ebana, K., Uga, Y., Hayashi, T., and Jannink, J.-L. (2010). Genome-wide association study of grain shape variation among oryza sativa l. germplasms based on elliptic Fourier analysis. *Mol. Breed.* 25 (2), 203–215. doi: 10.1007/s11032-009-9319-2

Iwata, H., and Ukai, Y. (2002). SHAPE: a computer program package for quantitative evaluation of biological shapes based on elliptic Fourier descriptors. *J. Heredity* 93 (5), 384–385. doi: 10.1093/jhered/93.5.384

Jirsa, O., and Polišenská, I. (2011). Identification of fusarium damaged wheat kernels using image analysis. *Acta Universitatis Agricult. Silvicult. Mendelianae Brunensis* 59 (5), 125–130. doi: 10.11118/actaun201159050125

Josse, J., and Husson, F. (2016). missMDA: a package for handling missing values in multivariate data analysis. *J. Stat. Software* 70, 1–31. doi: 10.18637/jss.v070.i01

Khaeim, H. M., Clark, A., Pearson, T., and Van Sanford, D. (2019). Methods of assessing fusarium damage to wheat kernels. *Al-Qadisiyah J. For Agric. Sci. (QJAS) (P-ISSN: 2077-5822 E-ISSN: 2617-1479)* 9 (2), 297–308. doi: 10.33794/qjas.Vol9.Iss2.91

Komyshev, E., Genaev, M., and Afonnikov, D. (2017). Evaluation of the SeedCounter, a mobile application for grain phenotyping. *Front. Plant Sci.* 7, 1990. doi: 10.3389/fpls.2016.01990

Kuhn, M., Wing, J., Weston, S., Williams, A., Keefer, C., Engelhardt, A., et al. (2020). Package 'caret'. *R. J.* 223, 7. doi: 10.18637/jss.v028.i05

Lê, S., Josse, J., and Husson, F. (2008). FactoMineR: an r package for multivariate analysis. *J. Stat. Software* 25, 1–18. doi: 10.18637/jss.v025.i01

Lipka, A. E., Tian, F., Wang, Q., Peiffer, J., Li, M., Bradbury, P. J., et al. (2012). GAPIT: genome association and prediction integrated tool. *Bioinformatics* 28 (18), 2397–2399. doi: 10.1093/bioinformatics/bts444

Liu, W., Liu, C., Jin, J., Li, D., Fu, Y., and Yuan, X. (2020). High-throughput phenotyping of morphological seed and fruit characteristics using X-ray computed tomography. *Front. Plant Sci.* 11, 601475. doi: 10.3389/fpls.2020.601475

Lobet, G. (2017). Image analysis in plant sciences: publish then perish. *Trends Plant Sci.* 22 (7), 559–566. doi: 10.1016/j.tplants.2017.05.002

Lu, B., Dao, P. D., Liu, J., He, Y., and Shang, J. (2020). Recent advances of hyperspectral imaging technology and applications in agriculture. *Remote Sens.* 12 (16), 26–59. doi: 10.3390/rs12162659

Menesatti, P., Antonucci, F., Costa, C., Santori, A., Niciarelli, I., and Infantino, A. (2009). Application of morphometric image analysis system to evaluate the incidence of fusarium head blight wheat infected kernels. *Proc. Bornimer Agrartechnische Berichte* 69), 157–161. Available at: https://www.scopus.com/inward/record.uri?eid=2-s2.0-84876683478&partnerID=40&md5=44c21b369e2d5fdc1b165442fd8dbb7d

Mesterhazy, A. (2020). Updating the breeding philosophy of wheat to fusarium head blight (FHB): Resistance components, QTL identification, and phenotyping–a review. *Plants* 9 (12), 1702. doi: 10.3390/plants9121702

Polak-Śliwińska, M., and Paszczyk, B. (2021). Trichothecenes in food and feed, relevance to human and animal health and methods of detection: A systematic review. *Molecules* 26 (2), 454. doi: 10.3390/molecules26020454

Rangarajan, A. K., Whetton, R. L., and Mouazen, A. M. (2022). Detection of fusarium head blight in wheat using hyperspectral data and deep learning. *Expert Syst. Appl.* 208, 118240. doi: 10.1016/j.eswa.2022.118240

Saccon, F. A., Parcey, D., Paliwal, J., and Sherif, S. S. (2017). Assessment of fusarium and deoxynivalenol using optical methods. *Food Bioprocess Technol.* 10 (1), 34–50. doi: 10.1007/s11947-016-1788-9

Schroeder, H., and Christensen, J. (1963). Factors affecting resistance of wheat to scab caused by gibberella zeae. *Phytopathology* 53 (1), 831–838.

Shahin, M. A., and Symons, S. J. (2011). Detection of fusarium damaged kernels in Canada Western red spring wheat using visible/near-infrared hyperspectral imaging and principal component analysis. *Comput. Electron. Agric.* 75 (1), 107–112. doi: 10.1016/j.compag.2010.10.004

Shiferaw, B., Smale, M., Braun, H.-J., Duveiller, E., Reynolds, M., and Muricho, G. (2013). Crops that feed the world 10. past successes and future challenges to the role played by wheat in global food security. *Food Secur.* 5 (3), 291–317. doi: 10.1007/s12571-013-0263-y

Stack, R. W., and McMullen, M. P. (1998). *A visual scale to estimate severity of fusarium head blight in wheat.* NDSu Extension Circular: n. pag

Steed, A., King, J., Grewal, S., Yang, C.-Y., Clarke, M., Devi, U., et al. (2022). Identification of fusarium head blight resistance in triticum timopheevii accessions and characterization of wheat-t. timopheevii introgression lines for enhanced resistance. *Front. Plant Sci.* 13. doi: 10.3389/fpls.2022.943211

Tanabata, T., Shibaya, T., Hori, K., Ebana, K., and Yano, M. (2012). SmartGrain: High-throughput phenotyping software for measuring seed shape through image analysis. *Plant Physiol.* 160 (4), 1871–1880. doi: 10.1104/pp.112.205120

Team, R. C. (2013). *R: A language and environment for statistical computing.*

Wang, L., Uilecan, I. V., Assadi, A. H., Kozmik, C. A., and Spalding, E. P. (2009). HYPOTrace: image analysis software for measuring hypocotyl growth and shape demonstrated on arabidopsis seedlings undergoing photomorphogenesis. *Plant Physiol.* 149 (4), 1632–1637. doi: 10.1104/pp.108.134072

Whan, A. P., Smith, A. B., Cavanagh, C. R., Ral, J.-P. F., Shaw, L. M., Howitt, C. A., et al. (2014). GrainScan: a low cost, fast method for grain size and colour measurements. *Plant Methods* 10 (1), 1–10. doi: 10.1186/1746-4811-10-23

Yipeng, L., Wenbing, L., Kaixuan, H., Wentao, T., Ling, Z., Shizhuang, W., et al. (2022). Determination of wheat kernels damaged by fusarium head blight using monochromatic images of effective wavelengths from hyperspectral imaging coupled with an architecture self-search deep network. *Food Control* 135, 108819. doi: 10.1016/j.foodcont.2022.108819

Zakieh, M., Gaikpa, D. S., Leiva Sandoval, F., Alamrani, M., Henriksson, T., Odilbekov, F., et al. (2021). Characterizing winter wheat germplasm for fusarium head blight resistance under accelerated growth conditions. *Front. Plant Sci.* 12. doi: 10.3389/fpls.2021.705006

Zhu, F., Paul, P., Hussain, W., Wallman, K., Dhatt, B. K., Sandhu, J., et al. (2021). SeedExtractor: an open-source GUI for seed image analysis. *Front. Plant Sci.* 11, 581546. doi: 10.3389/fpls.2020.581546

Appendix 1

Quantitative trait loci (QTL) detected in genome-wide association studies employing seven models at p = 0.0001 (LOD $\geq$ 4) for Fusarium head blight severity in winter wheat from the breeding, genebank, and combined sets (Zakieh et al., 2021). Chr., chromosome; FAF, favorable allele frequencies. The asterisk means also detected by these models at p = 0.0002. A, detected above Bonferroni corrected threshold (α = 0.05). B, the marker effects are estimated for only GLM, MLM, and CMLM and FarmCPU in GAPIT (Lipka et al., 2012).

QTL	Marker	Chr.	Position (cM)	FAF	Effect	Model (s)	Set
SLUfhbchr1B.1	BS00021877_51	1B	154.58	0.06	NA	Blink	Combined
SLUfhbchr2A.2	BobWhite_c16923_64	2A	125.33	0.06	NA	Blink; (SUPER)*	Combined
SLUfhbchr3A.3	Kukri_rep_c89183_282	3A	15.05	0.64	27.84 to 28.10	GLM, CMLM	Combined
SLUfhbchr3B.4	wsnp_Ex_c34975_43204180	3B	67.45	0.95 (CS), 0.94 (BS), 0.97 (GS)	65.78 to 82.47	GLM, MLM, CMLM, SUPER, MLMM, FarmCPU, Blink	All
	Kukri_c18009_398a	3B	67.67	0.95	78.20 to 80.15	GLM, MLM, CMLM, SUPER	Combined
	wsnp_Ex_c5378_9505533	3B	68.71	0.94	NA	SUPER	Combined
SLUfhbchr3D.5a	RFL_Contig4591_1759	3D	0.00	0.94	51.94 to 54.69*	MLMM; (GLM, MLM, CLM, SUPER, Blink)*	Combined
	RAC875_rep_c115090_5	3D	0.00	0.02	NA	Blink	Breeding
SLUfhbchr3D.5b	JD_c7714_954	3D	143.01	0.04	NA	Blink, SUPER	Genebank
SLUfhbchr5A.6	RAC875_rep_c106118_339	5A	39.02	0.03	-31.55 to -29.40	GLM, MLM, SUPER, MLMM	Combined
SLUfhbch6A.7	Tdurum_contig46670_911	6A	128.26	0.96	NA	SUPER	Combined
SLUfhbchr7A.8	Kukri_c11530_92	7A	232.11	0.84	44.1	CMLM, SUPER, MLMM	Combined
	RAC875_c12733_1509a	7A	228.37	0.83	40.41 to 45.14	GLM, MLM, CMLM, SUPER, MLMM, FarmCPU, Blink	Combined
SLUfhbchr7B.9	wsnp_Ex_c351_689415	7B	143.23	0.02	NA	Blink, SUPER	Breeding
	RAC875_c8752_1079	7B	158.98	0.84	39.97*	SUPER; (CMLM)*	Combined

III

Heat, drought and combined stress impact on yield, phenotypic and gluten protein traits: Capturing stability of spring wheat in excessive environments

Sbatie Lama[1†], Fernanda Leiva[1†], Pernilla Vallenback[2], Aakash Chawade[1] and Ramune Kuktaite[1]

[1]Department of Plant Breeding, Swedish University of Agricultural Sciences, SE-23422 Lomma, Sweden

[2]Lantmännen Lantbruk, SE-26881 Svalöv, Sweden

†These authors contributed equally to this work.

* **Correspondence:** sbatie.lama@slu.se

Keywords: Wheat, drought, heat, heat-drought, phenotyping, gluten protein quality, stability.

Abstract

Wheat production and end-use quality are severely threatened by drought and heat stresses. This study evaluated stress impacts on phenotypic and gluten protein characteristics of eight spring wheat genotypes (Diskett, Happy, Bumble, SW1, SW2, SW3, SW4, SW5) grown to maturity under controlled conditions (Biotron) using RGB imaging and size-exclusion high-performance liquid chromatography (SE-HPLC). Among the stress treatments compared, combined heat-drought stress had the most severe negative impacts on biomass (real and digital), grain yield, and thousand kernel weight (TKW). Conversely, it had a positive effect on most gluten parameters evaluated by SE-HPLC and resulted in a positive correlation between spike traits and gluten strength, expressed as unextractable gluten polymer (%UPP), and large monomeric protein (%LUMP). The best performing genotypes in terms of stability were Happy, Diskett, SW1, and SW2, which should be further explored as attractive breeding material for developing climate-resistant genotypes with improved bread-making quality. RGB imaging in combination with gluten protein screening by SE-HPLC could thus be a valuable approach for identifying climate stress-tolerant wheat genotypes.

1. Introduction

Wheat (Triticum aestivum L.) is the third most common cereal produced worldwide, with more than 771 million tonnes harvested in 2021 (https://www.fao.org/faostat). Wheat provides approximately 20% of global total human dietary calories and 21% of daily protein consumption (Shiferaw et al., 2013). With increasing population and urbanization, consumption and associated demand for wheat-based food products is increasing (Peña, 2007), so sustaining wheat production and quality is important for ensuring food security. With ongoing climate change and global warming, extreme climate events and abiotic stresses are becoming more severe and unpredictable (Le Gouis et al., 2020). Climate events such as heat, drought, excessive rainfall, and high atmospheric concentrations of CO_2 are already affecting production and quality of wheat world-wide (Yadav et al., 2020). The extent of the losses depends on the plant growth stage affected and the severity of the stress (Wahid et al., 2007; Lan et al., 2022). Therefore, development of wheat genotypes that are resistant to various abiotic stresses is crucial for food security under ongoing climate change.

Among the abiotic stresses imposed by climate change, heat and drought stresses are considered to cause the most damage to wheat growth and development (Mamrutha et al., 2020). Drought during stem elongation and heat stress during the grain-filling stage have been identified as particularly important environmental factors affecting the yield and quality of wheat (Guzmán et al., 2016; Le Gouis et al., 2020). This is because drought and heat impair growth and development of different wheat plant organs, rate of photosynthesis, fertility, number of spikes, grain-filling, and nutrient uptake by the plant (Hurkman and Wood, 2011; Guzmán et al., 2016; Lan et al., 2022). Yield losses due to individual or combined heat-drought stresses have been observed in multiple countries in Europe, including Finland, Sweden, France, Belgium, and Switzerland (Kumar et al., 2020; Le Gouis et al., 2020; Lama et al., 2022). Areas such as the Mediterranean and southern Europe are experiencing higher impacts of heat-drought stress than other regions, causing major economic and food production losses (EEA, 2020). A 1-3°C rise in mean global air temperature is suggested to decrease wheat production by up to 28% (Shew et al., 2020; Zhang et al., 2022). In fact, in a previous study by our research group on field-grown wheat in Sweden, a yield reduction of up to 40% was observed under combined heat-drought conditions compared with rainy and cold conditions (Lama et al., 2022).

Wheat yield is generally the main focus in research, due to its direct relationship to food security (Asseng et al., 2019). However, manufacturers of different wheat-based food products, such as bread and pasta, require wheat flours with a specific protein quality (Johansson et al., 2020). Wheat quality is mainly determined by its major protein, gluten, the quantity and quality of which are often negatively impacted by heat and drought. For instance, the relatively high content of protein and strong gluten required in wheat bread flour (Kuktaite et al., 2004) is severely affected by intense heat and drought stresses (Lama et al.,

2022). Total protein content and gluten content are reported to increase by 65% and 32%, respectively under combined heat-drought stress compared with control conditions (Sattar et al., 2020). In greenhouse studies, the relative proportions of different types of proteins, such as high molecular weight (HMW) and low molecular weight (LMW) glutenins, and omega-, alfa/beta- and gamma-gliadins, have been found to increase under heat stress (35°C day temperature) compared with a control environment (Zhao et al., 2022).

The susceptibility of wheat plants to abiotic stresses depends mainly on the duration, frequency, and intensity of the stress conditions to which the plants are exposed (Barnabás et al., 2008; Farooq et al., 2009; Qaseem et al., 2019). Due to the adaptive metabolic and physiological mechanisms that wheat plants have developed, physiological responses at different developmental stages can differ between genotypes (Rampino et al., 2006). Plants under drought stress decrease their leaf area and increase canopy temperature in order to prevent water loss (Anjum et al., 2011), although heat stress combined with appropriate irrigation can increase transpiration rates and decrease canopy temperature (Singh et al., 2007). In combined heat-drought stress, there is an extreme effect on the physiological responses of wheat plants at all growth and reproductive stages (Rizhsky et al., 2002; Prasad et al., 2011). In combination, these two stresses can have complex contradictory effects compared with when they occur separately (Zhou et al., 2017).

Physiological traits of wheat, such as growth and characteristics related to yield, are commonly assessed by visual or manual annotation methods, but these tend to be subjective, time-consuming, and laborious (Dhondt et al., 2013). Therefore non-destructive remote and proximal phenotyping techniques are becoming more popular and more widely used (Armoniené et al., 2018; Leiva et al., 2021; Tao et al., 2022). Such methods have been developed to extract data

mainly from images in the visual and electromagnetic spectrum on several plant traits with high accuracy, reliability, and time resolution (Humplík et al., 2015; Chawade et al., 2019; Reynolds et al., 2019). Cameras that provide spectral information for each pixel in an image, such as multispectral and hyperspectral data, have proven to be a valuable tool for studying plants under abiotic stresses (Cao et al., 2019). The main difference between multispectral and hyperspectral data is the number of bands in the light spectrum (5-10 bands and hundreds, respectively) (Sara et al., 2021). However, these cameras are expensive and require sophisticated statistical methods for data processing (Zubler and Yoon, 2020). Low-cost digital RGB cameras can readily estimate plant shoot biomass, development, and growth rate, and can be a suitable tool for mapping plant responses under heat and drought (Blum et al., 1997; Humplík et al., 2015).

Phenotypic traits such as plant growth and yield and grain quality characteristics are important for sustaining the supply of wheat-based food products. Thus, a clear understanding of wheat response mechanisms to heat, drought, and combined heat-drought stresses is essential. In addition, since phenotypic traits (e.g., yield/grain weight) and wheat protein quality parameters are usually negatively related (Daniel and Triboi, 2000; Johansson et al., 2005), the stability of these attributes under climate change is complex and needs to be investigated.

The aim of this study was to determine the effects of individual and combined heat-drought stresses on phenotypic plant growth characteristics, yield, and gluten protein quality parameters of spring wheat genotypes grown in highly controlled environments. Plant growth and development under heat, drought, and combined heat-drought stresses were monitored using RGB imaging, and gluten protein quality characteristics of wheat grain were assessed by SE-HPLC. The stability of yield and of gluten protein quality parameters

for different spring wheat genotypes grown under stress conditions was also evaluated.

2. Materials and Methods

2.1. Plant material

Eight spring wheat genotypes (Diskett, Happy, Bumble, SW1, SW2, SW3, SW4, and SW5) developed in the breeding program at Lantmännen Lantbruk, Svalöv, Sweden, were evaluated. The selected genotypes represented a range in gluten strength, as identified when grown in the field in our previous study (Lama et al., 2022). Diskett, Bumble, and SW3 represented genotypes with unstable gluten strength (>5% variation between years), while Happy, SW1, SW2, SW4, and SW5 represented genotypes with stable gluten strength (<5% variation between years) (Lama et al., 2022).

2.2. Experimental design and description of stress environments

The spring wheat plants were grown in a randomized complete block design under three stress environments (heat, drought, combined heat-drought), which were applied simultaneously. The plants were grown in plastic pots (20 cm x 16 cm, volume 3.5 L) in peat-based soil, with three plants per pot. Two weeks after emergence, a plant cone (61 x 25 cm) was inserted in each pot to support the growing plants. Each pot was considered a biological replicate, and four biological replicates were used per genotype.

The pots containing the eight genotypes were grown in two Biotron climate chambers with artificial lighting from February to June 2020 at SLU, Alnarp, Sweden (Tables S1 and S2, Supplementary Information (SI)). Growing conditions in terms of temperature, humidity, and day length (hours) were based on mean five-year (2016-2020) weather data for the growing period in Malmö, Sweden (22 April-11 August) obtained from the Swedish Meteorological and Hydrological Institute (SMHI) (www.smhi.se). Daylight intensity of

400 μmol m-2s-1, produced with LED lights, was provided during the growing period. Until the start of the stress treatments, all plants were watered every two days with approximately 500 mL water per pot. The drought, heat, and combined heat-drought stress treatments (information below) were introduced at the beginning of heading stage (Zadoks 50), at approximately 56 days after sowing, and were applied for five days, resulting in signs of stress in the plants (dry, yellow leaves) (Figure 1a).

Heat. In this treatment, the temperature was kept at 29°C during day and night for five days and the 56-day-old plants were watered as in the control (500 mL water/pot every two days) (Table S1). After five days, the temperature was returned to the control level (15°C) (Table S1).

Drought. Plants assigned to the drought treatment began heading (Zadoks 50) slightly earlier than the plants in the other treatments. Drought stress was thus applied to 51-day-old plants, by stopping all watering of the plants for five days. After five days, normal watering was resumed (500 mL water/pot every two days).

Combined heat-drought stress. In this treatment, the 56-day-old plants received no water for five days and the temperature was maintained at 29oC during day and night (Table S1). After five days normal watering was resumed and the temperature was set to control conditions (Tables S1 and S2).

Wheat plants still growing eight days after stopping the stress treatments were considered recovered plants. The digital biomass of all plants was recorded at three time points (Tp1 = no stress, Tp2 = after five days of stress treatment, Tp3 = after eight days of recovery) (Table 1).

2.3. Image acquisition

The biomass of the wheat plants was assessed digitally from the top and side through RGB imaging in a laboratory with LED light, using two Canon EOS 1300D DSLR cameras with an 18-55 mm kit lens (Armonienė et al., 2018). The cameras were mounted on a SpaceArm (Tristar) at 1 m for the top view and on a tripod at 1.5 m for the side view. Plant pots were placed manually on a top-quality Intelligent 360 Photography turntable platform (Shenzhen Comxim Technology Co., Ltd., Shenzhen, Guangdong, China) and individually photographed using the DigiCamControl software (Istvan, 2014). During the side-view imaging, the plant pot was rotated by 90° four times, to acquire four images (front, right, left, and back projections). Shadows and light differences were adjusted by camera settings and exposure. For both cameras, focal length was set at 18 mm and ISO 1600, while light exposure was set as F-Stop f/13 and exposure time 1/60 s for the top-view camera, and F-Stop f/8 and exposure time 1/40 for the side-view camera. The images obtained were stored in JPEG format, using resolution 3456 x 2304 pixels for top projection and 5184 x 3456 pixels for side projection.

2.4. Image processing

The digital biomass of each plant was automatically extracted with EasyLeaf software (Easlon and Bloom, 2014). Since all images were acquired under the same light conditions, the red and green thresholds in the software and the individual ratios of RGB values (green/red (G/R)) and green/blue (G/B)) were set using the first image of each measuring occasion (Tp) and then processed in batch. Finally, projected leaf area (PLA) was obtained from the average of the five plant images (top at 0° and four sides at 90°) as:

$$PLA = \sum_{1}^{n} pla$$

2.5. Phenotypic traits

The height of all three plants in each pot was measured with a ruler as the distance from the soil surface to the tip of the spike, excluding the awns. To measure the spike length (mm), the

tallest spike of each plant in the pot was selected and the length of the spikes was recorded from the base of the rachis to the tip of the terminal spikelet, excluding the awns. Spike width (mm) was measured on these same spikes, at a point halfway along the spike height. Weight of fresh biomass (g), including the weight of spikes (g), per pot was recorded. Thousand kernel weight (TKW) (g) was calculated as described by Wu et al. (2018). Number of spikes was counted for each plant per pot and grain yield (g) was recorded per plant.

2.6. Gluten protein parameters in the flour

Size exclusion-high-performance liquid chromatography (SE-HPLC) was used to evaluate the gluten protein characteristics of the harvested grain. Seeds from the different genotypes grown at different stresses and control samples were milled into flour using a homogenizer (Mixer Mill MM 400, Retsch) for 30 s at 30 Hz. The flours were freeze-dried (Cool safe Pro, LaboGene) for 24 hours in order to remove all moisture prior to SE-HPLC analysis. A two-step gluten protein extraction method was performed according to Lama et al. (2022), with some modifications where collected supernatant (after 1st and 2nd steps) in SE-HPLC vials was heated at 80°C for 2 min (to inactivate proteases) in a water bath according to Islas-Rubio et al. (2006). Samples were run on the SE-HPLC system in triplicate. Concentrations of TOTE (SDS-extractable proteins), TOTU (SDS-unextractable proteins), %UPP (percentage of SDS-unextracted polymeric proteins in total polymeric proteins), and %LUMP (percentage of large SDS-unextracted large monomeric proteins in total large monomeric proteins) were calculated according to Lama et al. (2022). Total polymeric proteins (TPP) and total monomeric proteins (TMP) were calculated as LPP+SPP+LPPs+SPPs and LMP+SMP+LMPs+SMPs, respectively, where LPP, SPP, LMP, and SMP are SDS-extractable large polymeric proteins, small polymeric

proteins, large monomeric proteins, and small monomeric proteins, respectively, and LPPs, SPPs, LMPs, and SMPs are the corresponding SDS-unextractable form.

2.7. Statistical analysis

Statistical analyses were performed using the software R (Team, 2013). Principal component analysis (PCA) using the R packages FactoMineR and two-way analysis of variance was conducted, with Tukey's post hoc test ($p<0.05$), to assess the effect of different treatments on the gluten protein parameters and phenotypic traits. Spearman correlation analysis ($p<0.05$) (R package Corrplot) was applied for all gluten protein parameters and phenotypic traits in plants in each treatment. GGE biplots analysis (R package Metan) was performed to evaluate the stability of the studied genotypes in the different growing environments. The selected GGE tools were "mean vs. stability", "which-won-where view of the GGE biplots", and "ranking genotypes". These tools facilitate the identification of the optimal genotypes based on performance and stability, identify the optimal genotype for each growing environment, and rank them according to suitability for a growing environment.

3. Results
3.1. Digital biomass assessment

The digital wheat biomass assessed by RGB imaging at time points Tp1, Tp2, and Tp3 differed between the genotypes for the different stress conditions tested (Figure 1). The greatest differences in plant appearance were observed for the genotype Diskett in the combined heat-drought stress treatment (Figure 1; at Tp2 and Tp3). The impact of drought was similar to that of combined heat-drought at Tp2 and Tp3, with both treatments resulting in semi-dry plants (Figure 1b, 1d). The heat stress treatment had mild effects on the plants (Figure 1c).

Mean digital biomass measured at flowering (anthesis) was similar for all genotypes at Tp1 and decreased for all genotypes at both Tp2 and

Tp3. The greatest impact of the stress treatments was observed in the drought and combined heat-drought treatments, followed by heat (Figure 2). The greatest variation in mean digital biomass between the different genotypes was observed under drought and combined heat-drought (Figure 2).

Under control conditions, rather similar digital biomasses at Tp1-Tp3 were observed for all genotypes except SW1 and SW3 (Figure 3a). Genotype SW3 had relatively higher digital biomass at Tp2 and Tp3, while in SW1 it was somewhat lower. Drought reduced the digital biomass of all genotypes compared with the control, and especially that of SW1 and SW4 (Figure 3b). Heat stress had almost no impact at Tp1 and Tp2, but some impact at Tp3, especially for Bumble, SW2, and SW4 (Figure 3c). Diskett, SW1, and SW3 showed relatively similar digital biomass at Tp1-Tp3 in the heat stress treatment (Figure 3c). In the heat-drought treatment, the digital biomass was significantly reduced in all genotypes at Tp2 and Tp3, although the reduction observed between Tp2 and Tp3 was somewhat smaller for Happy (Figure 3d).

3.2. Effect of genotypes and stress conditions on gluten protein parameters

The impact of genotype (G) and stress environment (E) on the protein parameters was significantly dominated by individual effect, and not by G and E interaction (G x E) (Table 2, Table S3 in SI). A significant impact of G x E interaction was observed on Mon/pol ratio (p<0.01) and TOTU (p<0.05) (Table 2). The G x E interaction had a significant impact in particular on unextractable gluten polymers (LPPs and SPPs) and smaller monomeric proteins (SMP) (Table S3).

Evaluation of the effect of the different treatments on the gluten protein parameters by Tukey's post hoc test indicated a major impact of the combined heat-drought stress conditions on the gluten protein parameters, with

significant effects on TOTE, TOTU, TPP, TMP, and %UPP in comparison with the other environmental conditions (Table 3).

A similar impact of heat-drought stress was observed on most gluten parameters studied (Table 3), and some impact of heat stress on TMP, %LUPP, SPP, and LMPs (Table 3, Table S4 in SI) in comparison with drought stress. Surprisingly, no significant differences between the drought stress treatment and the control were found for any of the gluten protein parameters studied except %UPP and %LUPP (Table 3). Lower amounts of %UPP and %LUPP (gluten strength) and, somewhat unexpectedly, a higher amount of LPP was found under the control environment compared with the drought and heat stress treatments (Tables 3 and S4).

3.3. Relationship between genotypes, phenotypic traits, and gluten parameters under different stress environments

In PCA plots, mean values of the phenotypic and gluten protein characteristics for plants in the four environments (treatments) explained 65.6% of the variation (PC1 52.9%, PC2 12.7%) (Figure 4). The strongest impact on the genotypes was observed in the combined heat-drought treatment, for genotypes Diskett and SW2 (Figure 4). Sensitivity to heat stress and heat-drought stress was observed for genotype SW1 (Figure 4).

Yield, phenotypic characteristics, and gluten protein parameters explained 52.8% of the variation in PCA (PC1 31.6%, PC2 21.2%) (Figure 5). The major contributors to these two PCs were %UPP (control and drought), TOTU (heat, heat-drought, and control), and spike length (all treatments), which impacted SW4 and SW2 most, further followed by Diskett. Happy, SW3, and SW5 showed a similar low response to the stresses, together with grain yield (all treatments) (Figure 5). Bumble displayed a similar response in spike width (all stress treatments and control), %LUMP

6

(control, heat, and heat-drought), and %UPP (heat and heat-drought) (Figure 5).

The Spearman's rank correlation results indicated a significant impact of the treatments on certain gluten protein parameters, yield, and phenotypic traits (Figure 6). In the control (unstressed) environment, a significant positive correlation was found between grain yield and digital biomass at all three time points (Tp1-Tp3) ($p<0.001$), and between grain yield and number of spikes ($p<0.01$) (Figure 6). Experimentally measured biomass showed a significant positive correlation with digital biomass at Tp1, Tp2, and Tp3 ($p<0.001$, $p<0.05$, and $p<0.001$, respectively) (Figure 6a). The strongest significant negative correlations were found between TKW and the protein parameters (TOTE, TMP, TPP ($p<0.001$); TOTU ($p<0.01$)) (Figure 6a).

In all stress treatments, grain yield was significantly positively correlated with biomass ($p<0.001$), while significant positive correlations were also found between grain yield and digital biomass under heat ($p<0.01$) and under combined heat-drought stress ($p<0.05$) (Figure 6c and 6d).

Under drought treatment, a negative significant correlation was found between digital biomass (at Tp2) and most of the protein parameters studied (TOTU, TPP TMP and TOTE; $p<0.001$) (Figure 6b). Additionally, TPP, TMP, and TOTE showed a significant negative correlation with grain yield (Figure 6b).

Under individual drought and heat stresses, a significant negative correlation between digital biomass (at Tp3 and Tp2) and %UPP ($p<0.01$ and $p<0.05$, respectively) was observed (Figures 6b and 6c). Under heat stress, only TKW was significantly positively correlated with plant height ($p<0.05$).

In combined heat-drought stress conditions, a significant negative correlation was found between grain yield and protein parameters (TOTE, TMP, and TPP; $p<0.001$) (Figure 6d).

TOTU showed significant positive correlations with digital biomass at Tp1 ($p<0.001$) and with the phenotypic traits spike length, number of spikes, and TKW ($p<0.05$). In addition, number of spikes was significantly positively correlated with %UPP ($p<0.001$) and %LUMP ($p<0.01$) (Figure 6d).

Comparisons of the impact of the stress treatments on selected yield traits (grain yield and TKW) and gluten parameters (%UPP, LPP, Mon/pol, and TOTE) for individual genotypes revealed some variation (non-significant) between the genotypes (Figure 7). Combined heat-drought stress decreased grain yield in most genotypes (Figure 7a). However, Bumble and SW1 in the combined heat-drought treatment showed similar grain yield as in the control. Regarding TKW, no impact of the stresses was observed for most genotypes, except a decrease due to combined heat-drought stress for SW3, SW4, and SW5 (Figure 7a).

In terms of gluten protein characteristics, a clear increase in both %UPP and LPPs (gluten strength) was noted for SW2, which had the highest %UPP (52.5%) of all genotypes studied (Figure 7b). Concerning Mon/pol ratio (describing extensibility vs. strength distribution), no difference due to the stresses was found between the genotypes. Total extractable protein (TOTE), a strong indicator of protein concentration, was found to be increased most under combined heat-drought stress in genotype SW2 (Figure 7b).

3.4. Stability of yield and protein quality traits under stress

The GGE biplots of PC1 and PC2 scores indicating stability and performance of the wheat genotypes in terms of grain yield, TKW, TOTE, and %UPP in the different treatments are shown in Figure 8. PC1 and PC2 together explained 93.61% of the variation in grain yield, 90.2% of the variation in TKW, 95.22% of the variation in %UPP (gluten strength), and 97.79% of the variation in TOTE (protein

7

concentration) (Figure 8). To identify stable genotypes, the GGE biplots of mean performance and stability across the environments were compared, where 1, 2, 3, and 4 in Figure 8 correspond to control, drought, heat, and combined heat-drought, respectively.

The grain yield (g/plant) plot for 'mean vs. stability' revealed the most promising genotypes (Figure 8a). SW3 showed the highest mean value for grain yield, followed by Happy, while Diskett and SW4 showed the lowest grain yield in the studied environments (Figure 8a). The five connected points in the 'which-won-where' GGE biplots showed that plants in the drought, heat, and combined heat-drought treatments clustered close to each other and indicated that the genotypes Bumble, SW5, Happy, and SW3 were the top performers in the studied environments (Figure 8b). Ranking the genotypes according to their location in the circles in the GGE biplots confirmed that the genotypes Happy and SW3 were the top performers, i.e., located closest to the "ideal line" (Figure 8c).

Stability in TKW appeared to be higher for the genotype Happy (Figure 8d). The genotypes Bumble and SW3 showed the highest stability, but the lowest mean values, for TKW (Figure 8d). The five connected points in the 'which-won-where' GGE biplots showed that the control, drought, and heat treatments (1, 2, 3, respectively) clustered in the same section, with Happy and SW4 indicated as the top performers (Figure 8e). For the combined heat-drought environment, the top performer in terms of TKW was Diskett (Figure 8e). Based on its location in the inner circle and position near the "ideal line", Happy was identified as the top-ranking genotype (Figure 8f).

The GGE biplots indicated that stability in %UPP among the genotypes in the studied environments was highest in terms of mean value for SW2, followed by Bumble (Figure 8g). The 'which-won-where' GGE biplots indicated that SW2 was the top performer in the

control, drought, and combined heat-drought treatments, while Bumble was the top performer in the heat and combined heat-drought treatments (Figure 8h). The highest ranking genotypes in all four environments were SW2 and Bumble (Figure 8i).

Stability evaluation of TOTE in the GGE biplots showed that the highest mean values across the studied environments were for Diskett and SW1 (Figure 8j). Based on the 'which-won-where' GGE biplots, Diskett was a top performer in all four environments, while SW1 was a top performer in the control, drought, and heat treatments (Figure 8k). SW2 and SW5 were the top performers in the combined heat-drought treatment (Figure 8k). To conclude, the top-ranked genotypes in all environments for TOTE were Diskett and SW1 (Figure 8l).

4. Discussion

Accurate tools for evaluating the yield, phenotypic traits, and quality traits of wheat genotypes under changing climate conditions are important when selecting new cultivars. Among the abiotic stresses to which plants are subjected, drought, heat, and combined heat-drought are major limiting factors affecting wheat plant development. In this study, combined heat-drought stress had the greatest impact on digital biomass (assessed by RGB imaging) in the eight wheat genotypes studied. The drought treatment also significantly reduced the digital biomass, whereas the heat stress treatment had a relatively mild impact (Figures 1 and 2). A similar pattern has been observed previously under combined heat-drought stress conditions for Nordic wheat grown in controlled conditions and Lithuanian winter wheat grown in the field (Statkevičiūtė et al., 2022). These observations suggest that the combined stress affects physiological plant traits such as stomatal closure, which leads to decreased CO_2 assimilation and lower TKW (Abdelhakim et al., 2021; Statkevičiūtė et al., 2022). The magnitude of the reduction in biomass is known to depend on the duration and

intensity of the stress and when the stress is imposed (Barnabás et al., 2008; Farooq et al., 2009; Qaseem et al., 2019).

In this study, wheat plants were exposed to the different five-day stress treatments during anthesis, which is known to be one of the most critical growth stages, explaining the strong impact of the treatments involving drought. Applying heat stress alone had a mild impact on plant development characteristics and biomass of individual genotypes, so it was not possible to evaluate plant response mechanisms to this stress. The chosen heat stress temperature (29°C) was based on findings in previous studies that a temperature of 27-30°C or higher prior to and during anthesis can substantially reduce grain size, numbers, and yield (Tashiro et al., 1989; Wheeler et al., 1996; Porter et al., 2005; Semenov and Shewry, 2011).

As expected, drought and combined heat-drought stress decreased biomass accumulation (Figure 3). The lack of impact of heat stress alone on biomass was most likely insufficiently high temperature and short treatment time resulting in little damage to photo-system II and thus to photosynthetic capacity (Sharkey, 2005), as seen for Bumble and SW2 at Tp2 (Figure 3c). For example, Diskett plants responded less to heat than to drought or combined heat-drought stress, despite the PCA results indicating some sensitivity of this genotype to heat stress (Figure 4). This can be explained by a different response mechanism of Diskett to heat and heat-drought stresses, as referred to our previous study (Lama et al 2022). For detailed examination of the heat response of Diskett, field studies under heat stress conditions are needed.

The digital tools used in this study to measure digital biomass showed good ability to evaluate wheat plants under severe drought and combined heat-drought stress conditions. The correlations observed between digital and measured biomass, e.g., under drought conditions (at Tp3) and combined heat-drought conditions (at Tp2), revealed strong potential of

RGB imaging to identify even small differences induced by stresses and to detect symptoms of the genotypes under the different environments. Under heat stress, the genotypes SW1 and SW3 were least affected (Figure 3c), while under combined heat-drought stress Happy and SW3 were the least affected genotypes (Figure 3d), suggesting somewhat different stress coping mechanisms.

In the control (no stress) growing environment, most gluten parameters (TOTE, etc.) showed a negative correlation with grain yield, TKW, biomass, plant height, and spike width (Figure 6a), as also observed previously (Bogard et al., 2011; Wang et al., 2018). Thousand kernel weight and grain yield are closely associated (Li et al., 2021) and are linked with starch accumulation. High accumulation of starch under the control conditions can dilute the gluten protein concentrations in wheat grain (Koga et al., 2015), which may be one explanation for the negative correlations between gluten proteins and yield-related parameters in this study.

This study examined the impact of stress factors on the most important gluten quality parameters, e.g., gluten strength, based on the concentrations of polymeric proteins. Under individual drought and heat stress, a negative correlation between %UPP and digital biomass (Tp2-Tp3) was observed. There was also a clear impact of stress on the %UPP and %LUPP fractions (Table 3), suggesting that these environmental stresses trigger mechanisms related to gluten polymer accumulation/regulation. In the presence of severe stress (combined heat-drought treatment), the wheat plants seemed still able to produce spikes, as number of spikes correlated positively with %UPP.

Spike length is a strong indicator of yield (Lan et al., 2022) and is directly related to starch accumulation, suggesting that wheat yield and protein polymerization are in some way related. Under stress conditions, gluten polymerization is triggered via formation of interchain

9

disulfide bonds (SS) between HMW and LMW glutenins and certain gliadins (alpha, beta, gamma) (Branlard et al., 2020). These gluten proteins form %UPP most likely at the expense of starch. Previous studies have found that, in particular, large polymeric protein fractions (e.g., uLPP and uSPP) increase at 12-18 days after anthesis (Johansson et al., 2005). Under combined heat-drought stress conditions in the present study, yield was significantly negatively correlated with protein concentration, confirming findings in previous studies in the field and greenhouse (Triboi et al., 2006; Malik et al., 2012).

A positive effect of abiotic stress on gluten protein polymerization has also been observed in previous studies performed in the field (Johansson, 2002; Johansson et al., 2002; Lama et al., 2022) and greenhouse (Malik et al., 2011; Leiva et al., 2021). The positive effect of heat stress on protein polymerization is known to occur at high temperatures (up to 30°C) during grain development stage (Johansson et al., 2002; Malik et al., 2011). The nature of the effect of drought stress on polymerization depends on the timing of the drought (Leiva et al., 2021; Lan et al., 2022). For example, a greenhouse study found a positive effect of drought at heading, which increased %UPP compared with drought at stem elongation stage (Leiva et al., 2021). Late drought (during ear emergence) is reported to have a stronger positive effect on %UPP than early drought (during tillering) (Lan et al., 2022). Among the three stress treatments tested in this study, combined heat-drought stress had the greatest effect on gluten protein polymerization.

The results obtained with the imaging tools employed to measure digital biomass at different stress time points (Tp1, Tp2, Tp3) in this study were significantly and positively correlated with grain yield and with actual measured biomass, suggesting that RGB imaging could be a useful method for evaluating the impacts of plant stresses on phenotypic characteristics, such as grain yield.

No significant effect was found for the interaction between genotype and environment (G x E) on gluten protein parameters (except for Mon/pol), contradicting findings in previous studies in the greenhouse (Malik et al., 2013) and in the field (Hernandez-Espinosa et al., 2018; Lama et al., 2022). This lack of effect may have been due to insufficiently challenging environmental background in this study.

Among the eight genotypes compared, Happy was the most promising in terms of stability of grain yield, TKW, %UPP, and TOTE in stressful growing environments. Happy also showed greater digital biomass in the combined heat-drought stress treatment. The breeding line SW2 showed lower digital biomass and yield under stress, but also the highest stability and mean gluten strength (%UPP) in the control and in all three stress treatments, supporting previous findings (Lama et al., 2022). Genotype SW3 showed the highest stability in TKW and higher grain yield than the other genotypes. Diskett, SW5, and SW1 appeared to be the most sensitive genotypes in terms of most parameters studied (yield, TKW, %UPP, etc.).

5. Conclusions

Assessing and controlling important phenotypic and grain quality-related traits in wheat is important for success in breeding programs seeking to produce desirable wheat material for use under future climate change. This study revealed significant impacts of combined heat-drought stress on plant phenotypic characteristics and gluten protein quality traits in eight spring wheat genotypes, while drought stress alone also had negative impacts. However, heat stress (29°C) had only mild effects on yield and phenotypic characteristics, although in field conditions the impact of heat stress could be much more severe.

There were significant positive correlations between grain yield and digital biomass, and between digital biomass and actual measured

biomass, in all stress treatments tested, indicating that RGB imaging can be a valuable tool in assessing stress in wheat plants.

Individual drought and heat stresses significantly affected gluten strength (%UPP and %LUPP). There was a negative correlation between digital biomass and most gluten protein parameters analyzed, although Mon/pol ratio was not affected by the experimental stresses studied.

A surprising finding was that number of spikes was significantly positively correlated with both %UPP and %LUMP under combined heat-drought stress, suggesting a correlation not only with polymeric glutenins (HMW and LMW) but also with large monomeric proteins (e.g., gliadin types). Number of spikes is an indicator of yield and, together with gluten protein quality traits, could potentially be explored in screening for high yield and gluten protein quality in wheat under climate stress.

The most promising genotypes in terms of performance and stability in the stress environments tested were SW3 and Happy for high yield, SW1 and Happy for high TKW, SW2 and Bumble for high %UPP, and Diskett and SW1 for high protein concentration (TOTE). In order to meet plant breeding targets for extreme climate resistance, these top-performing genotypes need to be further tested in field studies where their phenotypic and gluten protein characteristics are evaluated using the combination of tools tested in this study.

Conflict of Interest

The authors declare that the research was conducted in the absence of any commercial or financial relationships that could be construed as a potential conflict of interest.

Author Contributions

RK and AC conceived the study. RK, AC, SL, and FL planned the greenhouse experiments. PV developed the breeding population set. SL and FL performed the greenhouse experiments, analyzed the data, and wrote the manuscript, with inputs from RK and AC. RK acquired the funding. All authors contributed to data interpretation and approved the final version of the manuscript.

Supplementary Material

The Supplementary Material for this article can be found online at:

Data Availability Statement

The original data obtained in the study are presented in the article/Supplementary Information. Other inquiries can be directed to the corresponding author.

References

Abdelhakim, L.O.A., Rosenqvist, E., Wollenweber, B., Spyroglou, I., Ottosen, C.-O., and Panzarová, K. (2021). Investigating combined drought- and heat stress effects in wheat under controlled conditions by dynamic image-based phenotyping. Agronomy 11(2), 364.

Anjum, S., Xie, X.-y., Wang, L.-c., Saleem, M., Man, C., and Lei, W. (2011). Morphological, physiological and biochemical responses of plants to drought stress. Afr. J. Agric. Res. 6. doi: 10.5897/AJAR10.027.

Armonienė, R., Odilbekov, F., Vivekanand, V., and Chawade, A. (2018). Affordable imaging lab for noninvasive analysis of biomass and early vigour in cereal crops. Biomed Res. Int. 2018.

Asseng, S., Martre, P., Maiorano, A., Rötter, R.P., O'leary, G.J., Fitzgerald, G.J., et al. (2019). Climate change impact and adaptation for wheat protein. Glob. Chang. Biol. 25(1), 155-173. doi: 10.1111/gcb.14481.

Barnabás, B., Jäger, K. & Fehér, A. (2008). The effect of drought and heat stress on reproductive processes in cereals. Plant, Cell Environ. 31, 11–38.

Blum, A., Sullivan, C.Y., and Nguyen, H.T. (1997). The effect of plant size on wheat response to agents of drought stress. II. Water deficit, heat and ABA. Funct. Plant Biol. 24(1), 43-48. doi: https://doi.org/10.1071/PP96023.

Bogard, M., Jourdan, M., Allard, V., Martre, P., Perretant, M.R., Ravel, C., et al. (2011). Anthesis date mainly explained correlations between post-anthesis leaf senescence, grain yield, and grain protein concentration in a winter wheat population segregating for flowering time QTLs. J. Exp. Bot. 62(10), 3621-3636. doi: 10.1093/jxb/err061.

Branlard, G., Faye, A., Rhazi, L., Tahir, A., Lesage, V., and Aussenac, T. (2020). Genetic and environmental factors associated to glutenin polymer characteristics of wheat. Foods 9(5), 683.

Cao, Z., Yao, X., Liu, H., Liu, B., Cheng, T., Tian, Y., et al. (2019). Comparison of the abilities of vegetation indices and photosynthetic parameters to detect heat stress in wheat. Agric. For. Meteorol. 265, 121-136. doi: https://doi.org/10.1016/j.agrformet.2018.11.009.

Chawade, A., van Ham, J., Blomquist, H., Bagge, O., Alexandersson, E., and Ortiz, R. (2019). High-throughput field-phenotyping tools for plant breeding and precision agriculture. Agronomy 9(5), 258.

Condorelli, G.E., Maccaferri, M., Newcomb, M., Andrade-Sanchez, P., White, J.W., French, A.N., et al. (2018). Comparative aerial and ground based high throughput phenotyping for the genetic dissection of NDVI as a proxy for drought adaptive traits in durum wheat. Front. Plant Sci. 9, 893. doi: 10.3389/fpls.2018.00893.

Daniel, C., and Triboi, E. (2000). Effects of temperature and nitrogen nutrition on the grain composition of winter wheat: effects on gliadin content and composition. J. Cereal Sci. 32(1), 45-56. doi: 10.1006/jcrs.2000.0313.

Dhondt, S., Wuyts, N., and Inzé, D. (2013). Cell to whole-plant phenotyping: the best is yet to come. Trends Plant Sci. 18(8), 428-439. doi: https://doi.org/10.1016/j.tplants.2013.04.008.

Easlon, H.M., and Bloom, A.J. (2014). Easy Leaf Area: Automated digital image analysis for rapid and accurate measurement of leaf area. Appl. Plant Sci. 2(7). doi: 10.3732/apps.1400033.

EEA (2020). "Climate change threatens future of farming in Europe".).

Farooq, M., Wahid, A., Kobayashi, N., Fujita, D., and Basra, S.M.A. (2009). Plant drought stress: effects, mechanisms and management. Agron. Sustain. Dev. 29(1), 185-212. doi: 10.1051/agro:2008021.

Guzmán, C., Autrique, J.E., Mondal, S., Singh, R.P., Govindan, V., Morales-Dorantes, A., et al. (2016). Response to drought and heat stress on wheat quality, with special emphasis on bread-making quality, in durum wheat. Field Crops Res. 186, 157-165. doi: 10.1016/j.fcr.2015.12.002.

Hernandez-Espinosa, N., Mondal, S., Autrique, E., Gonzalez-Santoyo, H., Crossa, J., Huerta-Espino, J., et al. (2018). Milling, processing and end-use quality traits of CIMMYT spring bread wheat germplasm under drought and heat stress. Field Crops Res. 215, 104-112. doi: 10.1016/j.fcr.2017.10.003.

Humplík, J.F., Lazár, D., Husičková, A., and Spíchal, L. (2015). Automated phenotyping of plant shoots using imaging methods for

analysis of plant stress responses – a review. Plant Methods 11(1), 29. doi: 10.1186/s13007-015-0072-8.

Hurkman, W.J., and Wood, D.F. (2011). High temperature during grain fill alters the morphology of protein and starch deposits in the starchy endosperm cells of developing wheat (Triticum aestivum L.) grain. Journal of Agricultural and Food Chemistry 59(9), 4938-4946.

Islas-Rubio, A.R., Singh, H., Chittrakorn, S., and MacRitchie, F. (2006). Stability of wheat proteins in solution. J. Cereal Sci. 43(2), 169-174. doi: https://doi.org/10.1016/j.jcs.2005.08.009.

Istvan, D. (2014). DigiCamControl Software, 2.1.2.

Johansson, E. (2002). Effect of two wheat genotypes and Swedish environment on falling number, amylase activities, and protein concentration and composition. Euphytica 126(1), 143-149. doi: 10.1023/A:1019646916905.

Johansson, E., Branlard, G., Cuniberti, M., Flagella, Z., Hüsken, A., Nurit, E., et al. (2020). "Genotypic and environmental effects on wheat technological and nutritional quality," in Wheat quality for improving processing and human health. Springer), 171-204.

Johansson, E., Kuktaite, R., Andersson, A., and Prieto-Linde, M.L. (2005). Protein polymer build-up during wheat grain development: influences of temperature and nitrogen timing. Journal of the Science of Food and Agriculture 85(3), 473-479. doi: https://doi.org/10.1002/jsfa.2006.

Johansson, E., Nilsson, H., Mazhar, H., Skerritt, J., MacRitchie, F., and Svensson, G. (2002). Seasonal effects on storage proteins and gluten strength in four Swedish wheat cultivars. J. Sci. Food Agric. 82, 1305-1311.

Koga, S., Böcker, U., Moldestad, A., Tosi, P., Shewry, P.R., Mosleth, E.F., et al. (2015). Influence of temperature on the composition and polymerization of gluten proteins during grain filling in spring wheat (Triticum aestivum L.). J. Cereal Sci. 65, 1-8. doi: 10.1016/j.jcs.2015.05.012.

Kuktaite, R., Larsson, H., and Johansson, E. (2004). Variation in protein composition of wheat flour and its relationship to dough mixing behaviour. J Cereal Sci. 40(1), 31-39. doi: https://doi.org/10.1016/j.jcs.2004.04.007.

Kumar, D., Kushwaha, S., Delvento, C., Liatukas, Ž., Vivekanand, V., Svensson, J.T., et al. (2020). Affordable phenotyping of winter wheat under field and controlled conditions for drought tolerance. Agronomy 10(6), 882.

Lama, S., Vallenback, P., Hall, S.A., Kuzmenkova, M., and Kuktaite, R. (2022). Prolonged heat and drought versus cool climate on the Swedish spring wheat breeding lines: Impact on the gluten protein quality and grain microstructure. Food Energy Secur. 11(2), 1-17. doi: 10.1002/fes3.376.

Lan, Y., Chawade, A., Kuktaite, R., and Johansson, E. (2022). Climate change impact on wheat performance - Effects on vigour, plant traits and yield from early and late drought stress in diverse lines. Int. J. Mol. Sci. 23(6), 1-17. doi: 10.3390/ijms23063333.

Le Gouis, J., Oury, F.-X., and Charmet, G. (2020). How changes in climate and agricultural practices influenced wheat production in Western Europe. J. Cereal Sci. 93, 102960. doi: https://doi.org/10.1016/j.jcs.2020.102960.

Leiva, F., Vallenback, P., Ekblad, T., Johansson, E., and Chawade, A. (2021). Phenocave: An automated, standalone, and affordable phenotyping system for controlled growth conditions. Plants 10(9), 1817.

Li, S., Wang, L., Meng, Y., Hao, Y., Xu, H., Hao, M., et al. (2021). Dissection of genetic

basis underpinning kernel weight-related traits in common wheat. Plants 10(4). doi: 10.3390/plants10040713.

Malik, A.H., Andersson, A., Kuktaite, R., Mujahid, M.Y., Khan, B., and Johansson, E. (2012). Genotypic variation in dry weight and nitrogen concentration of wheat plant parts; relations to grain yield and grain protein concentration. J. Agric. Sci. 4(11). doi: 10.5539/jas.v4n11p11.

Malik, A.H., Kuktaite, R., and Johansson, E. (2013). Combined effect of genetic and environmental factors on the accumulation of proteins in the wheat grain and their relationship to bread-making quality. J. Cereal Sci. 57(2), 170-174. doi: 10.1016/j.jcs.2012.09.017.

Malik, A.H., Prieto-Linde, M.L., Kuktaite, R., Andersson, A., and Johansson, E. (2011). Individual and interactive effects of cultivar maturation time, nitrogen regime and temperature level on accumulation of wheat grain proteins. J. Sci. Food Agric. 91(12), 2192-2200. doi: 10.1002/jsfa.4439.

Mamrutha, H.M., Khobra, R., Sendhil, R., Munjal, R., Sai Prasad, S.V., Biradar, S., et al. (2020). Developing stress intensity index and prioritizing hotspot locations for screening wheat genotypes under climate change scenario. Ecol. Indic. 118, 106714. doi: https://doi.org/10.1016/j.ecolind.2020.106714.

Peña, R.J. (2007). Current and future trends of wheat quality needs. Dordrecht: Springer Netherlands.

Porter, J.R. and Semenov, M.A. (2005). Crop responses to climatic variation. Philos. Trans. R. Soc. B: Biol. Sci. 360(1463), 2021-2035.

Prasad, P.V.V., Pisipati, S.R., Momčilović, I., and Ristic, Z. (2011). Independent and combined Effects of high temperature and drought stress during grain filling on plant yield and chloroplast EF-Tu expression in spring wheat. J. Agron. Crop Sci. 197(6), 430-441.

doi: https://doi.org/10.1111/j.1439-037X.2011.00477.x.

Qaseem, M.F., Qureshi, R., and Shaheen, H. (2019). Effects of pre-anthesis drought, heat and their combination on the growth, yield and physiology of diverse wheat (Triticum aestivum L.) genotypes varying in sensitivity to heat and drought stress. Sci. Rep. 9(1), 6955. doi: 10.1038/s41598-019-43477-z.

Rampino, P., Pataleo, S., Gerardi, C., Mita, G., and Perrotta, C. (2006). Drought stress response in wheat: physiological and molecular analysis of resistant and sensitive genotypes. Plant Cell Environ. 29(12), 2143-2152. doi: 10.1111/j.1365-3040.2006.01588.x.

Reynolds, D., Baret, F., Welcker, C., Bostrom, A., Ball, J., Cellini, F., et al. (2019). What is cost-efficient phenotyping? Optimizing costs for different scenarios. Plant Sci. 282, 14-22. doi: https://doi.org/10.1016/j.plantsci.2018.06.015.

Reynolds, M., Dreccer, F., and Trethowan, R. (2006). Drought-adaptive traits derived from wheat wild relatives and landraces. J. Exp. Bot. 58(2), 177-186. doi: 10.1093/jxb/erl250.

Rizhsky, L., Liang, H., and Mittler, R. (2002). The combined effect of drought stress and heat shock on gene expression in tobacco. Plant Physiol. 130(3), 1143-1151. doi: 10.1104/pp.006858.

Sara, D., Mandava, A.K., Kumar, A., Duela, S., and Jude, A. (2021). Hyperspectral and multispectral image fusion techniques for high resolution applications: a review. Earth Sci. Inform. 14(4), 1685-1705. doi: 10.1007/s12145-021-00621-6.

Sattar, A., Sher, A., Ijaz, M., Ullah, M.S., Ahmad, N., and Umar, U.U.-D. (2020). Individual and combined effect of terminal drought and heat stress on allometric growth, grain yield and quality of bread wheat. Pak. J. Bot. 52(2). doi: 10.30848/pjb2020-2(5).

Semenov, M.A., and Shewry, P.R. (2011). Modelling predicts that heat stress, not drought, will increase vulnerability of wheat in Europe. Sci. Rep.1(1), 66.

Sharkey, T.D. (2005). Effects of moderate heat stress on photosynthesis: importance of thylakoid reactions, rubisco deactivation, reactive oxygen species, and thermotolerance provided by isoprene. Plant Cell Environ. 28(3), 269-277. doi: https://doi.org/10.1111/j.1365-3040.2005.01324.x.

Shew, A.M., Tack, J.B., Nalley, L.L., and Chaminuka, P. (2020). Yield reduction under climate warming varies among wheat cultivars in South Africa. Nat. Commun. 11(1), 4408. doi: 10.1038/s41467-020-18317-8.

Shiferaw, B., Smale, M., Braun, H.-J., Duveiller, E., Reynolds, M., and Muricho, G. (2013). Crops that feed the world 10. Past successes and future challenges to the role played by wheat in global food security. Food Secur. 5(3), 291-317. doi: 10.1007/s12571-013-0263-y.

Singh, R.P., Prasad, P.V.V., Sunita, K., Giri, S.N., and Reddy, K.R. (2007). "Influence of high temperature and breeding for heat tolerance in cotton: A review," in Adv. Agron., ed. D.L. Sparks. Academic Press), 313-385.

Statkevičiūtė, G., Liatukas, Ž., Cesevičienė, J., Jaškūnė, K., Armonienė, R., Kuktaite, R., et al. (2022). Impact of combined drought and heat stress and nitrogen on winter wheat productivity and end-use quality. Agronomy 12(6), 1452.

Suzuki, N., Rivero, R.M., Shulaev, V., Blumwald, E., and Mittler, R. (2014). Abiotic and biotic stress combinations. New Phytol. 203(1), 32-43. doi: https://doi.org/10.1111/nph.12797.

Tao, H., Xu, S., Tian, Y., Li, Z., Ge, Y., Zhang, J., et al. (2022). Proximal and remote sensing in plant phenomics: 20 years of progress, challenges, and perspectives. Plant Commun. 3(6), 100344. doi: 10.1016/j.xplc.2022.100344.

Tashiro, T., and Wardlaw, I.F. (1989). A comparison of the effect of high-temperature on grain development in wheat and rice. Ann. Bot. 64, 59–65.

Team, R.C. (2013). R: A language and environment for statistical computing. .

Triboi, E., Martre, P., Girousse, C., Ravel, C., and Triboi-Blondel, A. (2006). Unravelling environmental and genetic relationships between grain yield and nitrogen concentration for wheat. Eur. J. Agron. 25(2), 108-118. doi: https://doi.org/10.1016/j.eja.2006.04.004.

Wahid, A., Gelani, S., Ashraf, M., and Foolad, M.R. (2007). Heat tolerance in plants: an overview. Environ. Exp. Bot. 61(3), 199-223.

Wang, X., Hou, L., Lu, Y., Wu, B., Gong, X., Liu, M., et al. (2018). Metabolic adaptation of wheat grain contributes to a stable filling rate under heat stress. J. Exp. Bot. 69(22), 5531-5545. doi: 10.1093/jxb/ery303.

Wheeler, T.R., Hong, T.D., Ellis, R.H., Batts, G.R., Morison, J.I.L., and Padley, P.The duration and rate of grain growth and harvest index, of wheat (Triticum aestivum L) in response to temperature and CO2. J. Exp.Bot. 47, 623–630 (1996).

Wu, W., Zhou, L., Chen, J., Qiu, Z., and He, Y. (2018). Gain TKW: A measurement system of thousand kernel weight based on the android platform. Agronomy 8(9), 178.

Yadav, S., Modi, P., Dave, A., Vijapura, A., Patel, D., and Patel, M. (2020). "Effect of abiotic stress in crops. ," in Sustainable Crop Production, ed. M.C.M.T.F. M. Hasanuzzaman, M. Fujita & T.A.R. Nogueira. ntechOpen).

Zadoks, J.C.; Chang, T.T.; Konzak, C.F. A decimal code for the growth stages of cereals. Weed Res. 1974, 14, 415–421.

Zhang, T., He, Y., DePauw, R., Jin, Z., Garvin, D., Yue, X., et al. (2022a). Climate change may outpace current wheat breeding yield improvements in North America. Nat. Commun. 13(1), 5591. doi: 10.1038/s41467-022-33265-1.

Zhao, K., Tao, Y., Liu, M., Yang, D., Zhu, M., Ding, J., et al. (2022). Does temporary heat stress or low temperature stress similarly affect yield, starch, and protein of winter wheat grain during grain filling? J. Cereal Sci. 103. doi: 10.1016/j.jcs.2021.103408.

Zhou, R., Yu, X., Ottosen, C.O., Rosenqvist, E., Zhao, L., Wang, Y., et al. (2017). Drought stress had a predominant effect over heat stress on three tomato cultivars subjected to combined stress. BMC Plant Biol. 17(1), 24. doi: 10.1186/s12870-017-0974-x.

Zubler, A.V., and Yoon, J.-Y. (2020). Proximal methods for plant stress detection using optical sensors and machine learning. Biosensors 10(12), 193.

Tables

Table 1. Age of the plants in days (Zadoks scale) during recording the digital biomass of the wheat plants.

Time points (Condition of the plants)	Wheat growth stage in Zadoks Scale	Combined heat-drought, (days)	Heat, (days)	Drought, (days)
Tp1 (non-stressed)	Heading (Zadoks 50)	56	56	51
Tp2 (stressed)	Heading (Zadoks 59)	61	61	56
Tp3 (recovered)	Development of fruit (Zadoks 70)	70	70	65

Table 2. Analysis of variance (ANOVA) showing the effect of genotype (G), treatment (E) and their interaction (G x E) on the gluten protein parameters (total amount of SDS-extractable (TOTE) and SDS-unextractable (TOTU) protein, total polymeric protein (TPP), total monomeric protein (TMP), SDS-unextractable polymeric protein (%UPP), large SDS-unextractable polymeric protein (%LUPP), large SDS-unextractable monomeric protein (%LUMP) and monomer to polymer ratio (Mon/pol)) of wheat grown under control, heat, drought and heat-drought stresses measured by size exclusion liquid chromatography (SE-HPLC).

Factors	Df	TOTE 10^{16}	TOTU 10^{15}	TPP 10^{15}	TMP 10^{15}	%UPP 10^3	%LUPP 10^3	%LUMP 10^2	Mon/ pol
Genotype (G)	7	0.53***	0.60***	0.98***	3.05***	1.65***	3.23***	0.80***	0.38***
Treatment (E)	3	1.33***	2.49***	3.80***	10.62***	1.88***	3.87***	0.22**	0.38***
G x E	21	0.26	0.76*	0.95	1.87	0.84	0.87	0.36	0.72**
Residuals	96	1.09	1.78	2.77	7.41	2.45	3.60	1.44	1.28

***, **, and * indicate significance at the $p < 0.001$, $p < 0.01$, and $p < 0.05$, respectively.

Table 3. Tukey's post hoc test of different stress environments (drought, heat and combined) on the gluten protein parameters (total amount of SDS-extractable (TOTE) and SDS-unextractable (TOTU) protein, total polymeric protein (TPP), total monomeric protein (TMP), SDS-unextractable polymeric protein (%UPP), large SDS-unextractable polymeric protein (%LUPP), large SDS-unextractable monomeric protein (%LUMP) and monomer to polymer ratio (Mon/pol)) evaluated by SE-HPLC.

Factors	TOTE	TOTU	TPP	TMP	%UPP	%LUPP	%LUMP	Mon/pol
	10^7	10^7	10^7	10^7	10^3	10^3	10^2	
Control	6.15 b	1.22 c	2.44 b	4.92 bc	31.06 c	34.84 c	9.45 b	2.02 a
Drought	5.81 b	1.28 bc	2.32 b	4.75 c	35.62 b	41.18 b	9.50 b	2.06 a
Heat	6.49 b	1.54 b	2.62 b	5.41 b	37.93 b	46.07 a	10.23 ab	2.08 a
Combined	8.43 a	2.32 a	3.70 a	7.06 a	41.65 a	49.46 a	10.36 a	1.93 b

Different letters indicating significant difference according to Tukey's post hoc test at $p < 0.05$.
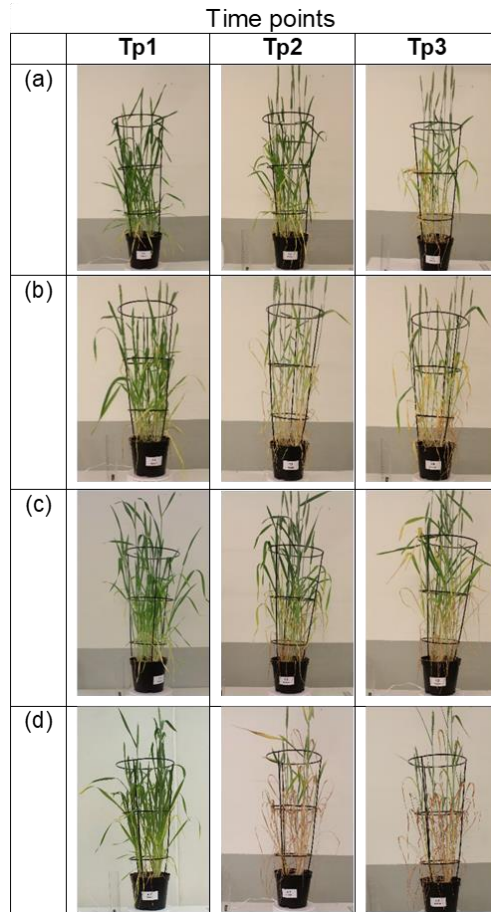
Figure 1. Digital RGB images of the spring wheat genotype Diskett in the heading stage (Zadoks 50) under diverse growing conditions (treatments); (a) control, (b) drought, (c) heat, and (d) combined heat-drought stresses measured along three time points (Tp) Tp1-Tp3; Tp1- no stress, Tp2-five days after induced the stress, and Tp3- after eight days of recovery.
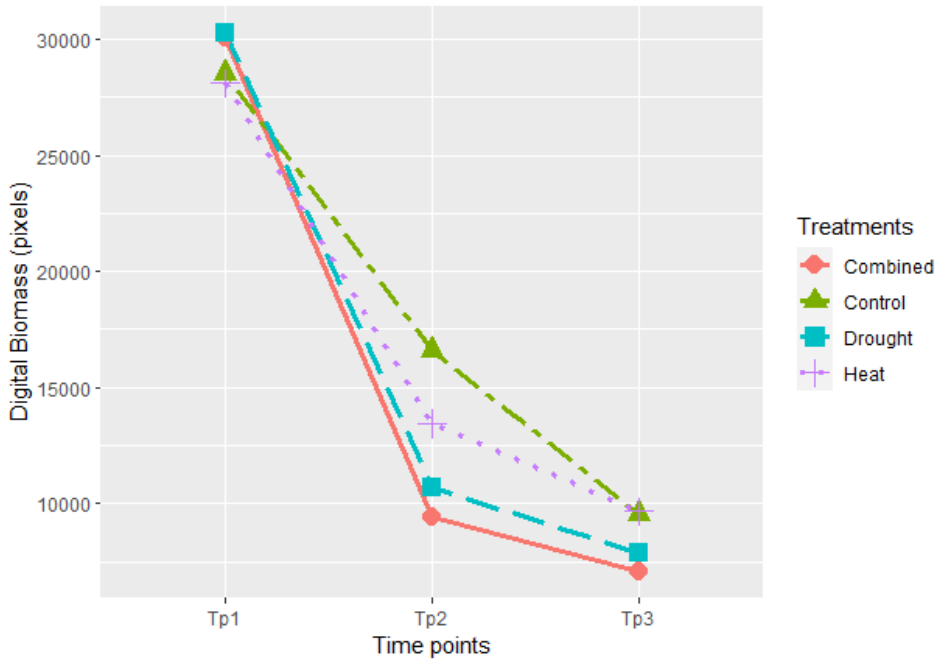
Figure 2. Mean digital biomass of the studied wheat genotypes obtained by RGB imaging (in pixels) at different growing conditions (treatments) such as, control, drought, heat, and combined heat-drought stresses measured along the three time points (Tp) Tp1-Tp3; Tp1 - no stress, Tp2- five days after induced the stress, and Tp3- after eight days of recovery.
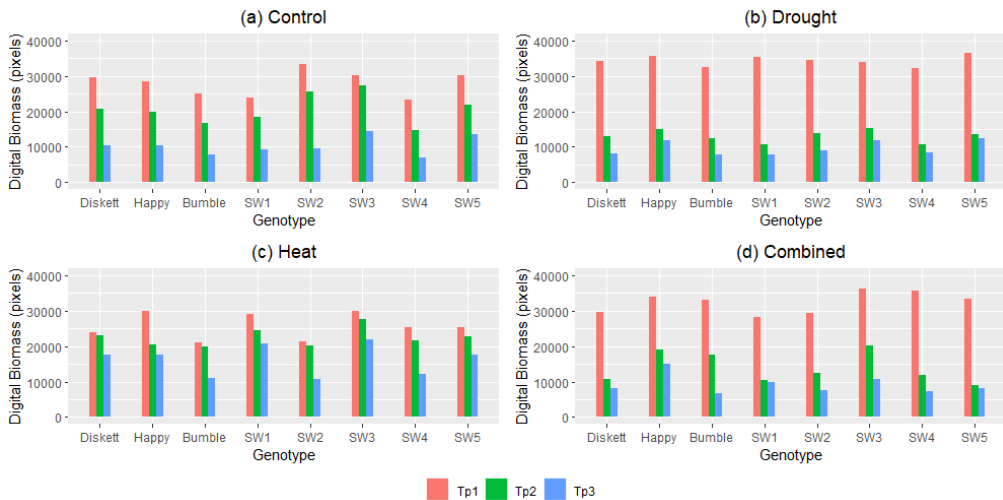
Figure 3. Digital biomass determined by RGB imaging (in pixels) of the eight spring wheat genotypes grown under diverse growing environments, (a) control, (b) drought, (c) heat, and (d) combined heat and drought stresses, evaluated along the three-time points (Tp) Tp1-Tp3; Tp1 - no stress, Tp2- five days after induced the stress, and Tp3- after eight days of recovery.
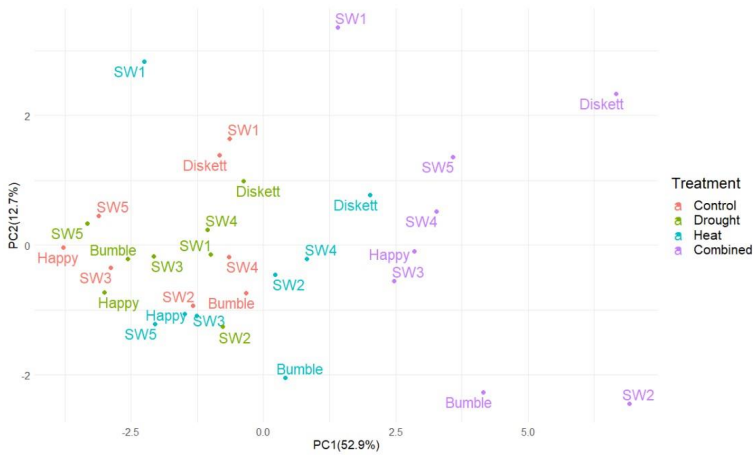
Figure 4. Principal component analysis (PCA) showing distribution of the eight wheat genotypes grown under control, drought, heat and combined heat-drought stresses (treatments).
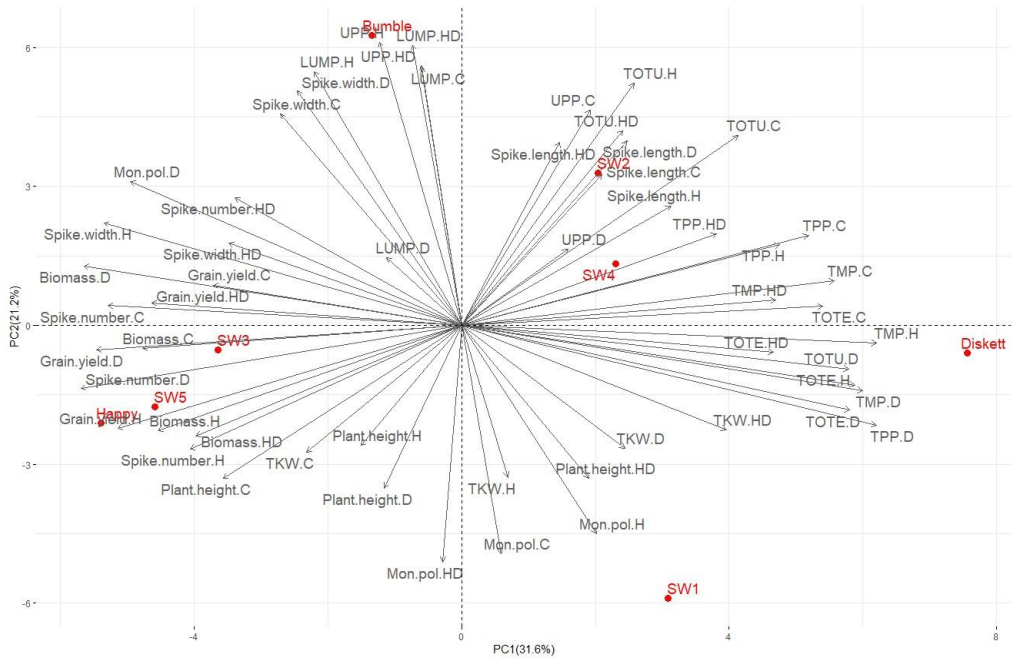
Figure 5. Principal component analysis (PCA) showing a relationship between the gluten protein parameters (TOTE, TOTU, TMP, TPP, %UPP and %LUMP) evaluated by SE-HPLC and the phenotypic traits (thousand kernel weight (TKW), plant height, spike length, biomass, spike width and grain yield) of the eight wheat genotypes grown under control (C), drought (D), heat (H), and combined heat-drought (HD) treatments.
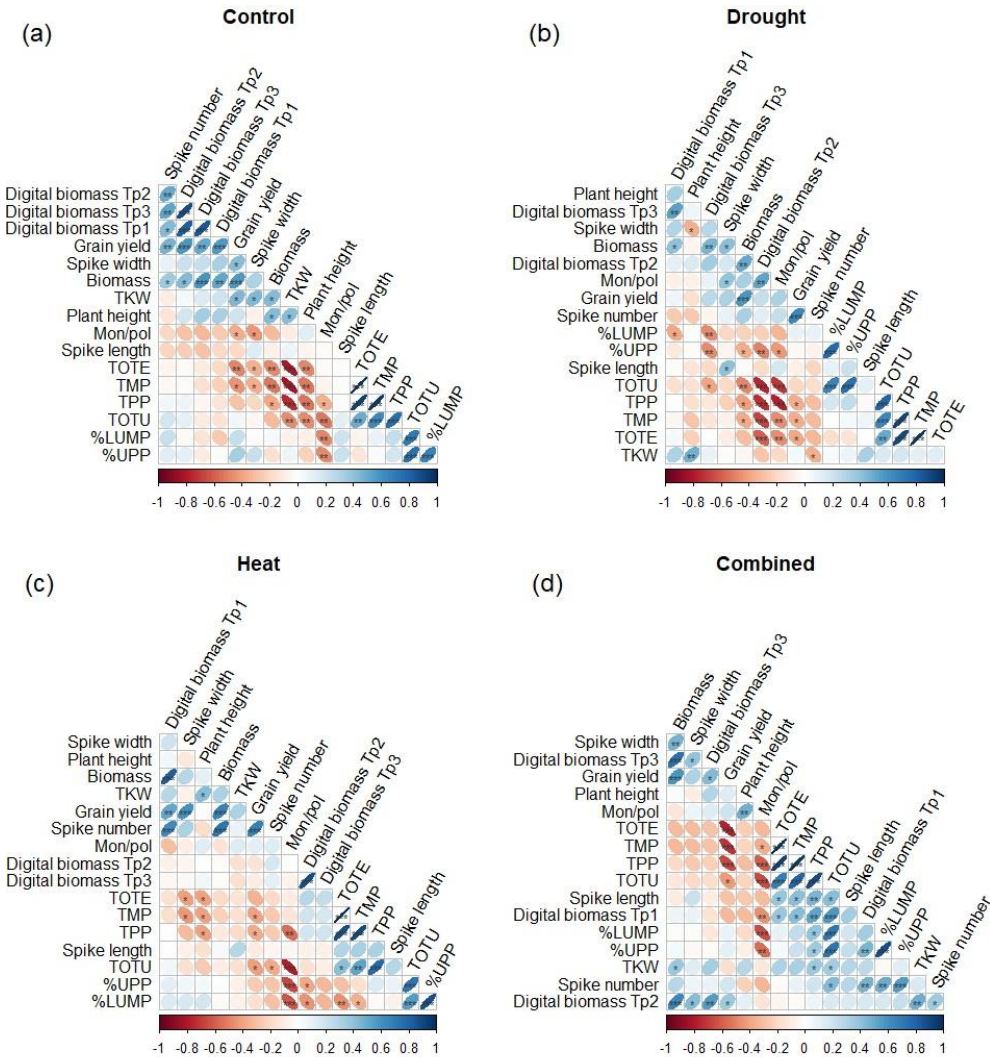
Figure 6. Spearman correlation of the gluten protein parameters (TOTE, TOTU, TMP, TPP, %UPP and %LUMP) and the phenotypic traits (grain yield, TKW, plant height, spike length, biomass, spike width and spike number) of the eight wheat genotypes grown under (a) control, (b) drought, (c) heat and (d) combined heat-drought conditions. ***, **, and * indicate significance at the $p < 0.001$, $p < 0.01$, and $p < 0.05$, respectively.
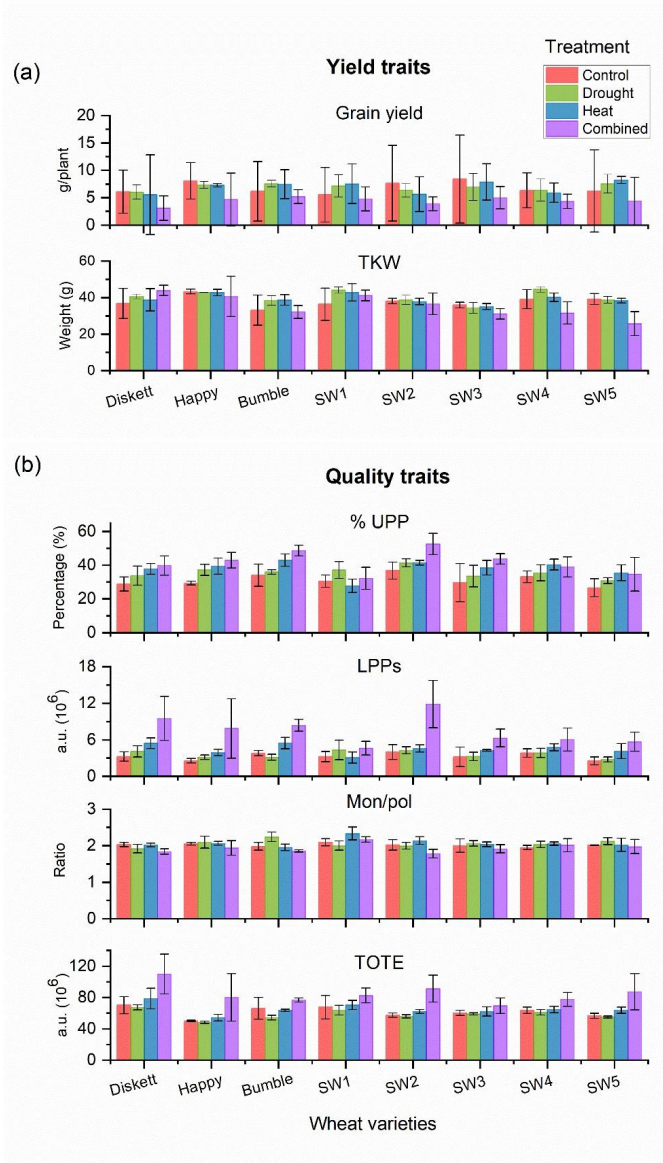
Figure 7. Yield traits (grain yield and TKW) (a) and gluten protein traits (%UPP, LPPs, Mon/pol and TOTE) (b) of the eight wheat genotypes grown under control, drought, heat and combined heat-drought conditions (treatments).
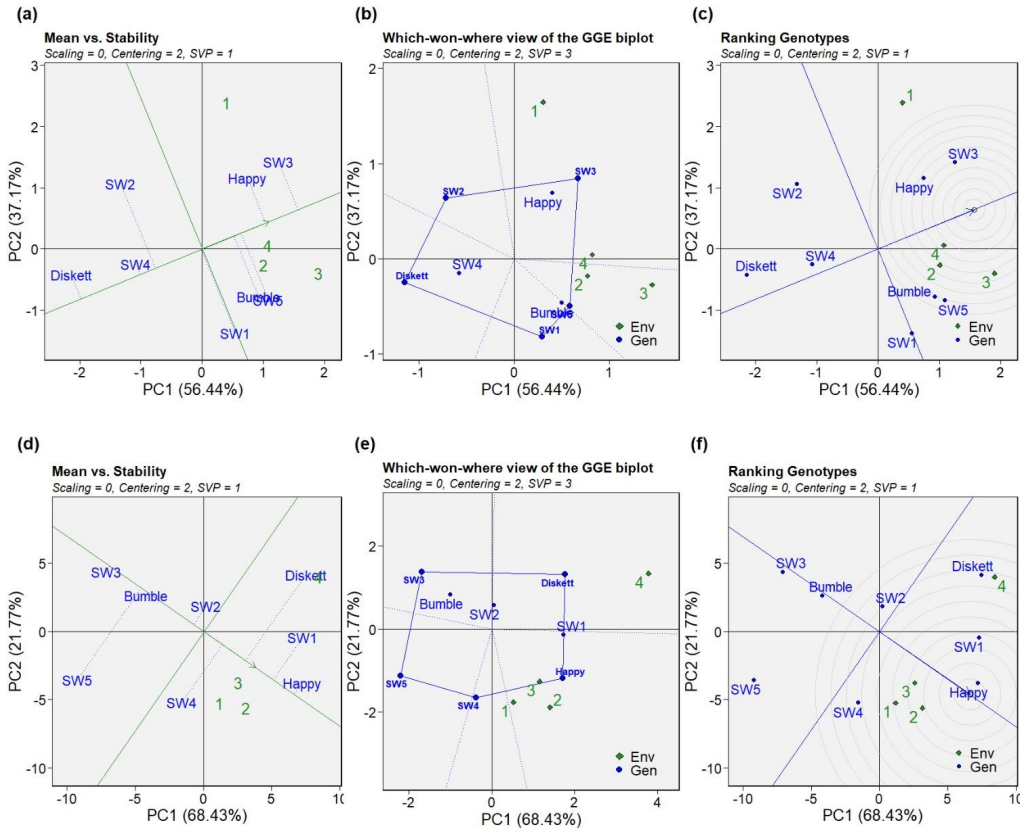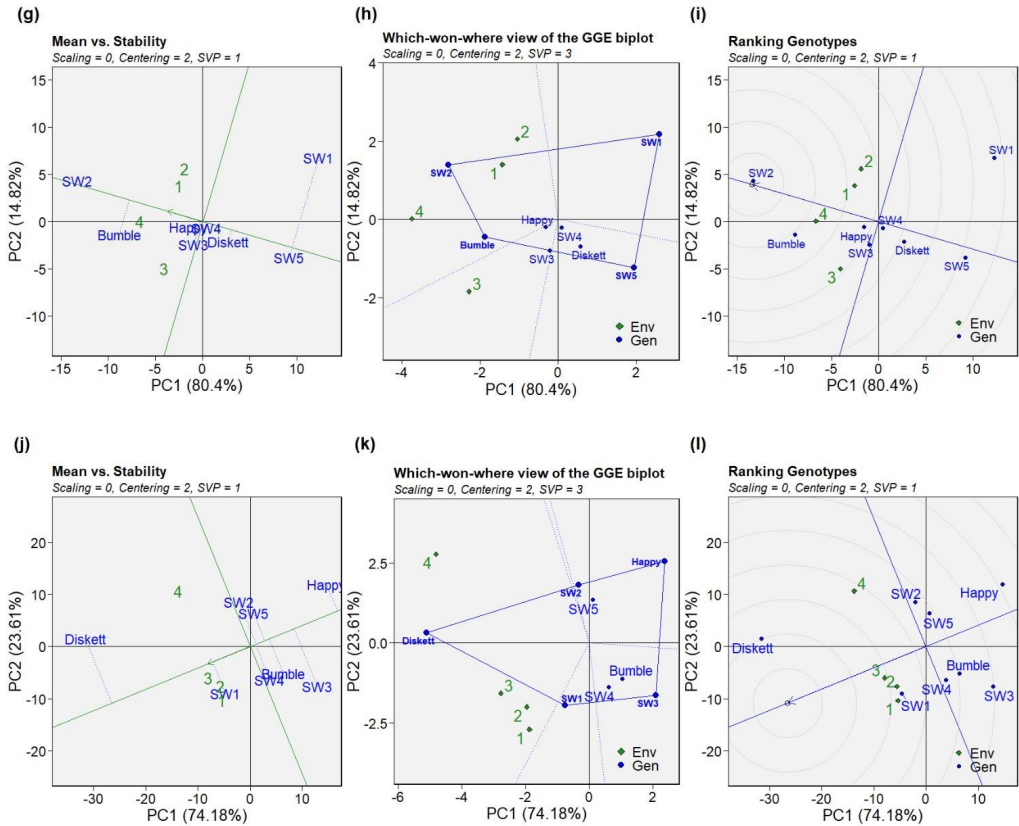
Figure 8. GGE biplots displaying the wheat genotypes according to their stability in the studied environments; (a-c) grain yield, (d-f) TKW, (g-i) %UPP and (j-l) TOTE (10^6). The biplots were based on genotype-focused singular value partitioning (SVP = 1), data were not scaled (scaling = 0), and were environment-centered (centering = 2). Environments designated as 1, 2, 3 and 4 correspond to control (no stress), drought, heat and combined heat-drought stresses, respectively.

Plant phenotyping is a pivotal tool for understanding the physiological and genetic basis of plant growth and development. However, phenotyping methods can be expensive and time-consuming, limiting their widespread adoption. This thesis presents the development and evaluation of affordable phenotyping methods that can be used to study a wide range of plant traits. These methods have the potential to increase the accessibility of plant phenotyping to researchers around the world, facilitating advances in plant breeding and physiology.

Fernanda Leiva-Sandoval received her doctoral education at the Department of Plant Breeding, Swedish University of Agricultural Sciences, Alnarp. She received her BSc in Electronics Engineering from the University of Ibague, Colombia.